SYNTHESIS AND CHARACTERIZATION OF HYDROXYAPATITE FROM CAPRINE (GOAT) BONE FOR MICROBIAL ADSORPTION AND ANTIMICROBIAL STUDY

A DISSERTATION SUBMITTED FOR THE PARTIAL FULFILLMENT OF THE REQUIREMENTS FOR THE MASTER OF SCIENCE DEGREE IN CHEMISTRY

By

Bibek Gautam

Symbol No.: CHEM. 709/073

T.U. Registration. No.: 5-2-37-83-2012

Submitted to:

CENTRAL DEPARTMENT OF CHEMISTRY

INSTITUTE OF SCIENCE AND TECHNOLOGY

TRIBHUVAN UNIVERSITY, KIRTIPUR, KATHMANDU, NEPAL

January, 2021

BOARD OF EXAMINER AND CERTIFICATE OF APPROVAL

This dissertation entitled **"SYNTHESIS AND CHARACTERIZATION OF HYDROXYAPATITE FROM CAPRINE (GOAT) BONE FOR MICROBIAL ADSORPTION AND ANTIMICROBIAL STUDY"** by **Mr. Bibek Gautam** under the supervision of **Asst. Prof. Dr. Kshama Parajuli**, Central Department of Chemistry, Tribhuvan University, Nepal, is hereby submitted for partial fulfillment of Master of Science (M. Sc.) degree in Chemistry. This dissertation has not been submitted in any other university or institution previously for the award of any degree.

……

Asst. Prof. Dr. Kshama Parajuli

Supervisor

Central Department of Chemistry

Tribhuvan University, Kirtipur, Nepal

……..	……..……..
Prof. Dr. Tulasi Prasad Pathak	**Asst. Prof. Dr. Hari Poudyal**
External Examiner	**Internal Examiner**
Central Department of Chemistry	Central Department of Chemistry
Tribhuvan University, Kirtipur, Nepal	Tribhuvan University, Kirtipur, Nepal

……

Prof. Dr. Ram Chandra Basnyat

Head

Central Department of Chemistry

Tribhuvan University, Kritipur, Nepal

Date: January, 2021

RECOMMENDATION LETTER

This is to certify that the dissertation work entitled "**SYNTHESIS AND CHARACTERIZATION OF HYDROXYAPATITE FROM CAPRINE (GOAT) BONE FOR MICROBIAL ADSORPTION AND ANTIMICROBIAL STUDY**" has been carried out by **Mr. Bibek Gautam**, as a partial fulfillment for the requirement M.Sc. degree in Chemistry under my supervision. To the best of my knowledge, this work has not been submitted to any other degree in this institution.

……..

Asst. Prof. Dr. Kshama Parajuli

Supervisor

Central Department of Chemistry

Tribhuvan University, Kritipur, Kathmandu, Nepal

Date: January, 2021

DECLARATION

I, **Bibek Gautam**, hereby declare that the work presented herein is genuine work done originally by me and has not been published or submitted elsewhere for the requirement of degree program. Any literature, data, or works done by other and cited in this dissertation has been given due acknowledgement and listed in the reference section.

……

Bibek Gautam

Exam Symbol No.: CHEM. 709/073

TU Registration No.: 5-2-37-83-2012

Central Department of Chemistry

Tribhuvan University, Kathmandu, Nepal

Date: January, 2021

ACKNOWLEDGEMENTS

This research work entitled "**SYNTHESIS AND CHARACTERIZATION OF HYDROXYAPATITE FROM CAPRINE (GOAT) BONE FOR MICROBIAL ADSORPTION AND ANTIMICROBIAL STUDY**" has been prepared in the partial fulfillment of the requirements for the degree of M.Sc. in Chemistry in Central Department of Chemistry, Tribhuvan University. This work is an outcome of numerous help and support provided by various people to whom I am highly indebted.

Firstly, I am profoundly grateful to my supervisor, Asst. Prof. Dr. Kshama Parajuli for her contributions, corrections, remarks, efforts and supervisory role in making this thesis a remarkable success and always spared some time to go through this work in spite of her very busy schedule.

I am heartily thankful to Prof. Dr. Ram Chandra Basnyat, Head of Department, Central Department of Chemistry, Tribhuvan University, for his help, suggestion and encouragement which helped me in carrying out my study effectively.

I am heartily thankful to Bijaya Laxmi Maharjan, Lab Assistant, Central Department of Microbiology, Tribhuvan University, for her help, suggestion and encouragements.

I am heartily thankful to Karan Khadayat, Lab Assistant, Central Department of Chemistry, Tribhuvan University, for his help and suggestions which helped me in carrying out my study effectively.

I would like to thank my friends, well-wishers and everyone who directly or indirectly helped me in conducting this study.

Finally, I am equally grateful to all faculty and staff of Central Department of Chemistry, Tribhuvan University, for providing direct and indirect moral support.

Bibek Gautam

Exam Symbol No.: CHEM. 709/073

TU Registration. No.: 5-2-37-83-2012

Central Department of Chemistry

ACRONYMS AND ABBREVIATIONS

ATCC	American Type Culture Collection
ATR-IR	Attenuated Total Reflection-Fourier Transform Infrared Spectroscopy
^{o}C	Degree Centigrade
CDM	Central Department of Microbiology
C_e	Equilibrium Concentration
cfu	Colony Forming Unit
cm^{-1}	Per Centimeter
DMSO	Dimethyl Sulfoxide
DTA	Differential Thermal Analysis
EDLC	Electric Double Layer Capacitor
EDS	Energy Dispersive Spectroscopy
EDX	Energy Dispersive X-ray
FTIR	Fourier Transform Infrared Spectroscopy
FWHM	Full Width at Half Maxmium
g	Gram
HAp	Hydroxyapatite
HPC	Hierarchical Porous Carbon
hr.	Hour
kW	Kilowatt
M	Molar Concentration
mg	Milligram
MHB	Mueller-Hinton Broth
mL	Mililitre

min.	Minute
MSA	Mannitol Salt Agar
µm	Micrometer
µL	Microliter
mm	Millimeter
m^2/g	Meter square per gram
MBC	Minimal Biocidal Concentration
MIC	Minimal Inhibitory Concentration
MOS	Microorganisms
nm	Nanometer
NA	Nutrient Agar
NADH	Nicotinamide Adenine Dinucleotide
NB	Nutrient Broth
NMR	Nuclear Magnetic Resonance
PBS	Phosphate Buffer Saline
ppm	Parts Per Million
PZC	Point of Zero Charge
%	Percentage
Q_m	Maximum Adsorption Capacity
s	Second
SEM	Scanning Electron Microscopy
TCP	Tri-Calcium Phosphate
TEM	Transmission Electron Microscopy
TGA	Thermogravimetric Analysis

TU	Tribhuvan University
W/V	Weight/Volume
Wt.	Weight
XRD	X-Ray Diffraction
XRF	X-ray Fluorescence
ZOI	Zone of Inhibition

ABSTRACT

In this work, natural hydroxyapatite (HAp) was extracted from bio-waste namely caprine (goat) bone by two different methods such as thermal treatment only and chemical method followed by thermal treatment. Thus produced HAp was characterized by different scientific tools like XRD, FTIR and SEM analyses.

The specific surface area of HAp was found to be 144.89 m^2/g measured by using methylene blue adsorption method. Similarly, pH_{PZC} value was calculated as 7.2 determined by using pH drift method. Adsorption study of different microorganisms on the extracted HAp as a functions of various parameters like concentration of adsorbate, contact time and adsorbent dose was studied. The maximum adsorption efficiency at pH 7 for *Escherichia coli, Candida albicans, Staphylococcus aureus* and *Acinetobacter baumanii* was found to be 32.57×10^5, 37.17×10^5, 6.7×10^5 and 43.47×10^5 cfu/mg respectively from Langmuir adsorption isotherm model. The contact time required for maximum adsorption fell within 25 mins. for all microorganisms. The experimental data was best fitted with pseudo-second order kinetics model.

HAp showed the antimicrobial activity only upon *Acinetobacter baumanii* among the studied microorganisms. MIC and MBC values of HAp were found to be 6.25 and 100 mg/mL respectively against *Acinetobacter baumanii*. Thus, hydroxyapatite was synthesized from bio-waste caprine (goat) bone which can be used as an adsorbent in microbial adsorption and an antimicrobial agent.

Keywords: Natural hydroxyapatite, Bio-waste, Adsorption, Microorganisms, Antimicrobial activity

LIST OF FIGURES

LIST OF TABLES

TABLE OF CONTENTS

CHAPTER 1: INTRODUCTION

1.1 General Introduction of Hydroxyapatite (HAp)

Hydroxyapatite is a bone repair material which is most commonly used to treat sarcoma and osteomyelitis (Shruthy, Mathew and Nair, 2016). Bones consist of organic (30%) and inorganic compounds (70%). Inorganic compounds mainly correspond to nonstoichiometric hydroxyapatite, $Ca_{10}(PO_4)_6(OH)_2$, that provide stiffness to bone (Smith and Smith, 1977). The organic compounds mostly correspond to collagen, along with several different types of proteins, lipids, and peptides. Protein covers a major portion of the surface of histological sections (Walters *et al*., 1990). The presence of small amounts of other mineral ions influences the reactivity and stability of natural hydroxyapatite (e.g. OH^-, CO_3^{--}etc.) inducing changes in their microstructural features (Meneghini *et al*., 2003; Bigi *et al*., 1997).

The analysis of burnt skeletal from animal bone and teeth is a topic of importance to scientists in several fields. The study of burnt remains mainly focus on color changes, changes in microscopic morphology, crystalline structural changes and shrinkage. Knowledge of the maximum temperature reached by a skeletal element suggest the mode of heating employed (Shipman, Foster and Schoeninge, 1984).

HAp shows biocompatible, osteoconductive, non-toxic, non-inflammatory and non-immunogenic properties to be a good bioactive agent. It could form a chemical bond with living tissue easily (Fathil, Hanifi and Mortazavi, 2008; Barakat *et al*., 2009).

1.2 Structure of Hydroxyapatite

Biological hydroxyapatite mainly consists of calcium phosphate framework with lots of embedded ions. Calcium, phosphorus and oxygen are the three major elements found in hydroxyapatite. The chemical composition and crystal structure of the hydroxyapatite depend upon the sources as well. Crystal size of the HAp is also related to the age of animal. The crystal obtained from the young animal is generally shorter and thicker than the mature one (Tong *et al*., 2003)**.**

Structure of hydroxyapatite is similar to the calcium phosphate in apatite form. In general, the ratio of Ca/P in hydroxyapatite is around 1.67. There are two different crystal forms of hydroxyapatite i.e. hexagonal with the lattice parameters $a = b = 9.43$ Å, $c = 6.88$ Å, and $\gamma = 120^0$ (Posner, Perloff and Diorio, 1958) and monoclinic with the

lattice parameters a = 9.42 Å, b = 2a, c = 6.88 Å, and $\gamma = 120^0$ (Elliott, Mackie and Young, 1980). In hexagonal HAp, two adjacent hydroxyl groups point in reverse direction while the hydroxyl groups have the same direction in the same column and opposite among columns in monoclinic HAp (Liu and Ma, 2009). In modified form of hydroxyapatite, the site of Ca^{2+} may be occupied by Sr^{2+}, Ba^{2+}, Na^{+} etc. Similarly, phosphorous and the hydroxyl groups may be replaced by C, As, V etc. and CO, F^{-} etc. (Vallet-Reg, 2008).

The crystal size and the degree of crystallinity depend upon the calcination temperature and the treatment methods. In general, the degree of crystallinity is found to increase with the increasing sintering temperature (Ooi, Hamdi and Ramesh, 2006; Barakat *et al*., 2009). Due to the higher crystallinity of synthetic HAp, its solubility is low as compared to the natural HAp (Zhuofan *et al*., 2009). **Figure 1.1** shows the hexagonal structure of hydroxyapatite.

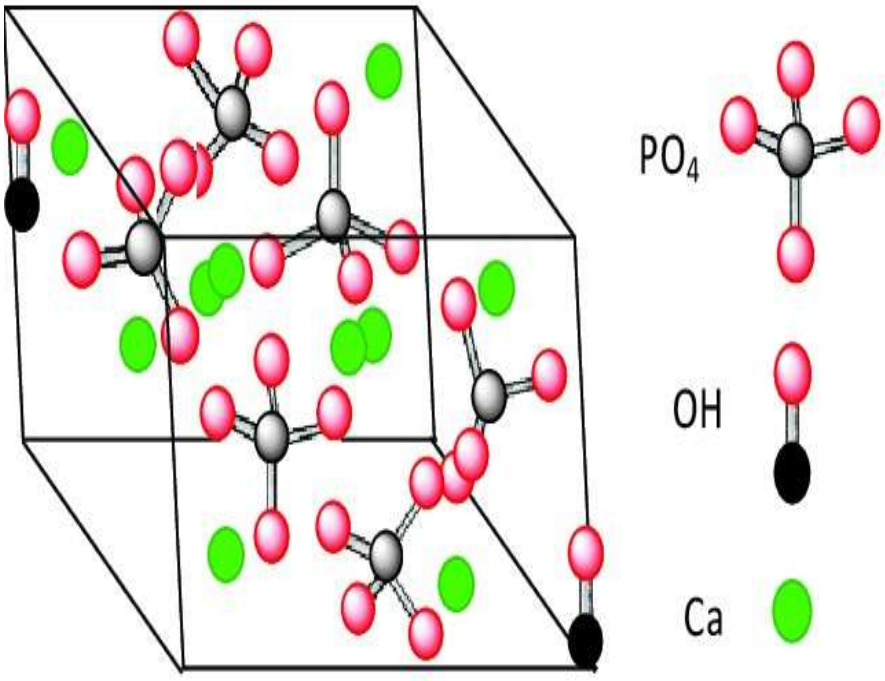

Fig 1.1: *Crystal structure of hydroxyapatite*

1.3 Methods of Synthesis (Barakat *et al*., 2009; Shojai *et al*., 2013)

Hydroxyapatite could be synthesized either from artificial chemicals or natural resources. First of all, different methods of synthesis of hydroxyapatite from artificial chemicals are described in the following paragraphs.

1.3.1 Dry methods

This method of synthesis of HAp does not require the solvent as well as the precise controlling condition. Dry methods are of two types.

1. Solid-state synthesis (Zhang and Zhu, 2006; Pramanik et al., 2007; Teshima et al., 2009)

In this process, precursors are first milled and then calcined at very high temperature (e.g. 1000^0C). The precursor can be calcium and phosphate containing chemicals of various types. Powder mixing and cold pressing are common processes applied in this synthesis. The powder obtained by this process often exhibit heterogenecity in its phase composition. So, a modified method, "Molten Salt Synthesis" is developed.

2. Mechanochemical method (Nasiri, Honarmandi and Ebrahimi, 2009; Mochales etal., 2011)

It is also known as mechanical alloying. Powder synthesized by this methods have well defined structure. It has the advantage of simplicity and reproducibility of a solid-state procedure to perform mass production. The materials are grounded on a planetary mill while the molar ratio between the reagents is kept at the stoichiometric ratio. Some of the relevant reactions involved are as follows:

$$6CaHPO_4.2H_2O + 4CaO \longrightarrow Ca_{10}(PO_4)_6(OH)_2 + 14H_2O$$

$$10CaCO_3 + 6(NH_4)H_2PO_4 \longrightarrow Ca_{10}(PO_4)_6(OH)_2 + 8H_2O + 10CO_2 + 6NH_3$$

$$3Ca_3(PO_4)_2.xH_2O + Ca(OH)_2 \longrightarrow Ca_{10}(PO_4)_6(OH)_2 + xH_2O$$

$$10Ca(OH)_2 + 3P_2O_5 \longrightarrow Ca_{10}(PO_4)_6(OH)_2 + 9H_2O$$

$$9CaO + Ca(OH)_2 + 3P_2O_5 \longrightarrow Ca_{10}(PO_4)_6(OH)_2 + 9H_2O$$

$$6CaHPO_4.2H_2O + 3CaO \longrightarrow Ca_9(HPO_4)(PO_4)_5OH + 14H_2O$$

1.3.2 Wet methods

This method is used to prepare the hydroxyapatite having nanosized structure with a regular morphology through solution phase reactions. Some of wet methods are shortly described in the following paragraphs.

1. Chemical precipitation (Gomez et al., 2001; Kong, Ma and Boey, 2002)

It is the simplest route for the synthesis of nanosize HAp. The precipitation reaction is conducted at a pH value higher than 4.2 and the temperature ranging from room temperature to boiling point of water. A typical procedure involves the dropwise addition of one reagent to another under continuous and gentle stirring, while the molar ratio of elements is kept at stoichiometry according to its ratio in HAp. At the last step, the resultant suspension may be aged under atmospheric pressure. To produce HAp particles, various calcium and phosphate containing reagents e.g. $Ca(OH)_2$ or $Ca(NO_3)_2$ act as the source of Ca^{2+} and H_3PO_4 or diammonium hydrogen phosphate act as the PO_4^{3-} source.

$$10Ca(NO_3)_2 + (NH_4)H_2PO_4 + 8NH_4OH \longrightarrow Ca_{10}(PO_4)_6(OH)_2 + 20\ NH_4NO_3 + 6H_2O$$

2. Hydrolysis (Durucan and Brown, 2000; Sturgeon and Brown, 2009)

By using hydrolysis method, calcium salt of phosphate are converted into HAp according to the following simplified equations.

$$10CaHPO_4 + 2H_2O \longrightarrow Ca_{10}(PO_4)_6(OH)_2 + 4H_3PO_4$$

$$10CaHPO_4 + 12OH^- \longrightarrow Ca_{10}(PO_4)_6(OH)_2 + 4PO_4^{3-} + 10H_2O$$

$$6CaHPO_4 + 4Ca(OH)_2 \longrightarrow Ca_{10}(PO_4)_6(OH)_2 + 6H_2O$$

$$6CaHPO_4 + 4CaCO_3 + 2H_2O \longrightarrow Ca_{10}(PO_4)_6(OH)_2 + 4H_2CO_3$$

$$10CaHPO_4.2H_2O \longrightarrow Ca_{10}(PO_4)_6(OH)_2 + 18H_2O + 12H^+ + PO_4^{3-}$$

$$6CaHPO_4.2H_2O + 4Ca(OH)_2 \longrightarrow Ca_{10}(PO_4)_6(OH)_2 + 18H_2O$$

$$10Ca_3(PO_4)_2 + 6H_2O \longrightarrow 3Ca_{10}(PO_4)_6(OH)_2 + 2PO_4^{3-} + 6H^+$$

$$10Ca_3(PO_4)_2 + 6OH^- \longrightarrow 3Ca_{10}(PO_4)_6(OH)_2 + 2PO_4^{3-}$$

Aqueous hydrolysis of HAp usually proceeds by dissolution and precipitation processes.

3. Sol-gel method (Sanosh et al., 2009; Kumar and Kalainathan, 2010)

It is one of the first method proposed for the wet synthesis of HAp. It offers advantage of molecular-level mixing of reactants improving the chemical homogeneity of the resulting powder. Low temperature formation and fusion of the prepared crystals are the notable advantage of sol-gel process. Powder obtained by sol-gel method usually

exhibits a stoichiometric structure with a large surface area and the small cluster size. The bioresorbility of the sol-gel HAp is higher than the conventional powder which is close to bioapatite. However, the generation of secondary phase and the high cost of starting materials are the major disadvantages of this process.

In the majority of cases, calcium diethoxide or calcium nitrate is treated with triethylphosphate either in an aqueous solution or organic solution.

$$6Ca(NO_3)_2 + 6(C_2H_5O)_3P(O) \longrightarrow Ca_{10}(PO_4)_6(OH)_2 + \text{byproducts}$$

4. Hydrothermal process (Xingyu et al., 2005; Neira et al., 2008)

It is a chemical precipitation method in which aging step is conducted at high temperature i.e. above the boiling point of water inside an autoclave. This method is used in the preparation of 1D nanosized HAp. The hydrothermal conditions are relatively stoichiometric and highly crystalline. HAp obtained by this process are irregular, spherical or at most rod like. During the hydrothermal treatment, Calcium ions are released and each individual nucleus will grow to the distinct single needle like particles and finally to well-separated long fibres. HAp powders of desired characteristics could be fabricated by the addition of organic modifiers e.g. Poly ethylene glycol, Tween-20 and d-sorbitol at different temperatures. Recently a novel hydrothermal method based on liquid-solid-solution had been developed to synthesize surface modified HAp nanorods of various aspect ratio. According to this strategy, controlled growth of HAp nanorods with tunable morphology could be achieved by properly tuning the interfaces between the surfactants and the central atom of HAp.

5. Emulsion (Hong, MinYing and ChangRen, 2008; Chen et al., 2009)

Emulsion process of synthesis of HAp is to refine the clustering and to restrict the formation of hard agglomerates. This process is more efficient to reduce the particle size, to control the morphology, and to limit the agglomeration of HAp particles. Emulsion process depends strongly on the type of surfactants used and concentration of the surfactants present in the liquid medium. There are three main categories of surfactants used in microemulsion synthesis of HAp including ionic surfactants, nonionic surfactants and block copolymers with different molecular weights. Depending on the nature of surfactants, HAp nanoparticles of different characteristics

(size, shape, crystallinity, etc.) could be produced. Incorporating alcohol as co-surfactants could improve the interfacial properties of the microemulsion.

6. Sonochemical method (Cao, Zhang and Huang, 2005; Rouhani, Taghavinia and Rouhani, 2010)

This method is based on chemical reactions activated by powerful ultrasound radiation. The physical mechanism behind the sonochemical synthesis is acoustic cavitation in an aqueous phase where the formation, growth and collapse of microbubbles occur. The sonication increases the rate of HAp crystal growth uo to 5.5 times. It also possess more uniform, smaller and pure crystals with minimal agglomeration. These nanoparticles can significantly enhance the sintering kinetics due to higher surface area. It is concluded that single phase HAp could be synthesized after the sonification of 60 mins.

1.3.2 High temperature processes

1. Combustion (Ayers et al., 2006; Aghayan and Rodriguez, 2012)

This method is used to prepare various oxide ceramics. The basis of combustion technique comes from the thermochemical concepts used in the field of propellants and explosives chemistry. The key feature of this process is its ability to quickly produce powder with high purity in a single step operation. Inexpensive raw materials, simple preparation process, and well chemical homogeneity are the advantages of this method. The solution combustion process of HAp involves a very rapid exothermic and self-sustaining redox reactions between the oxidants and a suitable organic fuel in aqueous phase. The aqueous stock solution of $Ca(NO_3)_2$ and $(NH_4)_2HPO_4$ are first mixed followed by the addition of concentrated HNO_3 to dissolve the resulting white precipitate.

2. Pyrolysis (Cho and Kang, 2008; Itatani et al., 2010)

Some post treatment and long term aging under elevated temperatures are required to achieve a high crystalline product. HAp particles prepared from this method are stoichiometric and homogenous with high degree of crystallinity. Particles can form from reactants in a gas phase generated by physical evaporation of liquid precursors. There is no need of fuel mixed with the reactants. Pyrolysis method is also known as spray pyrolysis which involves spraying the precursor solutions into a flame of an electric furnace using an ultrasonic generator which is followed by reactions of the

generated vapors and gases at high temperatures to produce final powers. The high temperature leads to the complete evaporation of precursor droplets followed by nucleation and growth of nanoparticles in the gas phase.

The properties of HAp prepared from above method mainly depend upon the following factors: (Baig *et al*., 1999)

1. Preparation methods
2. Ca/P ratios
3. Non-stoichiometries
4. Defects
5. Particle sizes etc.

However, synthetic HAp cannot mimic apatite extracted from natural sources due to the absence of other trace elements (e.g., Na, Mg, Al, C and other elements) in the bones (Akram et al., 2014). HAp synthesized from natural resources has high biocompatibility and good bioaffinity which stimulates osteoconduction (Chang et al., 2000). Similarly, it is economical and environmental friendly in terms of waste recovery. Therefore, it is slowly replaced by the host bone after implantation. HAp synthesized from animal bones inherits some properties of the raw bone powder which seems to be an alternative for numerous products based on synthetic HAp (Haberoka, Bucko and Miecznik, 2006). HAp synthesized from natural sources have broad applications which are classified on the basis of source in the following chart.

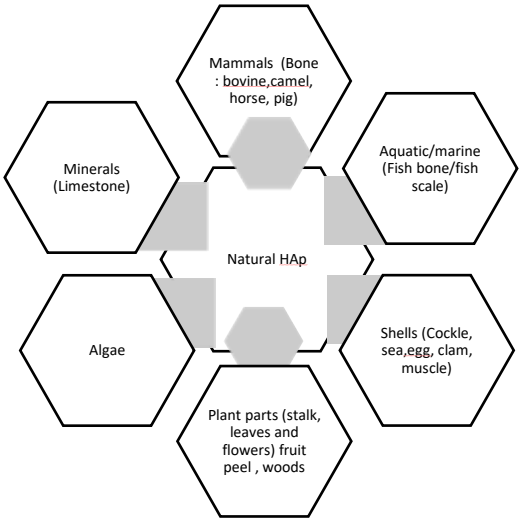

Fig 1.2: *Extraction of HAp from different natural sources*

There are some common steps applied in different methods for synthesis of HAp. Pretreatment is one of the crucial step which focus on the removal of the organics present in bone and other typical sources as depicted from **Table 1.1.**

Table 1.1: Pretreatment methods for the extraction of HAp from different natural sources

Methods		
Washing and removing the dirt, fats, protein, and other components such as bone marrows and soft tissues with boiling water for 8 hrs or more (Ruksudjarit *et al*., 2008)	Boiling and washing with solvents (acetone and Chloroform) (Ruksudjarit *et al*., 2008)	Washing alternatively with surfactant and alkali solutions to remove the soft tissues and decellularise it (Barakat *et al*., 2009)

After the pretreatment of the respective natural sources of HAp, following processes are performed in stepwise manner.

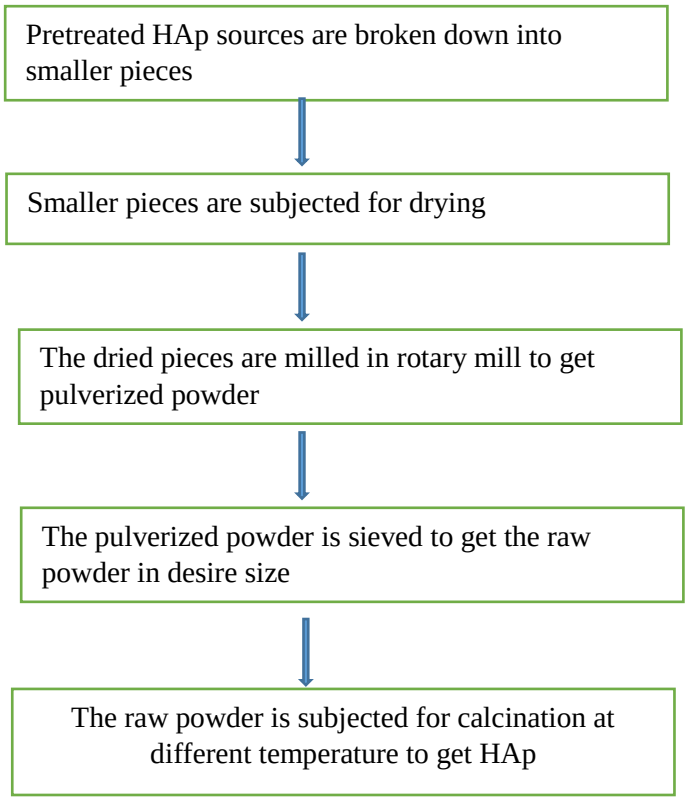

Beside this common process of extracting HAp, there are few modified methods extracting from animal bones:

1. Thermal decomposition (Barakat et al., 2009)

This is the direct heating of bone to decompose collagen and other organic compounds leaving the desire natural pure hydroxyapatite. These unwanted products are finally removed by calcination. In thermal decomposition process, raw bone powder placed in Alumina crucible is heated in the muffle furnace at different temperature. The rate of heating depends upon the type of rawmaterials. Most commonly, 10^0C/min is applied. In a typical process, nanorod shape hydroxyapatite with an average length of 300 nm was obtained by the thermal process at temperature of 750^0C during 6 hrs.of heat treatment.

2. Subcritical water process (Barakat et al., 2009)

This processs (pressurized low polarity water) is a type of fractionation technique which uses hot liquid water under pressure. The working temperature is between 100^0C and the critical value of water (379^0C). In this process, cylindrical hydrothermal stainless steel autoclave is used. The grinded bones are added to deionized water at solid to liquid weight ratio of 1:40. The mixture is placed in a Teflon crucible inside the autoclave. Nitrogen gas is used to remove the dissolved oxygen from the water and the surrounding atmosphere. The autoclave is heated in silicon bath at 275^0C for 1 hr. which is finally cooled by quenching in big amount of water. The obtained mixture is filtered and the solid product obtained is dried after washing. In a typical subcritical water process, pure hydroxyapatite nanoflakes have been obtained at temperature of 275^0C and holding time 1 hr.

3. Alkaline hydrothermal hydrolysis (Barakat et al., 2009)

The main aim of this process is to hydrolyze the collagen and other organic compounds present in the bones. The grinded bones are mixed with NaOH solution with solid/liquid weight ratio of 1:40 and heated to 250^0C for 5 hrs. In a typical alkaline hydrothermal hydrolysis, pure hydroxyapatite nanoparticles are produced at sodium hydroxide concentration of 25 wt% at 250 °C and holding time of 5 hrs.

4. Plasma processing (Yogananda et al., 2011)

During the plasma process, the organic component from the bovine bone get removed and HAp ceramic in the bulk is produced. In this process, bones are treated with NaOH to deproteinize and are cut into pieces. These pieces are used for plasma processing at 5 kW of plasma power in Argon plasma for different processing times by using DC transferred arc plasma torch operated at 10 kW. The arc is typically struck between the cathode and the anode to get the desired power level. In this way, plasma is generated and the bovine bone is processed by varying the melting times for 30, 45, 60, 90 and 120 s respectively.

5. Enzymatic hydrolysis (Huang, Hsiao and Chai, 2011)

This study analyzes the hydroxyapatite extracted from fish scale (FHAP) by enzymatic hydrolysis. Alkaline phosphatase is the most common enzyme used in this method. By using the enzyme, the alkaline hydrolysis method becomes too faster. The fish scale HAp particles are washed twice with PBS before adding the mixture of cell lysis buffer and p-nitrophenyl phosphate. After 30 mins. of incubation incubation at 37^0C, enzyme activity should be terminated by adding NaOH. Liberated p-nitrophenol was then measured by the light absorbance observed at 405 nm. The amount of p-nitrophenol corresponded to alkaline phosphatase activity**.**

6. Vibro-milling technique (Ruksudjarit et al., 2008)

In this process, the cut pieces of bones are boiled in distilled water for 8 hrs. for easy removal of the bone marrow and tendons. It is boiled to deproteinize. The boiled bone samples are dried overnight which are finally calcined. The resultant powder is crushed into small pieces and milled in a ball mill pot. Each 20 g of HA powders are regrounded by vibro-milling method (McCrone Micronizing Mill) using ethanol as a milling media and the milling time was varied from 0, 1, 2, 4 to 8 hrs. respectively.

In all process, heat treatment is the common method applied. Heat treatment is an important way to synthesize HAp from natural bone. The crystalline phase composition of sintered bovine bone is similar to natural bone mineral which is composed of $Ca_{10}(PO_4)_6(OH)_2$ at about 93 wt% and about 7 wt% of β-tricalcium phosphate ($Ca_3(PO_4)_2$, β-TCP) (Martin, 2000).

The properties of HAp prepared from natural bone through heat treatment mainly depend upon the following factors as: (Ooi et al., 2006)

1. Temperature
2. Duration of heat treatment
3. Ca/P ratio

It is reported that synthetic HAp with a Ca/P ratio near to 1.67 is stable below 1200^0C (Zhou et al., 1993). Above this temperature, it suffers poor thermal stability and will decompose to form secondary phases such as TCP. This shows the importance of temperature during extraction of HAp from bones (Kutty and Ramesh, 2000).

1.4 Applications of Hydroxyapatite

Natural HAp is one of the most important natural renewable feedstock. In general, vast numbers of applications are found in the plant based material from nature. However, animal based materials could not attract the experts to be researched on them. Hydroxyapatite is also animal based material which is most commonly used in skeletal reconstruction. It could also be used in other immense issues. They show good biocompatibility, bioaffinity and osteoconductive properties. Following lists summarize the major applications of HAp (Krzesinska and Majewska, 2015).

1.4.1 Purification process of food products

For the purification of food and meat products HAp could be used for dividing organic compounds in purification processes.

1.4.2 Adsorbents in purification

It is used as adsorbents of harmful substances (Fluoride, Arsenic ions etc.) in environmental protection (Moreno-Pirajan *et al*., 2010; Fu, Wang and Ho, 2013). Also, it can be used as an adsorbent for microbial adsorption (Gibbons, Moreno and Spinell, 1976; O'Brien *et al*., 1978; Berry and Siragusa, 1997; Zamora *et al*., 2007).

1.4.3 Electrodes in EDLC and supercapacitors

The Hierarchical Porous Carbon (HPC) is prepared from the natural hydroxyapatite. HPC is combination of micropores, mesopores and macropores which can be used for gas storage, biosensor, catalysis and in other fields. It can also be used as electrodes for

EDLC and supercapacitors. In EDLC preparation, the porous carbon from the hydroxyapatite acts as template (Huang *et al*., 2011; Goodman *et al*., 2013).

1.4.4 Bone substitute

HAp is a good biomaterial for filling bone defects. In tissue engineering, it can be used as bone substitute in bone grafting (Seol *et al*., 2013; Martinez-Vazquez *et al*., 2014)

1.4.5 Drug carrier in drug delivery system

It can be used as a drug carrier in drug delivery system (Martinez-Vazquez *et al*., 2014).

1.5 Microbial Adsorption

Microbial adsorption on HAp surface is studied in terms of adsorption sites and affinity constants (Gibbons *et al*., 1976). Researches mainly focus on oral bacteria during the study of microbial adsorption on HAp surfaces. Dental enamel contains HAp in large proportions and HAp could be used as model for the study of dental plaque formation (Hillman, Houte and Gibbons, 1970; Clark and Gibbons, 1977; Cowan, Taylor and Doyle, 1987; Clark *et al*., 1985). The adsorption of bacteria to saliva treated HAp surfaces and to teeth covered with an acquired salivary pellicle could be comparable. The presence of adsorbed salivary components on enamel or HAp surfaces change the selectivity of bacterial adsorption (Hillman, Houte and Gibbons, 1970; Orstavik, Kraus and Henshaw, 1974; Liljemark and Schauer, 1975; Clark and Gibbons, 1977). *S. mitis* and *S. sanguis* adsorb in high number in salivary treated HAp surfaces while *S. mutans* and *S. salivarius* adsorb in high number in saliva untreated HAp surfaces (Hillman, Houte and Gibbons, 1970; Orstavik, Kraus and Henshaw, 1974; Liljemark and Schauer, 1975; Olsson and Krasse, 1976; Clark and Gibbons., 1977; Clark *et al*., 1978).

By using the same model of microbial adsorption onto teeth surface, HAp could be also used as an adherence to concentrate the microorganisms. It is obvious need of non-cultural concentration of the microorganisms from food to shorten the time required for detection results. Efficient methods for bacterial concentration from foods help for the collection of larger and more representative samples increasing the probability of detection. There are variety of methods for separating and concentrating microorganisms from foods which are listed below (Payne and Kroll, 1991).

1. Centrifugation
2. Filtration
3. Use of anion- and cation exchange resins
4. Two-phase extraction systems

Centrifugation and Filtration are the most common methods for the concentrating the microorganisms in food products. However, they are limited due to interference from food particulates or chemical properties of food components (Payne and Kroll, 1991).

HAp could be used as an adsorbent material to concentrate bacteria from suspensions. It is shown that HAp adheres several different species of food-borne spoilage and pathogenic bacteria. It has great potential to remove and concentrate indigenous bacteria from ground beef, feces, and beef carcass sample suspensions (Berry and Siragusa, 1997). Also, it has been used extensively as a matrix for the purification and fractionation of an array of biochemical substances, including enzymes, nucleic acids, hormones, and viruses (Brooks, 1981).

HAp could also be applied to immobilize microorganisms that lead to a synergistic effect for the improvement of removal efficiencies of metal ions. Bacteria are particularly effective at higher metal concentrations (Piccirillo *et al*., 2013).

1.5.1 Mechanism of microbial adsorption on HAp surface.

In general, the surface of bacteria possess negative charge. The adsorption of such bacteria on HAp surface is similar to the adsorption of negatively charged proteins on HAp surface. An electrostatic attraction between the negatively charged bacterial surface and the positively charged Calcium atoms of the HAp occurs binding the two entities altogether (Rolla and Melsen, 1975).

Microroganisms possibly oral bacteria adsorbs on HAp surface to cause dental carries. This might be due to Ca^{2+} bridging between bacterial surface and HAp skeleton (Clark et al., 1978). Synthetic hydroxyapatite surfaces have been widely used for this purpose. The presence of adsorbed salivary material on enamel or HAp surfaces alters the selectivity of bacterial adsorption especially adsorption of proteins, dextrans and *S. mutans* on HAp (Gibbons *et al*., 1976).

Bacterial cell adsorption on saliva coated HAp might be due non-specific as well as specific interactions like hydrophobic, electrostatic and adhesion receptor interactions

(Beem *et al*., 1996). However, bacterial adsorption on saliva uncoated HAp is governed by non-specific van der waals and electrostatic attractions (Gibbons, Etherden and Moreno, 1985; Cowman *et al*., 1987).

1.5.2 Applications of microbial adsorption on HAp surface

1. Development of rapid microbial testing method in food and meat industry

For the implementation of hazard analysis and critical control point programs by the food industry there would be a great need in rapid microbial testing. Nucleic acid probe hybridization and immunological assays are the crucial rapid microbial testing method those lessen the time required for detection of bacterial pathogens. However, these methods require higher concentration of targeted microrganisms (10^4 to 10^6 cfu/mL or more). In general bacterial pathogens occur in very low number in food. To concentrate the bacterial pathogens in such sample HAp could be used as an adsorbent for pathogens in terms of non-cultural microbial concentration (Berry and Siragusa, 1997).

2. Purification and fractionating of biochemical substances

Biochemical substances like enzymes, nucleic acids, hormones, viruses etc. could be separated and fractionated through the use of hydroxyapatite in the form of matrix (Berry and Siragusa, 1997).

3. In the area of oral microbiology

The main inorganic fraction of dental enamel consists of hydroxyapatite. HAp could be used as a model for the study of dental plaque formation (Hillman *et al*., 1970; Orstavik, Kraus and Henshaw, 1974; Liljemark and Schauer, 1975; Olsson and Krasse, 1976; Clark and Gibbons., 1977; Clark *et al*., 1978).

4. Development an efficient adsorbent for the removal of heavy metal ions

HAp containing adsorbed microorganism could also be applied to improve the removal efficiencies of heavy metal ions. The combination of HAp with the bacterial strains led to higher adsorption capacity for heavy elements. In general, the maximum adsorption capacities are almost 4 and 3 times higher for Zn(II) with *Cupriavidus sp*.(1C2) and Cd(II) with *Microbacterium oxydans* (EC29) respectively (Piccirillo *et al*., 2013).

1.6 Antimicrobial Activity

Hydroxyapatite is used as the chief inorganic constituent in orthopaedics for decades. Metallic nanoparticles such as silver, copper, chromium, titanium, nickel, cobalt, zinc etc. are potent antibacterial agents. The incorporation of such nanoparticles in HAp reduces the risk of bacterial infections during bone implant (Sahithi *et al*., 2010). Hence, it should be cleared that the microorganisms adsorbed in hydroxyapatite are either viable or not. To know the exact details, the antimicrobial activity of HAp is necessary. Similarly, the antimicrobial activity of mesoporous hydroxyapatite and ZnO fibres is also studied. In general *Staphylococcus aureus* (*S. aureus*, ATCC6538) and *Escherichia coli* (*E. coli*, 8099) are used for the study of antibacterial activity. It shows that antimicrobial activity of meso-HAp/ZnO nanofibers depended on ZnO/HAp ratio and *S. aureus* is more sensitive to meso-HAp/ZnO nanofibers than *E. coli* (Cai *et al*., 2015).

MIC (Minimal Inhibitory Concentration) is the lowest concentration of the antimicrobial agent that inhibits the visible growth of the bacterium being investigated under the given conditions. MIC values are used to determine the susceptibilities of a particular bacteria towards the antimicrobial agent. MIC values are determined in 96-well microliter plate. Bacteria along with different concentrations of antimicrobial agent are inoculated. Bacterial growth is examined after 24 hrs. incubation followed by addition of dye (Resazurin). Aerobic bacteria contains NADH dehydrogenase enzyme in their cytoplasm which converts Resazurin (purple) into Resorufin (pink). The appearance of pink colour indicates the presence of bacteria in viable form. Control experiments are performed by using standard antibiotic solutions (Elshikh *et al*., 2016).

MBC (Minimal Biocidal Concentration) is the lowest concentration of the antimicrobial agent that kills the bacterium being investigated under the given set conditions. It is determined by plating the content of the wells with concentrations higher than the MIC values of sample and standard antibiotic solutions. It is calculated from the NA plate having no colony growth which was previously plated by the contents of the wells (Elshikh *et al*., 2016).

1.7 Adsorption

Adsorption is the process by which the certain amount of adsorbate is concentrated on the surface of adsorbent. Adsorption isotherm is the study adsorption process at constant temperature. A plot relating the adsorbate amount and equilibrium concentration of adsorbate gives this type of model.

1.7.1 Langmuir adsorption isotherm

In 1916, Irving Langmuir proposed adsorption isotherm for the explanation of variation of adsorption with pressure. Based on his theory, he derived Langmuir equation which depicted a relationship between the number of active sites of the surface undergoing adsorption and pressure. There are some assumptions that should be taken place before the application of Langmuir model in adsorption.

1. Adsorption takes place only at specific localized sites on the adsorbent surface.
2. Each site can occupy only and one molecule or atom.
3. There is no interaction between the adsorbed molecules or atoms.
4. There are no phase transitions.

The general form of Langmuir isotherm is (Langmuir, 1916)

$$\frac{Q_e}{Q_m} = bC_e + (1 + bC_e) \text{.....(i)}$$

where, Q_e is the number of moles of adsorbate adsorbed per gram of derived sorbent at equilibrium concentration C_e, Q_m is the number of moles of adsorbate per gram of sorbent required to form a monolayer (mg/g), $\frac{Q_e}{Q_m}$ is the fraction of adsorbent covered by adsorbate molecules, b is a Langmuir constant

On rearranging equation (i), we get

$$\frac{C_e}{Q_e} = \left(\frac{1}{Q_m}\right) C_e + \frac{1}{bQ_m} \text{.....(ii)}$$

The plot of $\frac{C_e}{Q_e}$ against C_e gives a straight line with slope equal to $\frac{1}{Q_m}$ and intercept equal to $\frac{1}{bQ_m}$.

1.7.2 Freundlich adsorption isotherm

This is another type of adsorption model used to explain the adsorption behavior at low pressure and constant temperature. Extent of adsorption is directly proportional to pressure at low pressure while it is independent to pressure at high pressure. Therefore, at intermediate value of pressure, adsorption is directly proportional to pressure raised to power $\frac{1}{n}$.

$$Q_e \, \alpha \, C_e{}^{\frac{1}{n}} \ldots\ldots\ldots\ldots\ldots\ldots\ldots\ldots\ldots\ldots\ldots\ldots \text{(iii)}$$

Where, 'n' is a variable having value greater than one. 'C_e' is the equilibrium concentration and Q_e is the amount of adsorbate adsorbed per unit mass of the adsorbent. Above equation becomes,

$$Q_e = K_f C_e{}^{\frac{1}{n}} \ldots\ldots\ldots\ldots\ldots\ldots\ldots\ldots\ldots\ldots\ldots\ldots \text{(iv)}$$

Where, 'K_f' is the constant of proportionality also known as adsorption constant. Freundlich adsorption isotherm is the special case of Langmuir adsorption model. Taking log on both sides of equation (iv),

$$logQ_e = logK_f + \frac{1}{n} logC_e \ldots\ldots\ldots\ldots\ldots\ldots\ldots\ldots\ldots\ldots \text{(v)}$$

Equation (v) is known as linearized form of Freundlich equation.

1.8 Adsorption Kinetics

Adsorption kinetics deals with the adsorption behavior of the adsorbate-adsorbent reaction with reference to time. It also facilitates the prediction of order of the adsorption process.

In general, there are three important steps during the adsorption mechanism

1. Transfer of adsorbate from its bulk solution to the external surface of the adsorbent
2. Internal diffusion of the adsorbate from the surface to the adsorption site
3. Sorption of the adsorbate itself

Some kinetics model predicts the sorption is the rate limiting step while other assumes the internal diffusion as rate limiting step (Largitte and Pasquier, 2016).

1. Pseudo-first order kinetics model

The pseudo-first order kinetic model is applied for the reversible reaction with an equilibrium established between liquid and solid phase. The differential form of pseudo-first order rate equation is generally expressed as

$$\frac{dQ_t}{dt} = K_1(Q_e - Q_t) \text{.....(vi)}$$

Where, Q_e is the amount of metal adsorbed at equilibrium (mg/g), Q_t is the amount of metal adsorbed at time t (mg/g), and K_1 is the rate constant of pseudo-first order adsorption (min^{-1}). After integration and applying boundary conditions from t = 0 to t and Q_t = 0 to Q_t then above equation becomes,

$$\log(Q_e - Q_t) = logQ_e - \frac{K_1 t}{2.303} \text{.....(vii)}$$

The plot of log (Q_e – Q_t) versus t gives a straight line from which K_1 and Q_e can be calculated from the slope and intercept of the plot respectively.

1. Pseudo-second order kinetics model

It states that the rate of occupation of adsorption sites is proportional to the square of the number of unoccupied sites.

$$\frac{dQ_t}{dt} = K_2 (Q_e - Q_t)^2 \text{.....(viii)}$$

Where, K_2 is the pseudo-second order rate constant (g mg^{-1} min^{-1}), Q_e is the amount of metal adsorbed at equilibrium (mg/g) and Q_t is the amount of metal adsorbed at time t (mg/g). After integration and applying boundary conditions from t = 0 to t and Q_t = 0 to Q_t, above relation becomes,

$$\frac{t}{Q_t} = \frac{1}{Q_e^2 K_2} + \frac{t}{Q_e} \text{ ..... (ix)}$$

where‘t’ is the contact time.

The initial adsorption rate could be expressed as;

Initial adsorption rate = $Q_e^2 K_2$

The plot of $\frac{t}{Q_t}$ versus t gives the straight line from which the value of Q_e and K_2 can be determined from slope and intercept respectively.

1.9 Specific Surface Area Calculation

Specific surface area of adsorbent is one of the important factor for the determination of amount of adsorbate upon particular size of adsorbent. It is calculated in laboratory conditions. Specific surface area is defined as the accessible area of solid surface per unit mass of material (Itodo *et al*., 2010b).

Different types of methods available for the determination of specific surface area are:

1. Brunauer-Emmett-Teller Method (BET Method)
2. Iodine Number Method
3. Methylene Blue Adsorption Method

The interference by the surrounding phase was especially problematical for the nitrogen adsorption/desorption isotherm method in which case the entire surface was modified by vacuum dried treatment before nitrogen adsorption (Chongrak *et al*., 1998). This method measures only the external and not the internal surface area.

The method of adsorption of methylene blue in liquid phase for specific surface area determination has been adopted widely for various natural solids: activated carbon, charcoal, graphite, and silica, for example. The method of methylene blue adsorption for measuring the specific surface area of fish carbon could provide a reference for adsorbent. In this method, different concentrations of methylene blue are prepared (in ppm) with known concentration which are then treated with adsorbent material for adsorption. The absorbance of supernatant solution was measured at 665 nm after shaking 24 hrs.

The Langmuir equation can be used to calculate the specific surface area of the adsorbent. Equation (i) an (ii) are used to calculate the number of moles of methylene blue per gram of sorbent required to form a monolayer (mg/g) i.e Q_m (Chongrak *et al*., 1998).

$$S_{MB} = \frac{(Q_m \times A_{MB} \times N_A \times 10^{-20})}{M} \text{.....(x)}$$

Where, A_{MB} is the adsorbent surface area covered by single molecule of methylene blue, N_A is Avogadro's number, M is the molecular weight of methylene blue and S_{MB} is the specific surface area in $10^{-3}km^2$ / kg.

1.10 Statement of the Problem

Animal bone is a bio-waste material. It plays an important role in environmental pollution especially in soil pollution as it is not degraded easily. Such type of waste material is used as the natural resource for the synthesis of hydroxyapatite as animal bones mainly consist 70% inorganic fraction made up of hydroxyapatite. Hydroxyapatite could further be used as an adsorbent to concentrate microorganisms from liquid food sample for rapid microbial testing. Thus a waste material could be converted into useful material for worthful purpose.

In general, bacterial pathogens occur in very low number in food and food products. Recent microbial testing methods like nucleic acid probe hybridization and immunological assays require higher concentration of targeted microrganisms (10^4 to 10^6 cfu/mL or more). To concentrate these bacterial pathogens in such food sample, HAp could be used as an adsorbent for pathogens in terms of non-cultural microbial concentration.

1.11 Objectives of the Study

1.11.1 General objective

To prepare low cost adsorbent hydroxyapatite from caprine (goat) bone by various methods for the adsorption of different microorganisms.

1.11.2 Specific objectives

The specific objectives of this present work are as follows:

1. Extraction of HAp from caprine (goat) bone at different temperatures with different chemicals.
2. Characterization of extracted HAp from caprine bone through XRD, FTIR and SEM analysis.
3. Determination of specific surface area as well as the particle size of prepared hydroxyapatite.
4. Investigation of the effect of contact time and initial concentration of adsorbate for the adsorption of different microorganisms.
5. Investigation of antimicrobial activity of HAp on *Escherichia coli*, *Staphylococcus aureus*, *Candida albicans*, *Acinetobactor baumanii*, *Bacillus sp.*

CHAPTER 2: LTERATURE REVIEW

2.1 Synthesis of Hydroxyapatite

In general, hydroxyapatite can be synthesized by using chemicals and natural sources. The starting materials are artificial chemicals and natural bones or tooth in chemical and natural synthesis respectively.

The morphology, crystal structure and shrinkage of burnt bones and teeth were observed. Color, microscopic morphology, crystalline structure and.shrinkage of burnt bones and teeth were studied after heating the specimen between 20^0C and 940^0C. Their results showed that changes in both color and microscopic morphology of burnt bones and teeth were fully dependent upon the particular temperature range (Shipman, Foster and Schoeninge, 1984).

Raman and Infrared spectroscopic investigation of biological hydroxyapatite were performed. Ox femur samples were treated with hydrazine to remove the organic components of bone. There was a large increase in the signal-noise ratio of the Raman spectrum resulted from the exposure of the mineral surface and the removal of fluorescent components of the organic component (Walters *et al*., 1990).

Hydroxyapatite was extracted from animal bones through the treatment of hot NaOH solution. Ca/P ratio in pig cortical bones was higher than that in the stoichiometric (synthetic) material. Fraction of carbonate groups decreased with temperature and CaO appeared at higher temperatures, but structure of hydroxyapatite became preserved even at 1000^0C. At temperatures greater than 700^0C, specific surface area of the powder decreased and compacts of such powder started to shrink (Haberoka, Bucko and Miecznik, 2006).

The properties of hydroxypatite produced by annealing of bovine bones between 400^0C and 1200^0C . The annealed body was characterized by DTA, SEM, XRD, EDX and FTIR. The XRD result showed that the annealing process enhanced the crystallinity of HAp phase above 700^0C. There was no secondary phase formation in bones annealed between 600^0C and 1000^0C. However, the decomposition of HAp to TCP was observed for samples heat treated at 1100^0C and 1200^0C (Ooi, Hamdi and Ramesh, 2006).

Hydroxyapatite was synthesized from animal bones and bone sludge along with calcined products were characterized by XRD, FTIR and SEM. Calcium and

phosphorus contents were 38% and 18%, respectively, which corresponded to the Ca/P molar ratio of nonstoichiometric hydroxyapatite (Sobczak, Kowalski and Wzore, 2009).

Hydroxyapatite and collagen were isolated from animal tendons. These were used in different proportions as composites. Sponges were prepared by freezing and lyophilization of corresponding composite solutions. The properties of composite sponges, such as microstructure, chemical and physical properties were studied. A collagen sponge and a composite sponge made up of composite of HAp/Col were prepared and were characterized by ATR-IR, TGA and SEM. The ATR-IR analysis did not indicate shift of the band corresponding to -COO- for none of the used HAp/Col ratios. Thermogravimetric results suggested that collagen chains had been embedded with HAp to several complexes with different thermal stabilities (Sionkowska and Kozlowska, 2010)

Hydroxyapatite was prepared and characterized hydroxyapatite from eggshell. The observed phases of the synthesized materials were dependent on mechanochemical activation method (ball milling and attrition milling). The structures of HAp were characterized by XRD, SEM and FTIR anylyses. Attrition milling proved to be more efficient than ball milling as it resulted nanosize homogenous HAp after milling (Gergely *et al*., 2010).

Natural hydroxyapatite was prepared from bovine femur bones using calcination at various temperatures. This study aimed to extract the natural HAp from bovine femur bone at different calcination temperatures with different particle size (Khoo *et al*., 2015).

The physical properties of continuous matrix of porous natural hydroxyapatite were studied at various annealing temperatures. This study reported the physical properties of porous blocks of nonstoichiometric natural hydroxyapatite from porcine and bovine bones by heat treatment between 400-950^{0}C in nitrogen atmosphere. Chemical characterizations were done by means of the CHN analysis (carbon, hydrogen and nitrogen content) and Inductively Coupled Plasma Optical Emission Spectrometry (ICP-OES) as well as by FTIR instrument. However, SEM was used to study the morphology of the samples (Krzesinska and Majewska, 2015).

Hydroxyapatite scaffold was synthesized and used as a potential bone tissue engineering substitute. Fish scales derived natural Hydroxyapatite (FS-HAp) scaffolds were prepared through solvent casting technique that resembles the structure of cortical and cancellous bone tissues of body system. The hydroxyapatite (HAp) biomaterial was synthesized by thermal decomposition of chemically treated fish scales (Mandal, Pal and Dey, 2016).

Organic derived hydroxyapatite scaffold was synthesized from pig bone waste for tissue engineering applications. They obtained HAp of rod like morphology with 38-52 nm in length. Porous HAp was prepared by using Ammonium bicarbonate as pore forming agent (Ofudje *et al*., 2017).

The physicochemical and biological properties of bovine derived porous hydroxyapatite were studied. The pure and natural HAp powders were prepared from the obtained HAp/collagen composite by two different methods (alkali-heat-treatment and calcination). XRD and FTIR studies of HAp/collagen composite and alkaline-HAp powder confirmed that the HAp phase is carbonate substituted HAp with a low crystallinity. The samples derived from bovine bone exhibited the major and trace elements of bone, whereas these elements were not found in the chemically synthesized HAp powder (Sun *et al*., 2017).

Hydroxyapatite was prepared by cold isostatic pressing method (CIP) and sintered at 1100^0C, 1200^0C and 1300^0C. XRD, XRF, FTIR, SEM and EDS analyses were carried out on the prepared hydroxyapatite. Hardness and compression tests were examined before and after sintering. Also, the morphology of the samples at different sintering temperatures was studied by SEM imaging. The obtained experimental results ascertained that with increasing the sintering temperature up to 1300^0C, relative density and hardness of the samples increased (Heidari *et al*., 2017).

Biogenic hydroxyapatite derived from animal bones were characterized for biomedical applications. In this work, the viability of producing biogenic hydroxyapatite from biowaste animal bones, namely bovine (cow), caprine (goat) and galline (chicken), through a heat treatment process had been investigated. The animal bones were cleaned to remove collagen and subsequently heat treated at different temperatures ranging from 600^0C to 1000^0C. From the range of sintering temperatures investigated, it was found that hydroxyapatite derived from bovine bone showed good thermal stability while

those produced from caprine and galline bone. The later exhibited phase instability with traces of TCP being detected after heat treatment beyond 700^0C (Ramesh *et al*., 2018).

2.2 Microbial Adsorption

Adsorption of microorganisms on hydroxyapatite is similar to the adsorption of negatively charged amino acids on hydroxyapatite as the microbial surface is negatively charged. In most of the cases, the normal flora present in saliva were used to study the adsorption process on hydroxyapatite.

The model delineating effects of salivary pellicle on adsorption of *S. miteor* onto hydroxyapatite were studied. A model describing the adsorption isotherms for *S. miteor* strain 26 to untreated and saliva-treated hydroxyapatite was developed. The strengths of the adsorption bonds in the two systems were similar (Gibbons, Moreno and Spinell, 1976).

The comparative study of bacterial affinities on the adsorption sites of hydroxyapatite surface were perforned. The adsorption of oral bacteria on hydroxyapatite (HAp) surfaces was studied by using Langmuir adsorption isotherm model. This permitted the comparative estimates of the number of adsorption sites and the strength ofthe adsorption bonds on untreated and salivatreated HAp surfaces for strain of *S. mutans, S. salivarius, S. sanguis, S. mitis, A. viscosus,* and *A. naeslundii*. The experimental data closely followed the adsorption model as judged by the high correlation coefficients obtained for all strains studied. Although some differences were observed in the adsorption of strains of *S. mutans.* However, the numbers attached to saliva treated HAp did not vary widely (Clark, Bammann and Gibbons, 1978).

The adsorption of *S. mutans* on hydroxyapatitce and dextran or chlorhexidine treated hydroxyapatite was studied. Zeta potentials of the chemically treated surfaces were obtained by electrophoretic mobility measurements. Surface morphologies were studied by scanning electron microscopy. Hydroxyapatite treated with chlorhexidine gluconate and with low molecular weight dextran gave higher potentials and lower *S. mutans* adsorption compared with untreated hydroxyapatite due to the changes in surface potentials and chemical properties of the chemically treated hydroxyapatite surfaces (O'Brien *et al*., 1978).

The surface modification of hydroxyapatite was studied to avoid bacterial adhesion. The surface of hydroxyapatite was modified through the adsorption of nonionic

polymers carrying phosphate groups as anchoring groups. A combination of alcohol ethoxylate and alkyl phosphate were also used (Olsson and Krasse, 1976).

Method to concentrate bacteria from foods through their adherence to hydroxyapatite was examined. Using HAp at a level of 10% and suspensions of an *E. coli* strain kinetic studies were performed which showed the maximum adherence was attained within 5 min for all cell concentrations.. Eleven species of spoilage and pathogenic bacteria were found to adhere to HAp, with seven species adhering at proportions of greater than 95%. Fluorescent viability staining revealed that cells bound to HAp remained viable. It was also revealed that there was 92% adherence of indigenous bacteria to HAp, indicating promise for the use of HAp for concentrating bacteria from meat and other food samples (Berry and Siragusa, 1997).

The inhibition of *S. mutans* adsorption to hydroxyapatite was studied by low molecular weight chitosans. In this work, the efficacy of a low molecular weight chitosan (LMWC) and its derivatives N-carboxymethyl chitosan (NCMC) and imidazolyl chitosan (IMIC) in preventing *S. mutans* attachment to HAp beads was assessed. The effects of chitosan on both sucrose dependent and independent adherence were evaluated. In both cases, a reduction in *S. mutans* adsorption ranging from 47 to 66% was observed. When HAp beads were coated with saliva after the treatment with chitosan, sucrose couldn't reduce the *S. mutans* adsorption suggesting that saliva deposition restored the HAp binding properties (Tarsil *et al*., 1997).

The influence of surface porosity and pH on bacterial adherence to hydroxyapatite and biphasic calcium phosphate bioceramics. The total porosity was 20% for HAp and 50% for BCP. Adherence of *S. aureus* and *S. epidermidis* was studied at a physiological pH of 7.4 and at a pH simulating bone infection of 6.8. The effect of pH on the potential of HAp, BCP and of both staphylococci was evaluated. Results showed that when pH decreased from 7.4 to 6.8, the adherence of both staphylococci to HAp and BCP surfaces decreased significantly. At both pH values, the number of *S. aureus* adhered to the HAp surface appeared to be lower than that for BCP. This study provides the evidence that HAp and BCP ceramics do not have pores sufficiently large to allow the internalization of staphylococci (Kinnari *et al*., 2007).

The bacterial immobilization on hydroxyapatite surface was studied for heavy metals removal. Selected bacterial strains were immobilised on the surface of hydroxyapatite

($Ca_{10}(PO_4)_6(OH)_2$ (HAp) of natural origin (fish bones). *Pseudomonas fluorescens* (S3X), *Microbacterium oxydans* (EC29) and *Cupriavidus* sp. (1C2) were chosen. These systems were tested using solutions of Zn(II), Cd(II) and in solutions containing both metals. It was observed that an effective approach for the removal of the target heavy metals on its own could be developed. The combination of HAp with the bacterial strains led to higher adsorption capacity for both elements. For the solutions containing only one metal, the synergistic effect was greater for higher metal concentrations. 1C2 and EC29 were the most effective strains for Zn(II) and Cd(II) respectively, while S3X was less effective (Piccirillo *et al*., 2013).

CHAPTER 3: MATERIALS AND METHODS

3.1 Chemical Reagents

Chemicals used in this research are listed in **Table 3.1**.

Table 3.1: List of chemicals

S.N.	Name of the chemicals	Company name	% purity
1.	Hydrochloric acid (HCl)	Merck Life Science Pvt. Ltd.	35%
2.	Sodium hydroxide (NaOH)	Merck Life Science Pvt. Ltd.	97%
3.	Methylene blue ($C_{16}H_{18}ClN_3S$)	Qualigens Fine Chemicals, India	N/A
4.	Buffer tablets of pH 4, 7, and 9.2	HiMedia Laboratories, India	N/A
5.	Sodium chloride (NaCl)	Merck Life Science Pvt. Ltd.	99.5%
6.	Phosphate buffer saline (PBS)	HiMedia Laboratories, India	N/A
7.	Acetone	Merck Life Science Pvt. Ltd.	N/A
9.	Nutrient agar	HiMedia Laboratories, India	N/A
10.	Nutrient broth	HiMedia Laboratories, India	N/A
11.	Potato Dextrose Agar (PDA)	HiMedia Laboratories, India	N/A

3.2 Instruments

Instruments used for the research work are listed in **Table 3.2.**

Table 3.2: List of instruments

S.N.	Name of the instrument	Company name
1	Magnetic stirrer hot plate	STUART SCIENTIFIC, UK
2	pH meter	MAX electronics, India
3	Electronic balance	SCALTEC instruments, Germany
4	Colorimeter	ELICO limited, India
5	UV/visible Spectrometer	SPECORD 200 PLUS, analytikejena, Germany
7	FTIR spectrometer	IR Prestige, SHIMADZU, Japan
9	XRD	D_2 phase Diffractometer, Bruker
10	Muffle furnace	Barnstead/Thermolyne, USA
11	Heating mantle	NIKE lab instruments
12	Autoclave	Fisher, US
13	Hot air oven	Narang scientific works Pvt. Ltd.
15	Bacteriological incubator	NIKE lab instruments
16	Water bath shaker	Grant instruments (Cambridge) Ltd., England

3.3 Synthesis of Hydroxyapatite from Caprine (goat) Bone

The tibia-fibula part of caprine (goat) bone was collected from the butcher house located in Kirtipur, Kathmandu. These were cleansed and thoroughly washed with water first and boiled for 3 hrs. in water to evacuate all of the attached meat and other soft tissues. Bone were left for sun drying for 2 days which were then washed with acetone for several times to remove fats and other impurities. Bone pieces were finally dried in hot air oven at 60^0C. The dried bone pieces were grinded and pulverized in rotary mill to get raw bone powder. The pulverized bone powders were sifted in smaller particle size using sieve shaker of 120 µm. Raw bone powder was then made hydroxyapatite by treating it with either acid or base or both followed by calcination at 750 an 950^0C. The whole process of synthesis of HAp is self-explained by **Figure 3.1.**

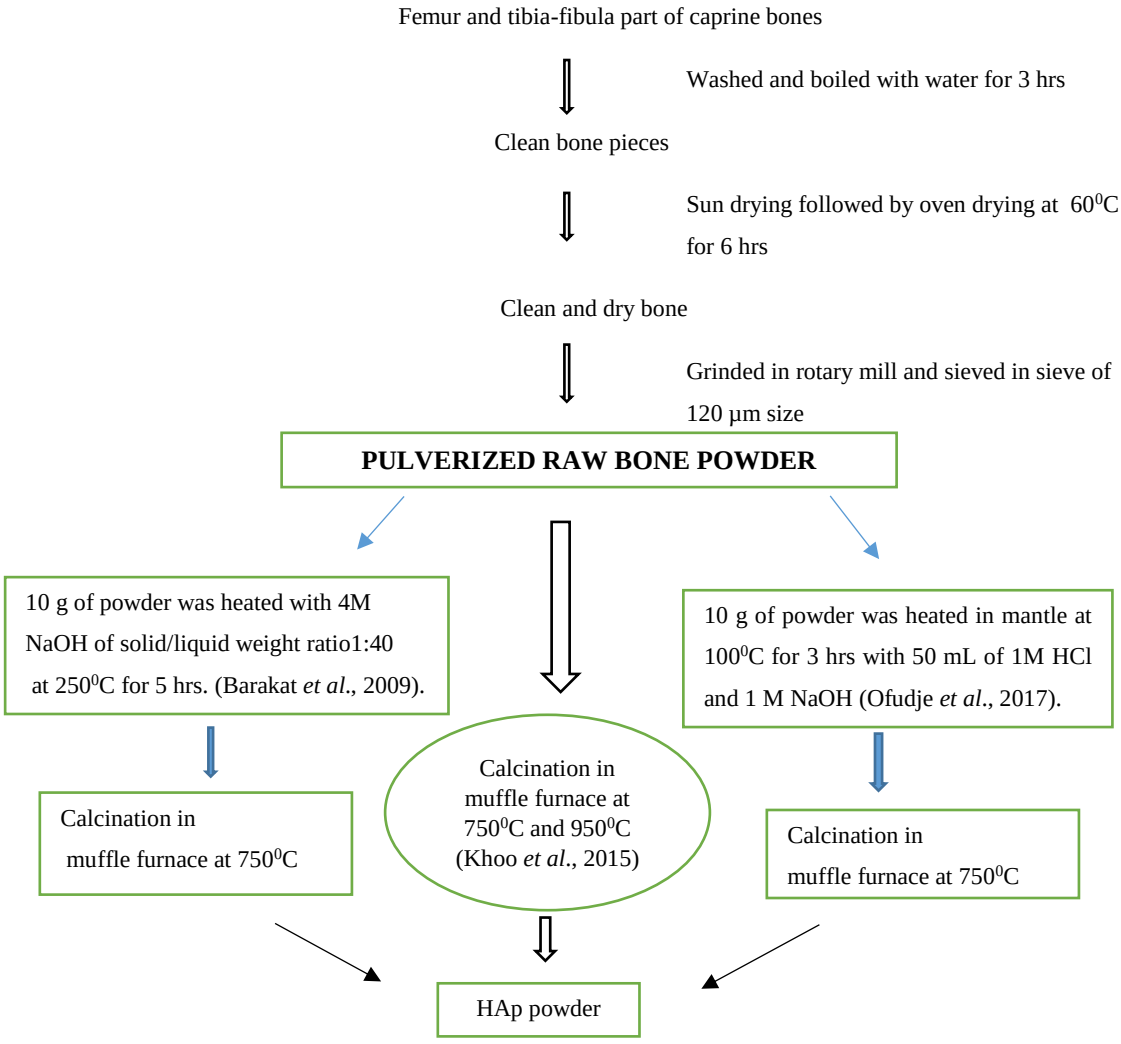

Fig 3.1: *Flow chart for the synthesis of hydroxyapatite (HAp)*

Finally, hydroxyapatite powders thus produced from different methods were washed with distilled water for several days to maintain pH 7.4 and were dried again to get powder.

3.4 Point of Zero Charge (pH_{PZC})

Accurately weighed 50 mg HAp was transferred into 10 reagent bottles. In all, 25 mL of 0.01M NaCl of different pH from 1 to 10 were transferred and the initial pH were calculated to get $pH_{initial}$. The whole contents were stirred for 24 hrs. and the final pH were calculated to get pH_{final} after filtration. The differences between initial pH ($pH_{initial}$) and final pH (pH_{final}) were calculated for all cases. These differences were plotted against initial pH to get a curve. The cross point between the curve and the straight line originating from the zero difference in pH parallel to x-axis gave the value of pH_{PZC} (Al-Degs *et al*., 2008).

3.5 Preparation of Stock Solution

3.5.1 Preparation of microbial suspensions

1. Bacterial (*E.coli*) suspension

The total number of *E.coli* (cultured in Nutrient broth) in original solution were enumerated by spread plate (Nutrient agar) technique followed by serial dilution method. It was found 72×10^6 cfu/mL of *E. coli* (ATCC 25923) from 10^{-5} dilution. From this stock solution, different concentrations of *E. coli* suspension were prepared by using appropriate volume of stock solution and distilled as well as sterilized water. The absorbance of this stock solution was measured as 0.99 at 550 nm.

2. Fungal (*C. albicans*) suspension

The total number of *C. albicans* (cultured in PDB) in original solution were enumerated by spread plate (PDA) technique followed by the serial dilution method. It was found 41×10^6 cfu/mL of *C. albicans* from 10^{-4} dilution. From this stock solution, different concentrations of fungal suspension were prepared by using appropriate volume of stock solution and distilled as well as sterilized water. The absorbance of this stock solution was measured as 0.83 at 550 nm.

3. Bacterial (*S. aureus*) suspension

The total number of *S. aureus* (ATCC 25923) (cultured in Nutrient broth) in original solution were enumerated by spread plate (Nutrient agar) technique followed by the serial dilution method. It was found 9×10^6 cfu/mL of *S. aureus* from 10^{-5} dilution. From this stock solution, different concentrations of bacterial suspension were prepared by using appropriate volume of stock solution and distilled as well as sterilized water. The absorbance of this stock solution was measured as 0.64 at 550 nm.

4. Bacterial (*A. baumanii*) suspension

The total number of *A. baumanii* (ATCC 19606) (cultured in Nutrient broth) in original solution were enumerated by spread plate (Nutrient agar) technique followed by the serial dilution method. It was found 25×10^6 cfu/mL of *A. baumanii* from 10^{-5} dilution. From this stock solution, different concentrations of bacterial suspension were prepared by using appropriate volume of stock solution and distilled as well as sterilized water. The absorbance of this stock solution was measured as 0.72 at 550 nm.

3.5.3 Preparation of 1000 mg/L stock methylene blue solution

Accurately weighed 1 g of methylene blue was transferred into 1000 mL of volumetric flask and the volume was made up to the mark by using distilled water. Solutions of different concentrations of methylene blue were prepared from the stock solution by serial dilution method.

3.6 Preparation of Chemical Reagents

3.6 .1 Preparation of 0.1M NaOH and 0.1M HCl

Accurately weighed 1 g of NaOH was transferred into 250 mL of volumetric flask and the volume was made up to the mark by using distilled water. About 2.5 mL of concentrated HCl from 35% HCl was transferred into 250 mL volumetric flask and and the volume was made up to the mark by using distilled water.

3.6.2 Buffer solutions

In order to calibrate the pH meter, buffer solutions of pH 4.0, 7.0, and 9.2 were prepared by dissolving buffer tablet of pH 4.0, 7.0 and 9.2 in 100 mL volumetric flasks with triple distilled water.

3.6.3 Preparation of 0.01M NaCl solution

Accurately weighed 0.15 g of NaCl was transferred into 250 mL of volumetric flask and the volume was made up to the mark by using distilled water.

3.7 Preparation of Calibration Curves

3.7.1 Preparation of calibration curve for the methylene blue solution

At first, λmax was found through maximum absorbance by using 1 mg/L methylene blue solution. The absorbance was measured against wavelength ranging from 400 to 700 nm using spectrophotometer at Central Department of Chemistry, Tribhuvan University. This showed that λmax was 665 nm. Then methylene blue solutions of 1, 2, 3, 4, 5, 6, 7, 8, 9 and 10 mg/L were prepared from the stock solution of 1000 mg/L in 25 mL volumetric flasks. The absorbance of all these differently concentrated solutions were taken at 665 nm. Finally, a plot of absorbance versus concentration (mg/L) was drawn to get a calibration curve.

3.7.2 Calibration curve for microorganisms

3.7.2.1 Collection of microorganisms

E.coli (ATCC 25923) (Gram –ve bacteria), *C. albicans* (unicellular fungi), *S. aureus (ATCC 25923)* (Gram +ve bacteria) and *A. baumanii* (ATCC 19606) were obtained from Central Department of Microbiology (CDM, TU).

3.7.2.2 Enumeration of microorganisms in original solution

1. Preparation of culture media

Nutrient Agar

About 7.0 g of Nutrient agar powder was suspended in 250 mL of purified/distilled water in a conical flask. The whole content was heated to dissolve the medium completely. The hot content inside the flask was transferred into the sterile petri plates which were finally sterilized by autoclaving at 15 lbs pressure (121^0C) for 15 mins. This is solid culture necessary to grow bacteria.

Nutrient Broth

About 3.25 g of nutrient broth powder was suspended in 250 mL of purified/distilled water in a conical flask. The whole content was heated to dissolve the medium

completely. The hot content inside the flask was transferred into the culture tubes which were finally sterilized by autoclaving at 15lbs pressure (121^0C) for 15 mins. This is broth culture necessary to grow bacteria.

Potato Dextrose Agar

About 9.75 g of PDA powder was suspended in 250 mL of purified/distilled water in a conical flask. The whole content was heated to dissolve the medium completely. The hot content inside the flask was transferred into the sterile petri plates and left to cool which were finally sterilized by autoclaving at 15lbs pressure (121^0C) for 15 mins. This is solid culture necessary to grow fungi.

Potato Dextrose Broth

About 2.4 g of PDB powder was suspended in 1000 mL of purified/distilled water in a conical flask. The whole content was heated to dissolve the medium completely. The hot content inside the flask was transferred into the culture tubes which were finally sterilized by autoclaving at 15lbs pressure (121^0C) for 15 mins. This is broth culture necessary to grow fungi.

2. Serial dilution of the original microbial solutions

1 mL microbial suspension from the original solutions of each microorganism was transferred into the sterile tube containing 9 mL distilled and sterile water to form 10^{-1} dilution. Similarly, 1 mL microbial suspension from 10^{-1} dilution of each microorganism was transferred into the sterile tube containing 9 mL distilled and sterile water to form 10^{-2} dilutiion. This procedure was repeated till 10^{-8} dilution for all cases of different microbial suspension.

3. Inoculation of the microorganisms

From the 10^{-4}, 10^{-5} and 10^{-6} dilutions of all microorganisms, 0.1mL of sample was transferred into separate, dried NA plates. The inoculated sample was spreaded using throughout the media plate. The plate was incubated at 37^0C for 24 hrs.

4. Colony count

The number of colonies were counted in each incubated plate. Finally, number of microorganisms per mL (cfu/mL) of the original sample were calculated by using following formula.

Number of microorganisms per mL of stock solution (cfu/mL) = $\frac{\text{Number of colonies}}{\text{inoculum size} \times \text{dilution}}$

3.7.2.3 Preparation of different concentrations of microbial suspension

Different concentrations of different microorganisms were prepared by using stock solution of each microorganism by dilution method.

Volume of the stock solution to be used (V_1) =

$$\frac{\text{Volume of the required concentration} \times \text{required concentration}}{\text{Concentration of microorganisms in stock solution } (N_1)}$$

Where, volume of the required concentration was 5mL for all microorganisms.

Table 3.3: Concentrations of different microorganisms in stock solution.

S.N.	MOS type	Concentrations (cfu/mL)
1	*E. coli*	720×10^5
2	*C. albicans*	410×10^5
3	*S. aureus*	90×10^5
4	*A. baumanii*	250×10^5

By using above dilution formula and the concentration of stock solution for each of the microorganisms, microbial suspension of required concentrations were prepared. *E.coli, C. albicans, S. aureus* and *A. baumanii* suspensions were 23×10^5 to 242×10^5 cfu/mL, 13×10^5 to 139×10^5 cfu/mL, 3×10^5 to 30×10^5 cfu/mL and 23×10^5 to 223×10^5 cfu/mL respectively in 5 mL total volume of microbial suspension and sterile distil water.

1. *E. coli*

For calibration curve of *E. coli*, 5 mL bacterial suspension of different concentrations (23, 72, 120, 169, 218 and 242) $\times 10^5$ cfu/mL were transferred to each sterile test tube. Control experiments were performed with distill and sterile water. Optical densities of the microbial suspension from each tube were measured from colorimeter at 550 nm. Six measurements were made and calibration curve was drawn.

2. *C. albicans*

For calibration curve of *Candida albicans*, 5 mL fungal suspension of different concentrations (13, 41, 69, 97, 125 and 139) $\times 10^5$ cfu/mL were transferred to each

sterile test tube. Control experiments were performed with distill and sterile water. Optical densities of the microbial suspension from each tube were measured from colorimeter at 550 nm. Six measurements were made and calibration curve was drawn.

3. *S. aureus*

For calibration curve of *Staphylococcus aureus,* 5 mL bacterial suspension of different concentrations (3, 9, 15, 21, 27 and 30) $\times 10^5$ cfu/mL were transferred to each sterile test tube. Control experiments were performed with distill and sterile water. Optical densities of the microbial suspension from each tube were measured from colorimeter at 550 nm. Six measurements were made and calibration curve was drawn.

4. *A. baumanii*

For calibration curve of *Acinetobacter baumanii,* 5 mL bacterial suspension of different concentrations (23,73,123,173 and 223) $\times 10^5$ cfu/mL were transferred to each sterile test tube. Control experiments were performed with distill and sterile water. Optical densities of the microbial suspension from each tube were measured from colorimeter at 550 nm. Six measurements were made and calibration curve was drawn.

3.8 Characterizations of Material

3.8.1 XRD analysis

Information regarding phase composition and crystallinity of samples were obtained by X-ray diffractometer (D_2 phase Diffractometer, Bruker) with CuKα radiation. Five samples (Raw bone powder, NaOH untreated HAp calcined at 750^0C and 950^0C, NaOH treated HAp calcined at 750^0C and NaOH/HCl treated HAp calcined at 750^0C) were analyzed at Nepal Academy of Science and Technology (NAST). The samples were scanned over a range of 2θ angles from 10^0 to 80^0. By using Debye-Scherrer's formula, crystallite size was calculated relating through peak broadening which was explained in introduction section**.**

$$\text{Crystallite size } (D) = \frac{k\lambda}{\beta \cos\theta} \ldots\ldots\ldots\ldots\ldots\ldots \text{(xi)}$$

Where, k is the Scherrer's constant (0.9), λ is the wavelength of X-ray used (0.15406 nm), β is FWHM in radians and D is the crystallite size in nm.

3.8.2 FTIR analysis

Information regarding functional groups of samples were obtained by FTIR spectrometer (IR Prestige, SHIMADZU, Japan). Five samples (Raw bone powder, calcined bone powders at 750^0C and 950^0C, NaOH treated bone powder calcined at 750^0C and NaOH/HCl treated bone powder calcined at 750^0C) were analyzed at Department of Plant Resources, Thapathali, Kathmandu. The samples were scanned over a range of 500 cm^{-1} to 5000 cm^{-1} .

3.8.3 SEM analysis

Informations regarding surface morphology and the microstructure evolution of the bone samples calcined at various temperatures of samples were obtained by Scanning Electron Microscopy. Single sample of NaOH /HCl treated bone powders calcined at 750^0C was analyzed in Korea.

3.8.4 Determination of specific surface area of HAp

Accurately weighed 0.05 g HAp were transferred into six reagent bottles containing varying concentration of methylene blue solutions from 50 – 300 mg/L. The solutions were then shaken for 24 hrs. in a mechanical shaker and were left to settle down for 30 min. The supernatant solutions were pipetted out. The absorbance of the supernatant solution was noted at 665 nm to calculate the Q_m value from Langmuir adsorption isotherm. By using this Q_m value specific surface area of HAp was determined.

3.9 Adsorption Studies

3.9.1 Adsorption studies of different microbial suspension

For adsorption isotherm studies, 5 mL of *E.coli* suspension (23, 72, 120, 169, 218 and 242) × 10^5 cfu/mL , 5 mL fungal suspension (13, 41, 69, 97, 125 and 139) × 10^5 cfu/mL, 5 mL *S. aureus* suspension (3,9,15,21,27 and 30) × 10^5 cfu/mL and 5 mL *A. baumanii* suspension (36, 86, 136, 186, 236 and 286) × 10^5 cfu/mL were added to each tubes containing 15 mg. hydroxyapatite. Control experiments were performed on hydroxyapatite treated with distilled and sterile water. The tubes were immersed in a 37^0C constant temperature water bath and were shaken for 30 mins. in a shaker. The contents were then left to settle. After 5 minutes, 3.5 mL of the (supernatant) suspension were withdrawn from each tubes. Optical densities of the supernatant from each tube

suspension were measured after addition of 2 drops of 2.5N HCI to dissolve any suspended hydroxyapatite particles. Six measurements were made from each organism (O'Brien *et al*., 1978).

3.9.2 Adsorption kinetics studies

For adsorption kinetics studies, 5 mL *E.coli* suspension (218 and 242) $\times 10^5$ cfu/mL , 5 mL fungal suspension (125 and 139) $\times 10^5$ cfu/mL, 5 mL *S. aureus* suspension (27 and 30) $\times 10^5$ cfu/mL and 5 mL *A. baumanii* suspension (236 $\times 10^5$ cfu/mL) were added to each tubes containing 15 mg hydroxyapatite. For each organism with different concentration, four tubes were prepared for each concentration. Control experiments were performed on hydroxyapatite treated with distilled and sterile water. All tubes were immersed in a 37^0C constant temperature water bath and were shaken for 30 mins. in a shaker. During the course of shaking, at 5, 15, 25 and 30 mins. test tubes were withdrawn one by one. 3.5 mL of the (supernatant) suspension were taken from each tubes. Optical densities of the supernatant from each tube suspension were measured after addition of 2 drops of 2.5N HCl to dissolve any suspended hydroxyapatite particles. Eight measurements were made from each organism for two different concentrations (O'Brien *et al*., 1978).

3.10 Antibacterial/Antifungal Activity

3.10.1 Qualitative screening

To know whether the microorganisms adsorbed on HAp might be viable or not qualitative screening was carried out. By measuring the zone of inhibition (ZOI) using ruler, the antimicrobial activity was performed. Different (*E. coli*, *S. aureus*, *A. baumanii* and *Bacillus* sp.) suspensions were grown in nutrient broth at 37^0C for 24 hrs. in an incubator. The sterile Nutrient Agar (NA) plates were labelled with the name of the bacteria and the name code of the disc. Bacterial suspensions were incubated again for sometime to match the turbidity of 0.5 McFarland standards equivalent to 1.5 $\times 10^8$ cfu/mL. 0.1mL of the inoculums were lawn cultured with the help of sterile cotton swab in NA. Then, with the help of sterile 5 mm cork borer, wells were made in the Nutrient agar. Different concentrations of HAp solutions were placed in wells. DMSO was taken as negative control. Finally, NA plates with HAp and bacteria were incubated at 37^0C for 24 hrs. ZOI was manipulated with the help of ruler after the 24 hrs. of incubation. Similarly, for antifungal activity, fungal (*C. albicans*) suspensions were

grown in potato dextrose broth at 37^0C for 24 hrs. in an incubator. The sterile Potato Dextrose Agar (PDA) plates were labelled with the name of the fungi and the name code of the disc. 0.1 mL of the inoculums were lawn cultured with the help of sterile cotton swab in PDA. Then, with the help of sterile 5 mm cork borer, wells were made in PDA. Different concentrations of HAp solutions were placed in wells. DMSO was taken as negative control. Finally, PDA plates with HAp and were incubated at 37^0C for 24 hrs. Zone of inhibition was manipulated with the help of ruler after the 24 hrs. of incubation.

3.10.2 MIC and MBC study

Minimal inhibitory concentration and minimal biocidal concentration of hydroxyapatite were determined by using a redox indicator (resazurin). The protocol for the study follows the **Figure 3.4** (Elshikh *et al*., 2016).

Bacterial (*A. baumanii*) suspensions were grown in NA plate at 37^0C for 24 hrs. in an incubator. 0.1mL of the inoculums were again cultured in MHB at 37^0C for 24 hrs. followed by incubation to match the turbidity of 0.5 McFarland standards equivalent to 1.5×10^8 cfu/mL which was finallly diluted to make 1.5×10^6 cfu/mL. 200 mg/mL of HAp in DMSO and 0.25 mg/mL antibiotic solutions were also prepared. All the wells of sterile 96 well plate were filled by 200 µL MHB. Then, 200 µL of HAp and antibiotic solutions of each were transferred into the wells in sterile 96 well plate. The concentrations of HAp and antibiotic solutions were serially decreased by 2 fold serial dilution in respective wells. 5 µL bacterial suspension was added in well containing HAp, antibiotic and control for bacterial growth. Then, the sterile well plate was incubated at 37^0C for 24 hrs. followed by the addition of 30 µL Resazurin (0.0003%) in all well. The whole contents were incubated at 37^0C for 4 hrs. Finally, the change in color of Resazurin from purple to pink was monitored to determine the MIC values of HAp and antibiotic solutions. Again, the wells containing HAp and antibiotic solutions with no change in color were cultured in NA plate to determine MBC values after incubation at 37^0C for 24 hrs.

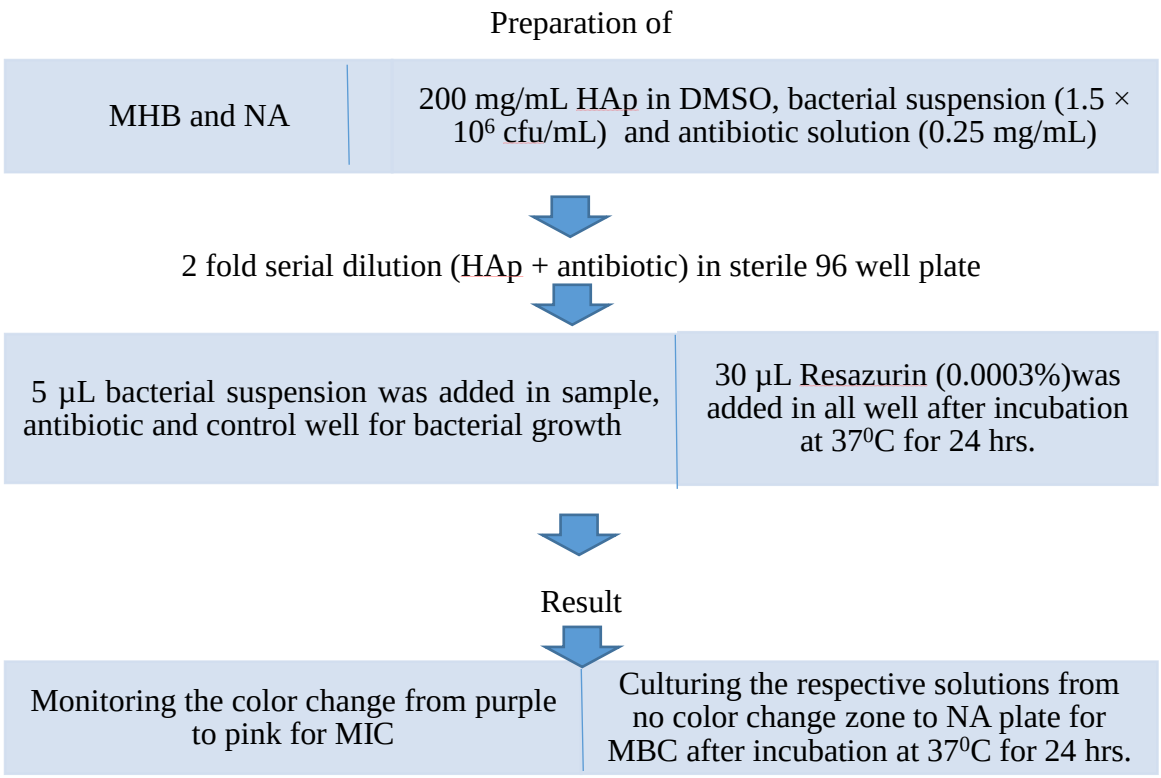

***Fig 3.2**: Flow chart for MIC and MBC study*

CHAPTER 4: RESULTS AND DISCUSSION

4.1 Characterizations of Isolated HAp

In this section, natural hydroxyapatite (HAp) extracted from bio-waste caprine (goat) bone was characterized by different scientific tools like XRD, FTIR and SEM analyses. It is necessary to compare the characters of synthesized HAp with the standard one.

4.1.1 XRD analysis

The XRD diffraction patterns of different powders prepared from thermal only and chemical followed by thermal treatments are shown in **Figure 4.1.**

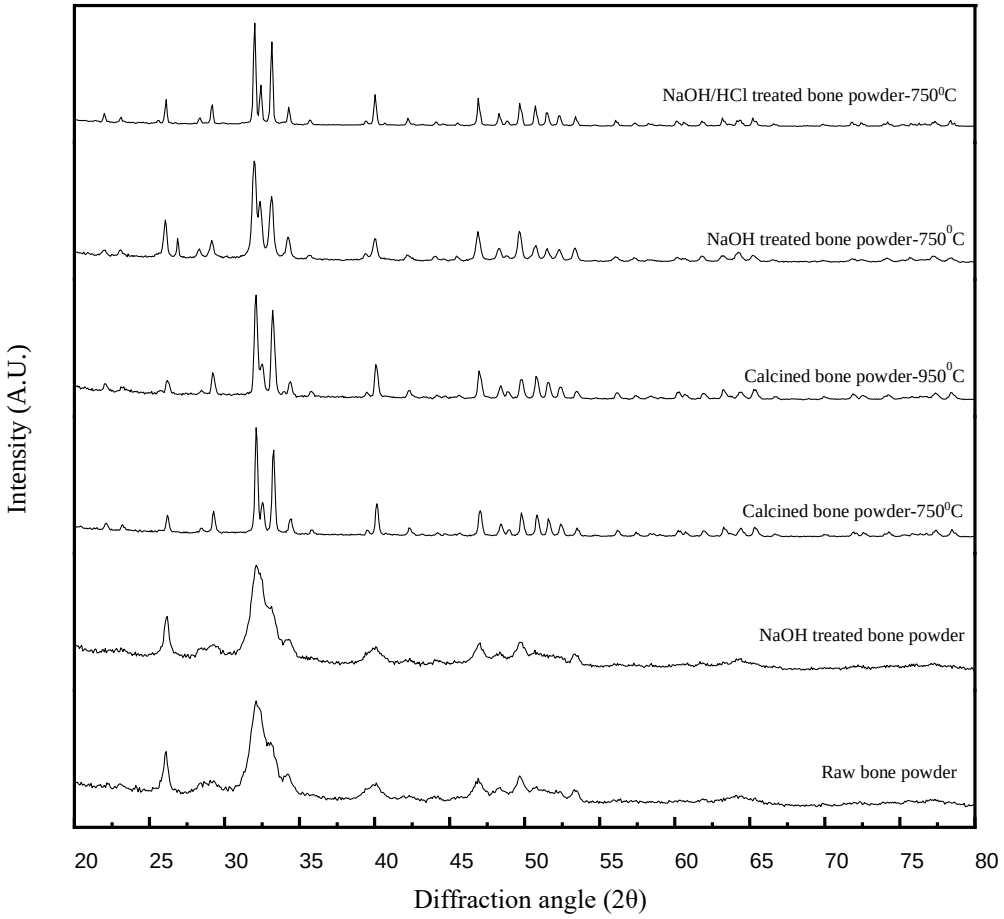

Fig 4.1: *XRD pattern of bone powder obtained by different methods*

The broad diffraction peaks at about 2θ = 26.21, 29.28, 32.12, 32.53, 33.26, 40.16, 47.04, 49.81, 50.84 and 51.61^o for different bone powders calcined at 750^{0}C and 950^{0}C, NaOH treated bone powder calcined at 750^{0}C and NaOH/HCl treated bone powder

calcined at 750^0C suggest the synthesized nanoparticle were hydroxyapatite (Kutty and Ramesh, 2000; Ooi *et al*., 2006; Barakat *et al*., 2009; Khoo *et al*., 2015; Ofudje *et al*., 2017). The diffraction peaks and their peak position for the respective 2θ value of different bone powders prepared by different methods resemble to the standard one (JCPDS card number 9-0432). The crystalline sizes of the bone powders prepared by different methods were calculated with the help of equation (xi) and are shown in **Table 4.1**.

Table 4.1: Average crystallite sizes of different bone powders prepared from thermal only and chemical followed by thermal treatments.

S.N.	Bone powders type	Average crystallite size (nm)
1	Calcined bone powder-750^0C	36.02
2	Calcined bone powder-950^0C	31.67
3	NaOH treated bone powder-750^0C	30.63
4	NaOH/HCl treated bone powder-750^0C	45.79

With the increase in calcination temperature, the intensity of the respected diffraction peaks increases which become sharper and narrower resulting the increase in crystallinity and the crystal size (Khoo *et al*., 2015) when compared with raw and NaOH treated bone powder. Similarly, degree of crystallinity also increases with increase in calcination temperature due to greater removal of organic part associated with HAp lattice resulting more exposure of phosphate group. There is no any significant difference found in the diffraction peaks for the bone powder obtained either through the base treatment or acid + base treatment.

The XRD patterns of the caprine (goat) bone show the presence of nanocrystalline hydroxyapatite in the bone matrix. XRD pattern of different bone powders calcined at different temperatures as well as different chemicals are almost similar with no any significant differences (Ooi *et al*., 2006; Barakat *et al*., 2009). However, there occurs some differences in average crystallite sizes of different bone powders as depicted from **Table 4.1**.

4.1.2 FTIR analysis

FTIR analysis is used to know the functional groups present in different bone powders prepared from thermal and chemical treatments. The FTIR spectra of different bone powders are shown in **Figure 4.2.**

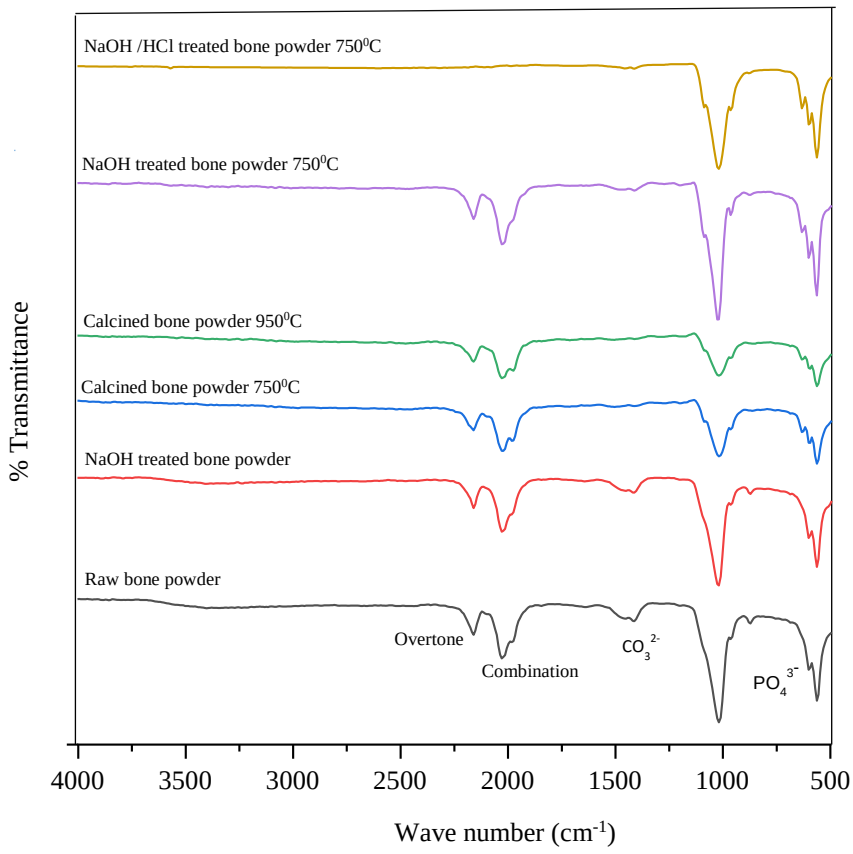

Figure 4.2: *FTIR spectra of bone powders prepared from thermal and chemical treatments*

The large number of bands in FTIR spectra at 3572.17, 2029.11-2160.27, 1411.89 to 1473.62, 1018.41 to 1087.85, 964.41, 864.11- 871.82, 632.65, 601.79, 563.21, 470.63 and 439.77 cm^{-1} of different bone powders prepared from chemical and thermal treatments show the presence of necessary functional groups to be a hydroxyapatite (Walters *et al*., 1990; Ooi *et al*., 2006; Ofudje *et al*., 2017). FTIR study reveals the presence of PO_4^{3-}, CO_3^{2-} and OH^- in raw, heated treated and heat + chemical treated bone powders. Corresponding bands of these groups are more clearly visible in calcined bone powder as the calcination process destroys the cross linked structure present in raw caprine bone (Khoo *et al*., 2015).

Table 4.1: Different functional groups and vibration modes of peaks obtained in different samples of bone powders

Mode of vibrations	Raw bone powder (cm^{-1})	NaOH treated bone powder (cm^{-1})	Calcined bone powder at 750^0 C (cm^{-1})	Calcined bone powder at 950^0 C (cm^{-1})	NaOH treated bone powder calcined at 750^0 C (cm^{-1})	NaOH/HCl treated bone powder calcined at 750^0 C (cm^{-1})
OH^- stretching	-	-	-	-	-	3572.17
OH^- liberation	-	-	632.65	632.65	632.65	632.65
PO_4^{3-} stretching	1018.41, 964.41	1018.41, 964.41	1018.41, 1087.85, 964.41	1018.41, 1087.85, 964.41	1026.13, 1087.85, 964.41	1018.41, 1087.85, 964.41
PO_4^{3-} bending	601.79, 563.21, 439.77	601.79, 563.21, 455.20	601.79, 563.21, 439.77	601.79, 563.21, 439.77	601.79, 563.21, 439.77	601.79, 563.21, 470.63
PO_4^{3-} overtone	2160.27	2160.27	2160.27	2160.27	2160.27	-
PO_4^{3-} combination	2029.11	2029.11	2029.11	2029.11	2029.11	-
CO_3^{2-} vibration	1411.89, 1450.47, 871.82	1411.89, 1450.47, 871.82	1411.89, 1504.48	1411.89, 1504.48	1411.89, 1473.62	1411.89, 1458.18

Analysis of hydroxyl group

Bands at 3572.17 and 632.65 cm^{-1} are due to stretching and liberation mode of OH^- present in the structure of HAp. However, significant band at 3572.17 cm^{-1} is observed only in NaOH/HCl treated HAp calcined at 750^0C (Markovic, Fowler and Tung, 2004; Ooi, Hamdi and Ramesh, 2006; Ofudje *et al.*, 2017).

Analysis of phosphate group

Intense and sharp bands at 1018.41 cm^{-1} and 1087.85 cm^{-1} arise from asymmetric stretching vibration (v_3) of P-O bond present in PO_4^{3-} group of HAp (Markovic, Fowler and Tung, 2004; Ofudje *et al*., 2017).

The presence of bands at 964.41, 563.21 and 601.79 cm^{-1} as well as at 470.63 cm^{-1} refer to the v_1 (symmetric stretching vibration), v_4 (bending mode) and v_2 PO_4^{3-} group (Markovic, Fowler and Tung, 2004; Ooi, Hamdi and Ramesh, 2006).

The group of weak intensity bands at 2160.27 to 1975.11 cm^{-1} are due the overtone and combination of v_3 and v_1 mode of PO_4^{3-} group (Markovic, Fowler and Tung, 2004; Ooi, Hamdi and Ramesh, 2006). Overtone band appears due to excitation of fundamental asymmetric stretching mode for higher energy level than first excited energy level from ground state. Similarly, combination band appears due to the simultaneous excitation of fundamental symmetric and asymmetric stretching mode to first excited energy level from ground state. However, these bands are not observed in NaOH/HCl treated HAp calcined at 750^0C.

Analysis of carbonate group

The presence of weak bands at about 1411.89 cm^{-1} and 1450.47 cm^{-1} to 1473.62 cm^{-1} are due to the (v_3) stretching vibration mode of CO_3^{2-}. However, the intensity of such bands gradually decrease in calcination process (Markovic, Fowler and Tung, 2004) indicating more and more loss of carbon content of bone powder. The absence of bands relating v_1 and v_4 (bending mode) is due to their weak intensity. A significant band at about 871.82 cm^{-1} is present only in bone powder without calcination. This arises due to asymmetric stretching vibration (v_2) of CO_3^{2-} (Markovic, Fowler and Tung, 2004; Ooi, Hamdi and Ramesh, 2006).

Analysis of amide group

Band at 1643.35 cm^{-1} indicates the presence of amide I of collagen in HAp. This band is observed only in bone powder without calcinations. However, bands at 1273.02 cm^{-1} (amide III of collagen) are observed only in the calcined bone powder without base treatment (Barakat *et al*., 2009).

Other analysis

The sharpness of band at 563.21, 601.79 and 632.65 cm^{-1} indicates well crystallized HAp. (Markovic, Fowler, & Tung, 2004). In all type of bone powders, bands at these respective position are obtained with intense sharpness. The sharp narrow band at 632.65 cm^{-1} due to -OH group in all cases of calcined bone powder confirms that there is no secondary phase (TCP) detectable in all sample (Ooi, Hamdi and Ramesh, 2006).

4.2.1 Effect of temperatures

Temperature plays an important role to prepare hydroxyapatite from raw bone powder. At higher temperature, some essential functional groups (OH^-) might be eliminated (Khoo *et al*., 2015). Similarly, at very high temperature the structure of the Hydroxyapatite might change into TCP phase (Ooi, Hamdi and Ramesh, 2006).

1. Band at 1643.35 cm^{-1} (amide I of collagen) is observed only in raw bone powder. This shows that the collagen protein is substantially reduced in calcination process (Barakat *et al*., 2009).
2. A wide peak is seen at 3363.85 cm^{-1} corresponding to adsorbed water molecule by the sample in raw bone powder. This peak is also seen in raw and NaOH treated bone powder. However, the intensity of such peak is gradually decreased in calcination process. It shows that the adsorbed water molecules were removed during calcination (Khoo *et al*., 2015).
3. Band at 632.65 cm^{-1} (liberation mode of OH^-) is seen in all cases of calcined bone powder except the bone powder without calcination. It shows that the effect of –OH in HAp structure is pronounced only after calcination (Barakat *et al*., 2009). As the temperature increases during the heat treatment of bone powder some of the water molecules associated with the hydroxyapatite back bone are removed (Ofudje *et al*., 2017).
4. In raw bone powder, peaks at 871.82 and 1411.89 cm^{-1} are associated to CO_3^{2-} groups. The intensity of such peaks decrease gradually on increasing temperature during the synthesis of HAp. These peaks are at same intensity level in uncalcined, NaOH treated bone powder and raw bone powder indicating that there will be no loss of carbon content during alkali treatment (Khoo *et al*., 2015). However, bone powder calcined at 750^0C and 950^0C show significant reduction in intensity of CO_3^{2-} peak at 864.11 and 1411.89 cm^{-1} respectively as

compare to that of raw bone powder. This results show that calcination is the crucial step to reduce the carbon content of raw bone powder during HAp synthesis (Khoo *et al*., 2015; Ofudje *et al*., 2017).

5. There are large number of bands such as 1180.44, 1273.02, 1697.36 cm^{-1} in the spectra for bone powder obtained after the calcination at 950^0C. These bands are not present in other cases where the bone powder is calcined at 750^0C. This may be due to the thermal instability of HAp above 900^0C (Ooi, Hamdi and Ramesh, 2006).

4.2.2 Effect of acid and base treatment prior to calcination

The calcination of raw bone powder is crucial step for the preparation of hydroxyapatite. Prior to calcination the raw bone powder is treated with either acid or base or the combination of both to make it easy for the removal of organic part attached to the bone. Acid or base reacts with amide to dissolve it from the phosphate back bone of raw bone (Barakat *et al*., 2009; Ofudje *et al*., 2017).

Effect of NaOH

1. Bands at 1273.02 cm^{-1} (amide III of collagen) are observed only in alkali untreated HAp. This shows that NaOH is responsible for the reduction of collagen (Barakat et al., 2009). Amide reacts with NaOH as given by the following reaction.

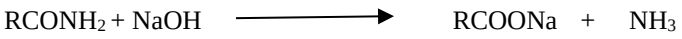

2. A band at 1504.48 cm^{-1} is observed in all HAps which are not treated with NaOH. This band arises due to “B” type carbonate substitution. It shows that NaOH is responsible for the removal of “B” type carbonate substitution. (Markovic, Fowler and Tung, 2004).

Effect of HCl

1. A significant band at 3572.17 cm^{-1} is observed only in NaOH/HCl treated HAp calcined at 750^0C (Markovic *et al*., 2004). However, the significant band is not observed in NaOH treated HAp calcined at 750^0C.
2. The sharpness of band at 632.65 cm^{-1} (liberation mode of -OH) is more pronounced in NaOH/HCl treated HAp than in NaOH treated HAp calcined at

same temperature. This indicates that HCl increases the degree of crystallinity in prepared HAp (Ofudje *et al*., 2017).

3. A band at 1195.87 cm^{-1} is observed in all HAps which are treated with NaOH. This band is also present in raw bone powder. However, this band is absent in NaOH/HCl treated HAp calcined at 750^0C. This band may correspond to some organic impurities which are better removed by HCl as compared to NaOH.
4. The sharpness of band at 632.65 cm^{-1} (liberation mode of -OH) is more pronounced in NaOH/HCl treated HAp than in NaOH treated HAp calcined at same temperature. This indicates that HCl increases the degree of crystallinity in prepared HAp (Ofudje *et al*., 2017).

From above discussion, it is observed that the FTIR spectra of different samples of bone powders show the presence of phosphate, carbonate and hydroxyl groups in all of them including the raw one. These spectra are more clearly appeared in calcined samples as the calcination process has destroyed the cross linked structure in the raw caprine bone. Similarly, the degree of removal of organic matter has been compared in different samples with FTIR spectra measurements. The bands in the FTIR spectra of the caprine bone at different temperatures as well as different chemicals are in close agreement with some literature reports which matched the major characteristic bands of pure HAp (Markovic, Fowler and Tung, 2004; Ooi, Hamdi and Ramesh, 2006; Barakat *et al*., 2009; Khoo *et al*., 2015; Ofudje *et al*., 2017).

4.1.3 SEM analysis

The surface morphology of acid + base treated caprine bone powder calcined at 750^0C was investigated by SEM. The result of SEM indicated that the bone powders were irregular in shape. The SEM image exhibited the presence of rounded nanoparticles of HAp in isolated and agglomerated forms. Based on the observation, the HAp particles can be regarded as nanospheres with crystal size ranging well below 50 nm. The morphology showed the agglomerated particles sizes of the hydroxyapatite containing mixture of particles with different sizes (Barakat *et al*., 2009). SEM images are shown in **Figure 4.3**.

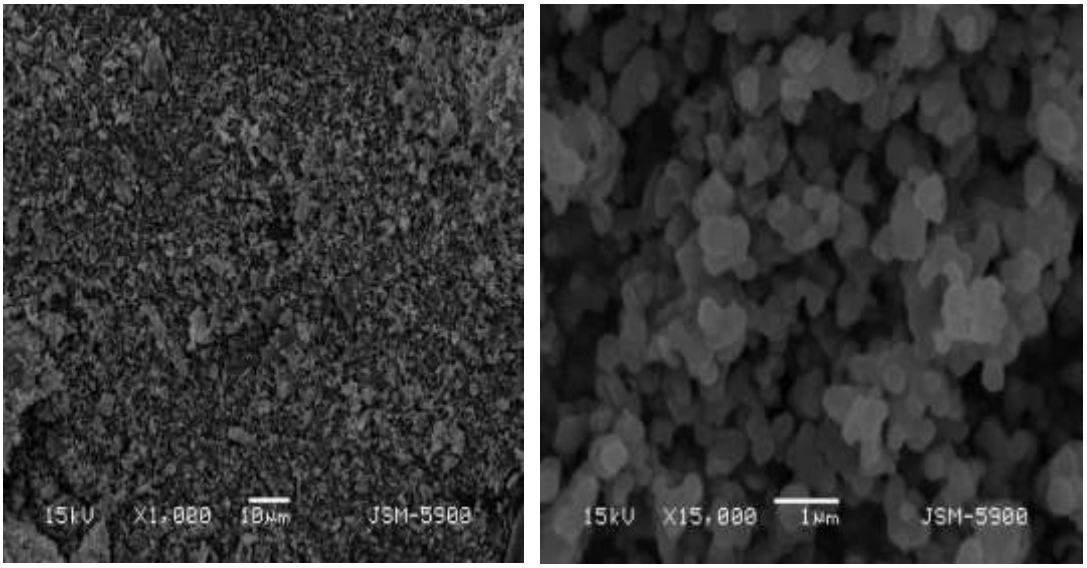

(a) (b)

***Fig 4.3**: SEM images of NaOH/HCl treated bone powder a) low magnification b) high magnification*

4.1.4 Determination of specific surface area

1. Determination of λ_{max} for methylene blue solution

Maximum absorption of methylene blue solution for a particular wavelength (λ_{max}) of light was obtained by using spectrophotometer. The concentration of methylene blue solution used was 1 ppm. The absorbance of methylene blue solution at different wavelengths were found to be increased as wavelength increased upto $\lambda_{max.}$ Beyond $\lambda_{max,}$ the absorbance declined. For, methylene blue solution λ_{max} was found to be 665nm. The plot of absorbance against wavelength in nm is shown in **Figure 4.4.**

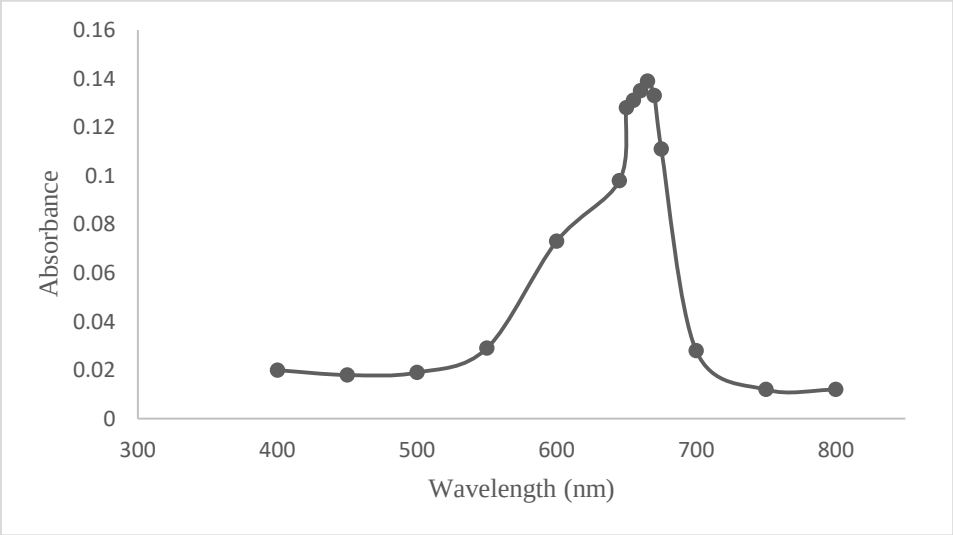

***Fig 4.4:** Absorbance against wavelength plot for methylene blue solution*

2. Calibration curve for methylene blue solution

Calibration curve establishes the relationship between absorbance and concentration of methylene blue solution on the basis of Lambert-Beer's law. The absorbance of methylene blue solution was measured at 665 nm. The absorbance at different concentrations were found to be increased linearly with the increase in methylene blue concentrations as depicted from **Figure 4.5.**

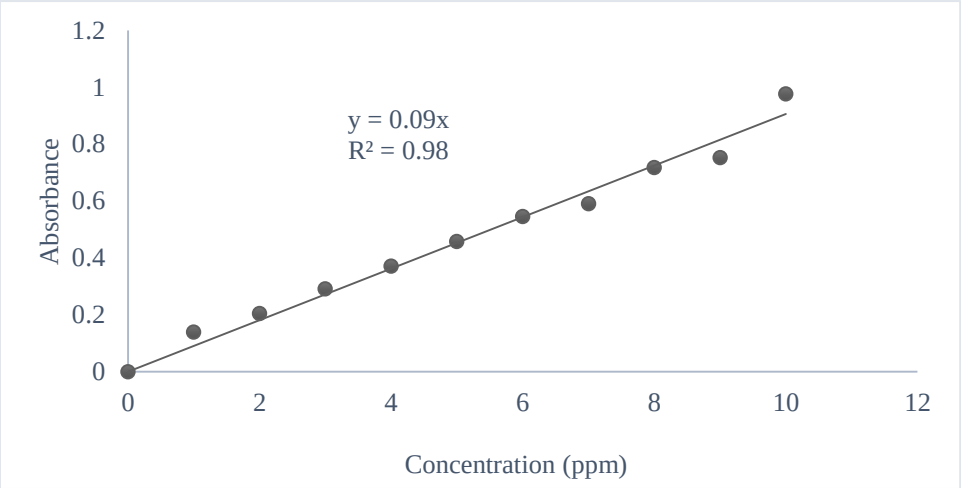

Fig 4.5: *Absorbance against concentration plot for methylene blue solution*

3. Determination of specific surface area

Langmuir plot was drawn to determine the specific surface area of HAp (acid + base treated). It was calculated by using the slope of the line obtained from the plot of $\frac{C_e}{Q_e}$ against equilibrium concentration (C_e) as depicted from **Figure 4.6.**

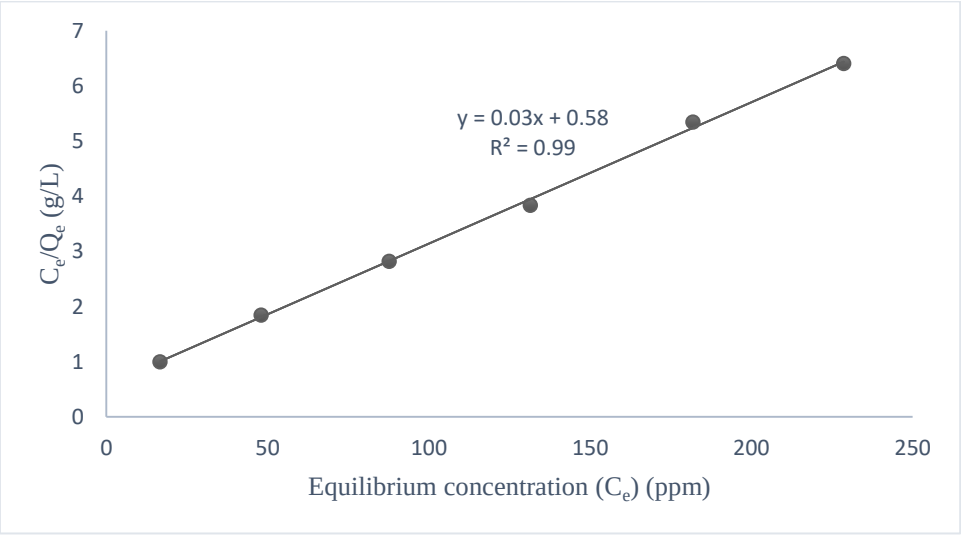

Fig 4.6: *Langmuir plot of C_e/Q_e against equilibrium concentration of methylene blue solutions (C_e)*

From the above plot, the slope of the line was found to be 0.03. The maximum concentration of methylene blue adsorbed per g of HAp (Q_m) is 39.06 mg/g. Specific surface area is calculated with the help of following equation (viii) and is found to be 144.89 m^2/g. This specific surface area is calculated on the basis of Langmuir plot. It shows the formation of monomolecular layer on the surface of HAp. For the adsorption experiment, it is better to have adsorbent with greater specific surface area as the adsorbate-adsorbent interaction becomes easier. In previous study, the specific surface area of HAp from buffalo bone was found to be 167.11 m^2/g (Panchen, 2019).

4.1.5 Point of zero charge of HAp (pH_{PZC})

To understand the bio-adsorption mechanism point of zero charge (pH_{PZC}) determination is very important. It refers pH value of the medium at which there will be no any charge present on HAp surface. To calculate the pH_{PZC} value a graph between change in pH against initial pH was plotted as shown in **Figure 4.7.**

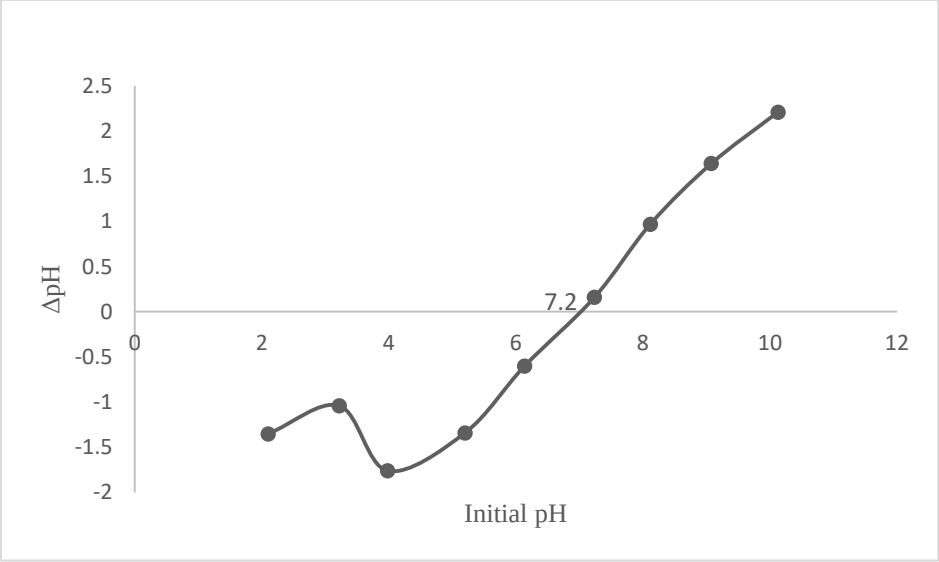

Fig 4.7: *ΔpH against initial pH of HAp for pH_{PZC} measurement*

The pH_{PZC} value was found to be 7.2. At pH_{PZC}, the surface of HAp is expected to be neutral. It doesnot carry any positive or negative charge at pH 7.2. This surface may become either positive or negative charged with varying pH of the medium on which experiment was conducted. At pH < pH_{PZC}, the adsorbent surface is positively charged resulting anion adsorption on its surface. However, at pH > pH_{PZC}, the adsorbent surface is negatively charged anion repulsion from its surface. Most of the microorganisms including fungi possess negative charge on their cell wall surface. So, for adsorption of

these microorganisms on HAp, the adsorbent surface should be positively charged and the medium must be in lower pH. In previous study, pH_{PZC} of HAp from buffalo bone was found to be 6.8 (Panchen, 2019).

4.2 Adsorption Study of Microorganisms on Hydroxyapatite (HAp)

4.2.1 Adsorption study of *E. coli* on HAp

1. Calibration Curve

Calibration curve establishes the relationship between absorbance and concentrations of *E. coli* suspensions on the basis of Lambert-Beer's law. The absorbance of *E. coli* suspension was measured at 550 nm. The absorbance at different concentrations were found to be increased linearly with the increase in concentrations of *E. coli* suspension as depicted from **Figure 4.8.**

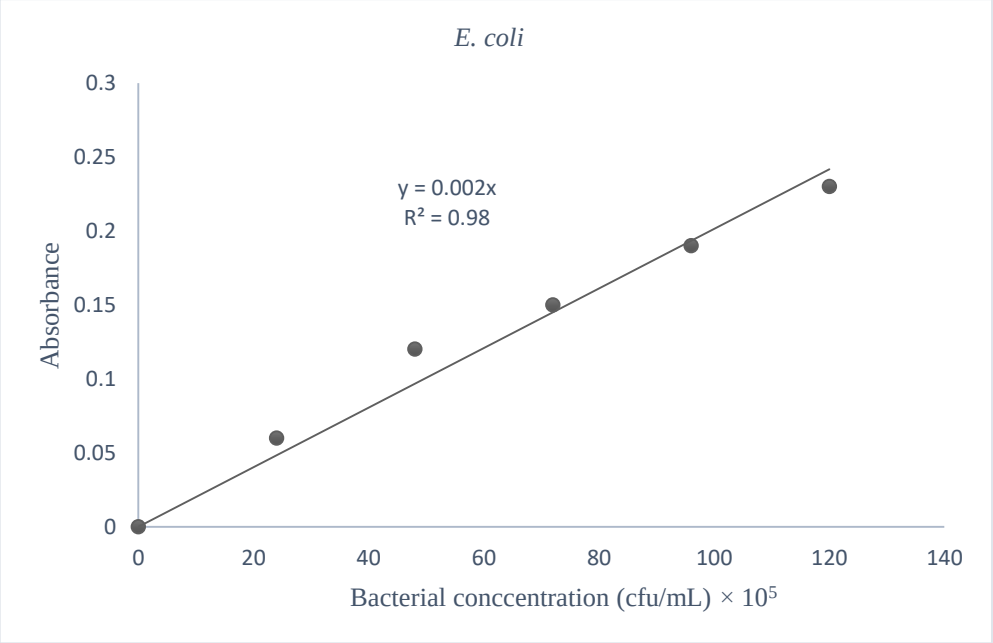

Fig 4.8: *Plot of absorbance against bacterial concentration of E. coli*

2. Adsorption study

A plot of *E. coli* adsorbed against bacterial equilibrium concentration was drawn to show the nature of adsorption during contact time as shown in **Figure 4.9.**

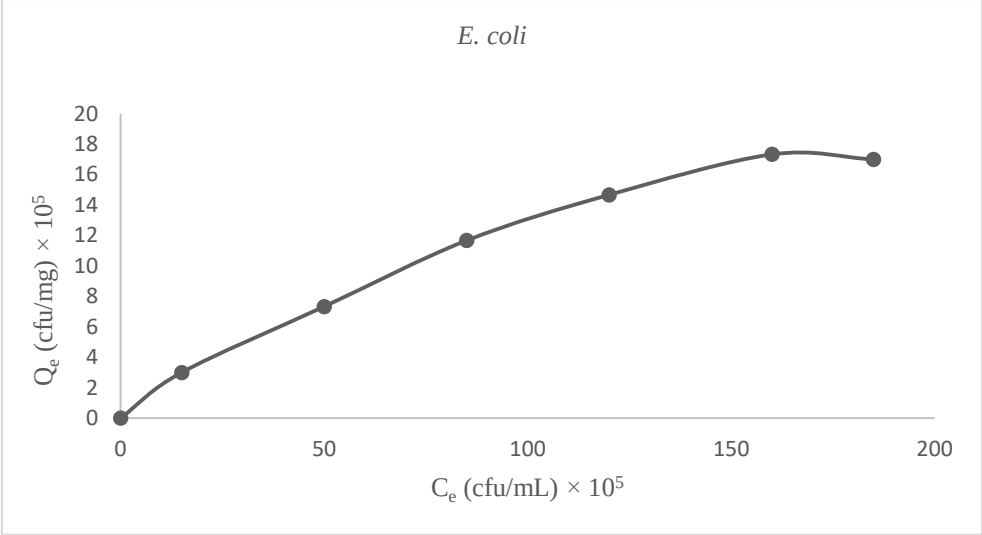

Fig 4.9: *Plot of E. coli adsorbed (Q_e) against equilibrium concentration (Ce)*

From the above plot, we can find the number of bacteria adsorbed in 1mg of HAp by using following formula.

Bacteria adsorbed per mg of HAp (Q_e) = $\frac{(C_i - C_e) \times 10^5}{M} \times V$ cfu/mg. It shows that the adsorption of bacteria on HAp increases upto the bacterial equilibrium concentration 134×10^5 cfu/mL. Plateau is formed in a plot of bacteria adsorbed against bacterial equilibrium concentration beyond this equilibrium concentration which indicates that no bacterial adsorption occurs. It is a major sign to find the adsorption capacity of HAp to adsorb *E. coli* suspension. Most of the adsorption sites of HAp are completely covered by monolayer of *E.coli* and further adsorption is stopped. The linearized Freundlich curve was also drawn as shown in **Figure 4.10.**

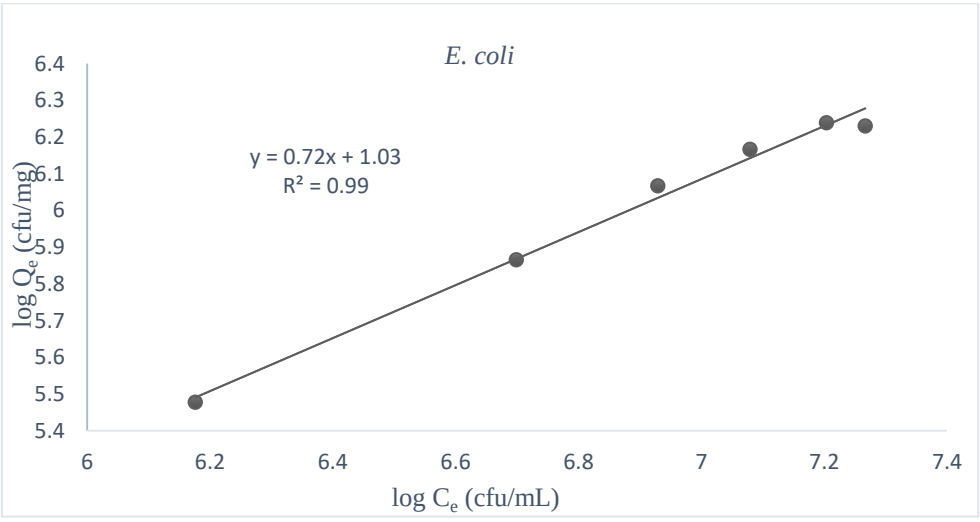

Fig 4.10: *Linearized Freundlich plot of logQ_e versus logC_e for E.coli*

Further, a langmuir plot is drawn to find the maximum number of bacteria that could be adsorbed in 1 mg of HAp as shown in **Figure 4.11.**

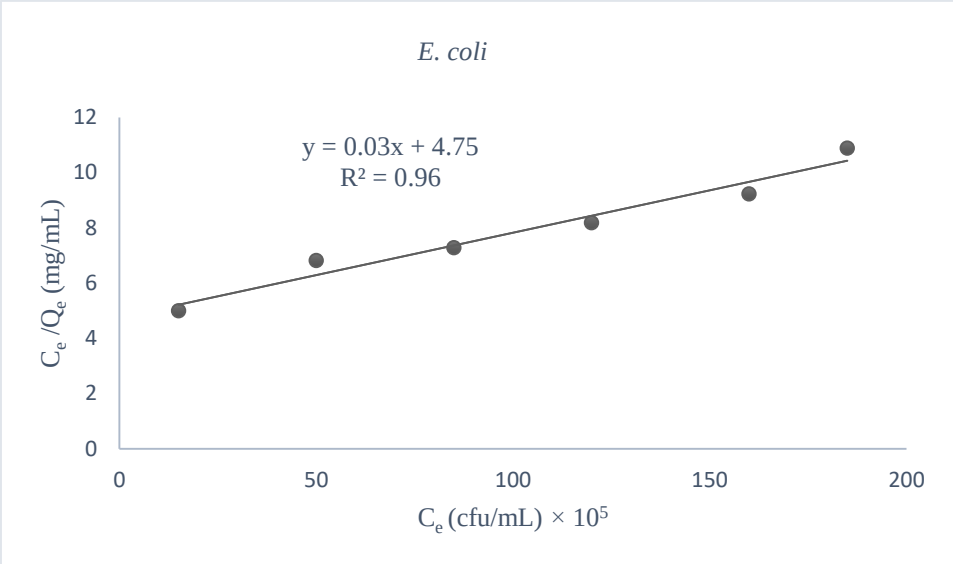

Fig 4.11: *Linearized Langmuir plot of C_e/Q_e against E. coli equilibrium concentration (C_e)*

Slope of the line obtained from the above Langmuir plot is found to be 0.03. The maximum number of bacteria adsorbed on 1 mg of HAp is calculated as

Q_m = 1/0.0307= 32.57 × 10^5 cfu/mg. It shows that 1 mg of HAp could adsorb 32.57 × 10^5 number of *E. coli* under the conditions of present study.

Table 4.2: Parameters of Langmuir and Freundlich constants for *E. coli*

Langmuir model			
	Q_m (cfu/mg)	b (mL/cfu)	R^2
E .coli	32.57 × 10^5	6.5 × 10^{-8}	0.96
Freundlich model			
	logK_f (cfu/mg)	n (mL/mg)	R^2
E. coli	1.03	1.39	0.99

Langmuir constant ‘b’ signifies the adsorption affinity of adsorbate on adsorbent during adsorption. In case of adsorption of *E. coli* onto HAp surface, the lower value of ‘b’ indicates the weak interaction between bacteria (adsorbate) and hydroxyapatite (adsorbent). The correlation coefficients of Langmuir and Freundlich adsorption isotherm of *E. coli* were 0.96 and 0.99 respectively. This shows that the experimental data fitted with the Freundlich model.

3. Adsorption kinetics study

Bacterial suspension having concentration 212×10^5 cfu/mL was prepared. The kinetics plot of bacteria adsorbed at particular time (Q_t) against time is shown in **Figure 4.12.**

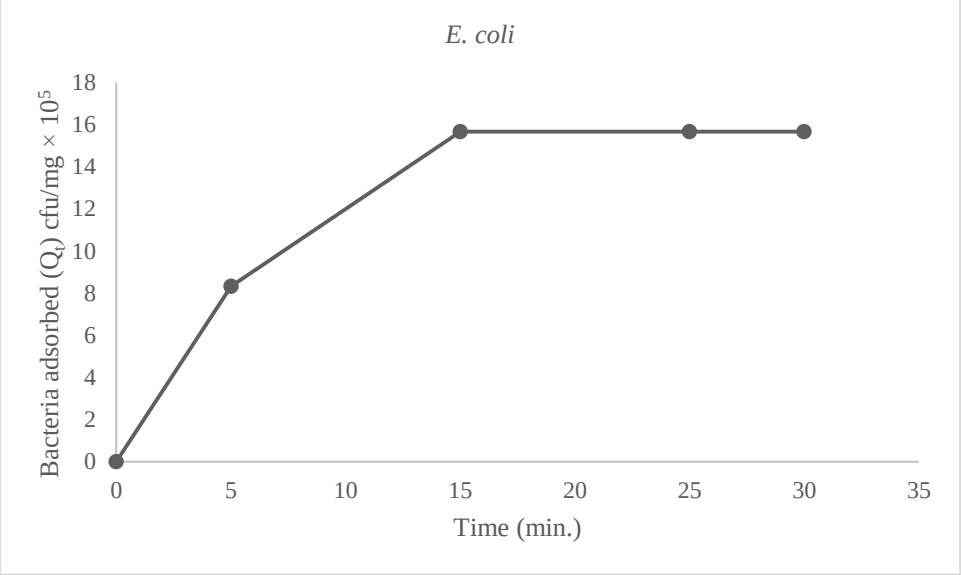

Fig 4.12: *Adsorption kinetics of E .coli onto HAp surface*

It shows that the adsorption of bacteria on HAp increases upto 15 minutes. Plateau is formed in a plot of bacteria adsorbed against contact time beyond 15 minutes which indicates that no bacterial adsorption occurs after this. Most of the adsorption sites of HAp are completely covered by monolayer of *E.coli* and further adsorption is stopped.

Pseudo-first order and pseudo-second order model were employed to the experimental kinetics data as shown in **Figure 4.13** and **Figure 4.14** respectively.

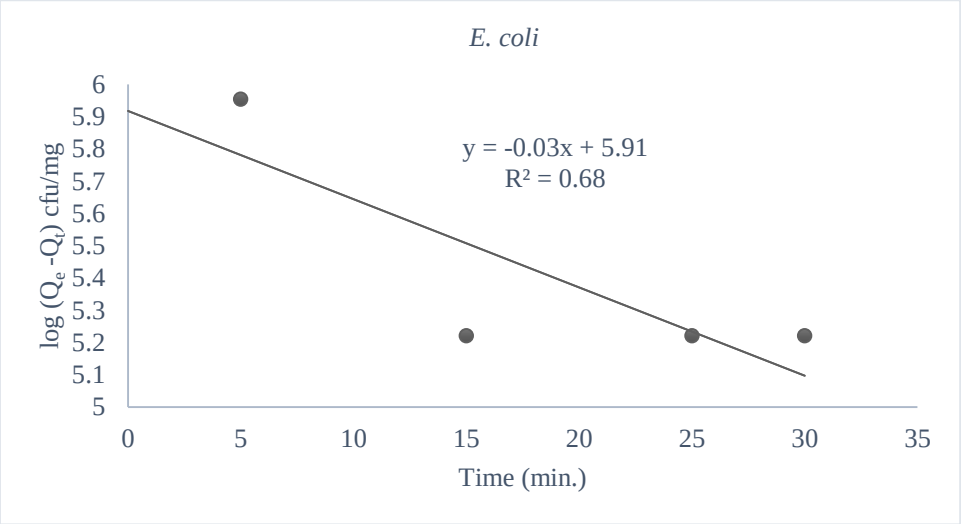

Fig 4.13: *Pseudo-first order kinetics model of adsorption for E. coli on HAp*

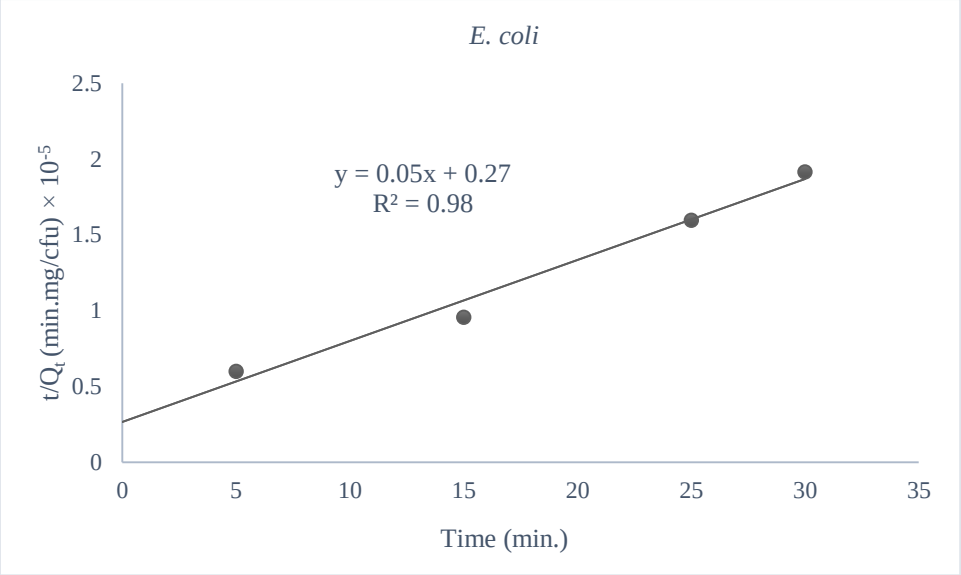

Fig 4.14: *Pseudo-second order kinetics model of adsorption for E. coli on HAp*

Table 4.3: Different parameters of pseudo-first and pseudo-second order kinetics model for *E. coli*

S.N.	Kinetics model	Rate constants	Q_e (cfu/mg) × 10^5	R^2
1.	Pseudo-first order	0.06 (cfu $mg^{-1}min^{-1}$)	8.26	0.68
2.	Pseudo-second order	1.05×10^{-12} (mg min^{-1} cfu^{-1})	18.76	0.98

The larger value of correlation coefficient for pseudo-second order kinetics model (R^2 = 0.98) than pseudo-first order model (R^2 = 0.68) indicates that most of the bacteria adsorb on hydroxyapatite following the pseudo-second order equation.

4. Effect of adsorbent dose

The effect of variation of adsorbent dose on bacterial adsorption was studied only for *E. coli*. The concentration of *E. coli* (236 × 10^5 cfu/mL) was kept constant during the adsorption study. **Figure 4.15** depicts the result.

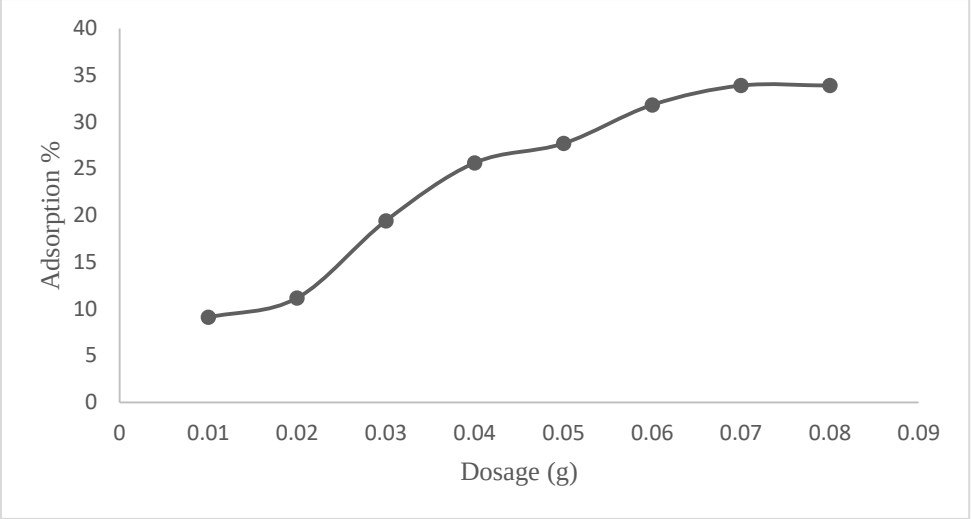

Fig 4.15: *Effect of adsorbent dose on adsorption of E. coli*

The adsorption % of *E. coli* increases with the addition of adsorbent (HAp) upto 0.07g. Beyond this amont of HAp, a plateau is formed which shows no more increase in adsorption. It might be due to increase in adsorption sites in adsorbent for bacteria to be adsorbed. However, at a particular concentration of adsorbent, all of the adsorption sites fill up and a plateau is produced beyond it.

4.2.2 Adsorption study of *C. albicans* on HAp

1. Calibration Curve

The calibration curve of different concentrations of *C. albicans* on hydroxyapatite is shown in **Figure 4.16.**

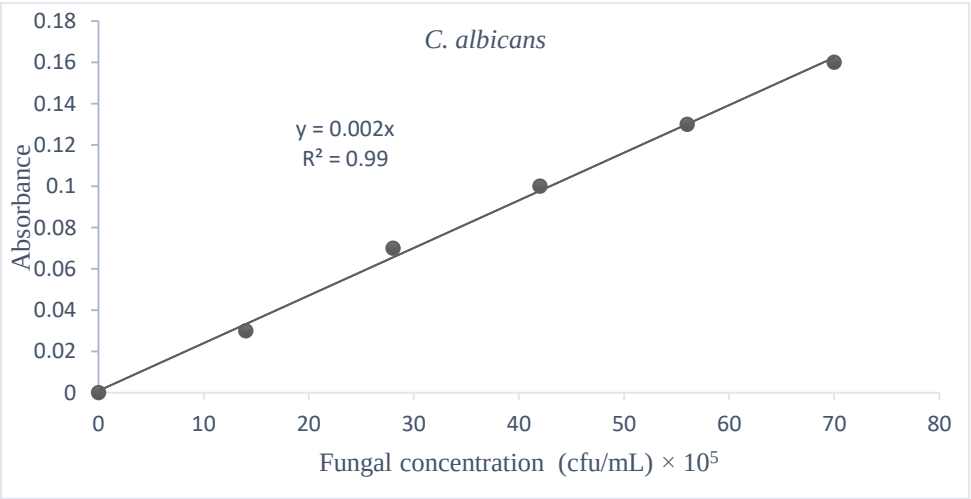

Fig 4.16: *Plot of absorbance against fungal concentration of C. albicans*

2. Adsorption study

A plot of *C. albicans* adsorbed against fungal equilibrium concentrations was drawn to show the nature of adsorption during contact time as shown on **Figure 4.17.**

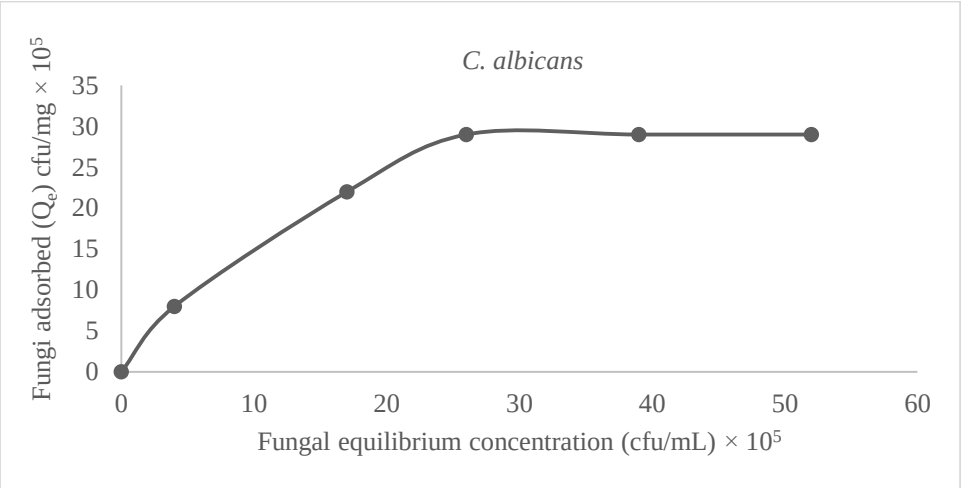

Fig 4.17: *Plot of fungi adsorbed against fungi equilibrium concentration*

It shows that the adsorption of fungi on HAp increases upto the fungal equilibrium concentration 25 × 10^5 cfu/mL. Plateau is formed in a plot of fungi adsorbed against fungal equilibrium concentration beyond this equilibrium concentration which indicates that no bacterial adsorption occurs. It is a major sign to find the adsorption capacity of HAp to adsorb *C. albicans* suspension. Most of the adsorption sites of HAp are completely covered by monolayer of *C. albicans* and further adsorption is stopped.

A linearized Freundlich plot for the adsorption of fungi was also drawn as shown in **Figure 4.18.**

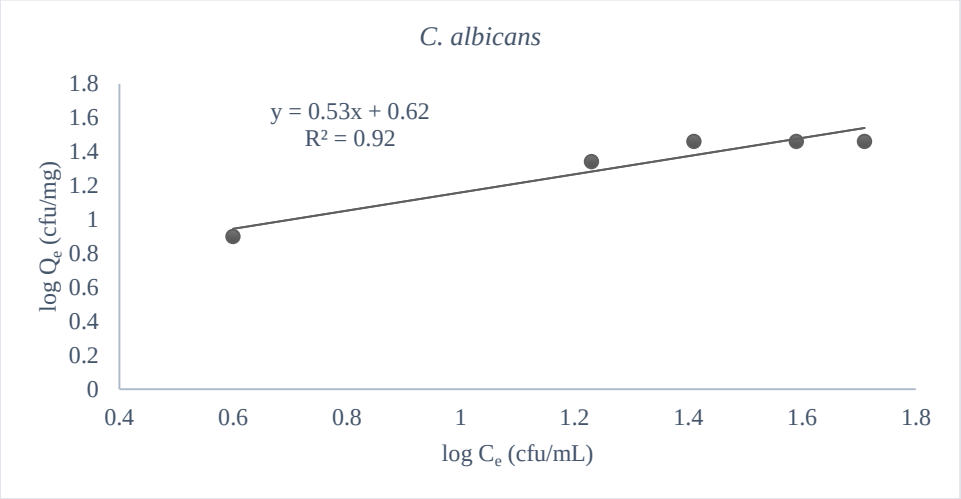

Fig 4.18: *Linearized Freundlich plot of logQ_e against logC_e for C. albicans*

Further, a Langmuir plot is drawn as shown in **Figure 4.19.**

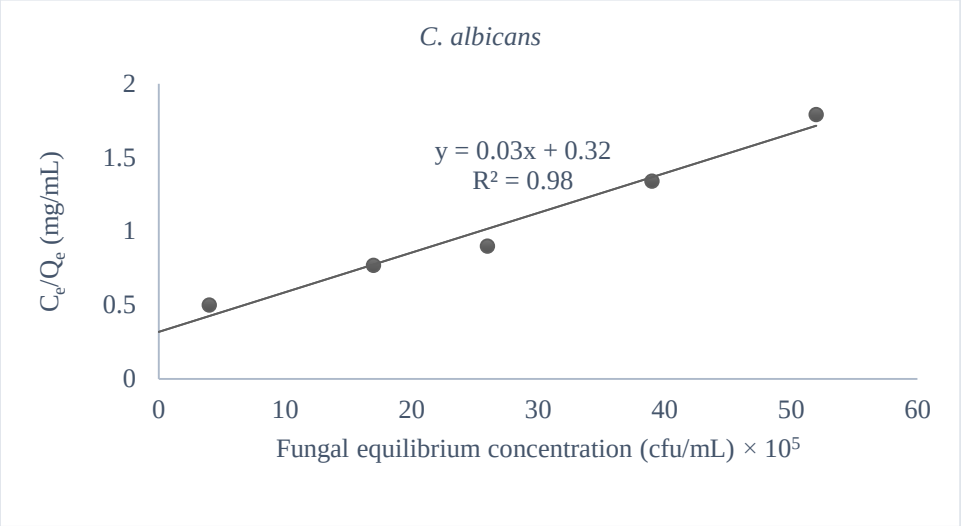

Fig 4.19: *Linearized Langmuir plot of C_e/Q_e against fungi equilibrium concentration (C_e)*

Slope of the line obtained from the above Langmuir plot is found to be 0.0269. The maximum number of fungi adsorbed on 1 mg of HAp is calculated as

$Q_m = 1/0.03 = 34 \times 10^5$ cfu/mg. It shows that 1 mg of HAp could adsorb 34×10^5 number of *C. albicans*

Table 4.4: Parameters for Freundlich and Langmuir constants for *C. albicans*

Langmuir model			
	Q_m (cfu/mg)	b (mL/cfu)	R^2
C. albicans	37.17×10^5	0.08×10^{-6}	0.98
Freundlich model			
	$\log K_f$ (cfu/mg)	n	R^2
C. albicans	0.62	1.87	0.92

In case of adsorption of *C. albicans* onto HAp surface, the lower value of Langmuir constant 'b' indicates the weak interaction between fungi (adsorbate) and hydroxyapatite (adsorbent).The correlation coefficients of Langmuir and Freundlich adsorption isotherm of *C. albicans* are 0.98 and 0.92 respectively. This shows that the experimental data fitted with the Langmuir model.

3. Adsorption Kinetics study

The adsorption kinetics study establishes the relationship between contact time of HAp and the adsorbed fungal concentration. Fungal suspension having concentration 126 × 10^5 cfu/mL was prepared and the kinetics plot of fungi adsorbed against time is as shown in **Figure 4.20.**

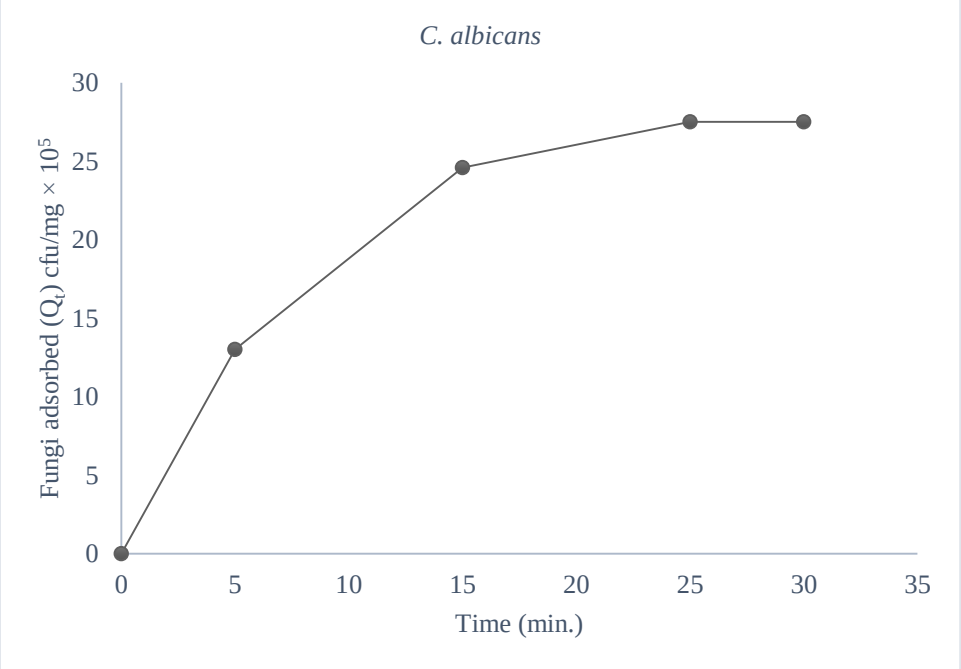

***Fig 4.20**: Adsorption kinetics of C. albicans onto HAp surface*

At first, the initial fungal concentration was used as 126 × 10^5 cfu/mL. It shows that the adsorption of fungi on HAp increases upto 25 minutes. Plateau is formed in a plot of bacteria adsorbed against contact time beyond 25 minutes which indicates that no fungal adsorption occurs after this. Most of the adsorption sites of HAp are completely covered by monolayer of *C. albicans* and further adsorption is stopped.

Pseudo-first order and pseudo-second models were employed to the experimental kinetics data as shown **Figure 4.21** and **Figure 4.22** respectively.

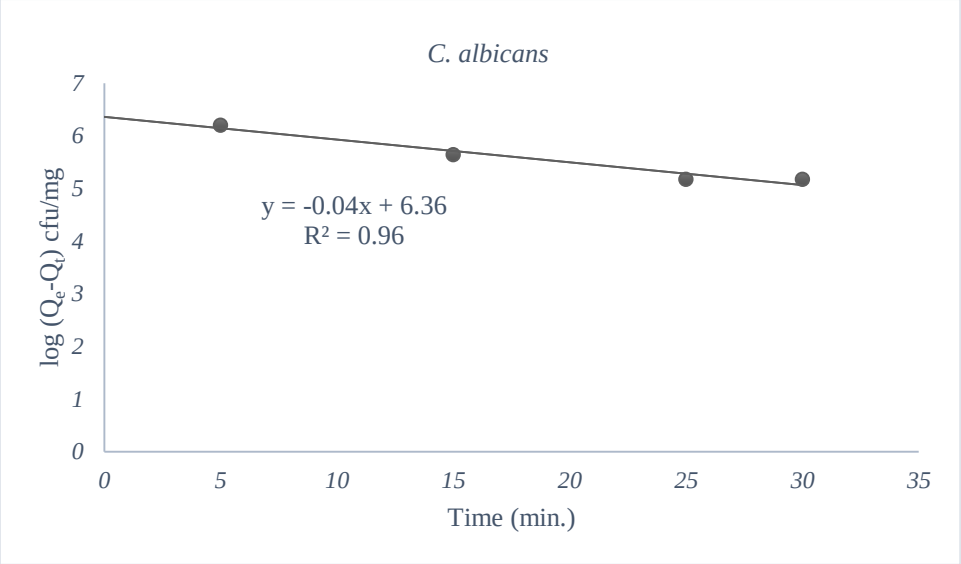

Fig: 4.21: *Pseudo-first order kinetic model of adsorption for C. albicans on HAp*

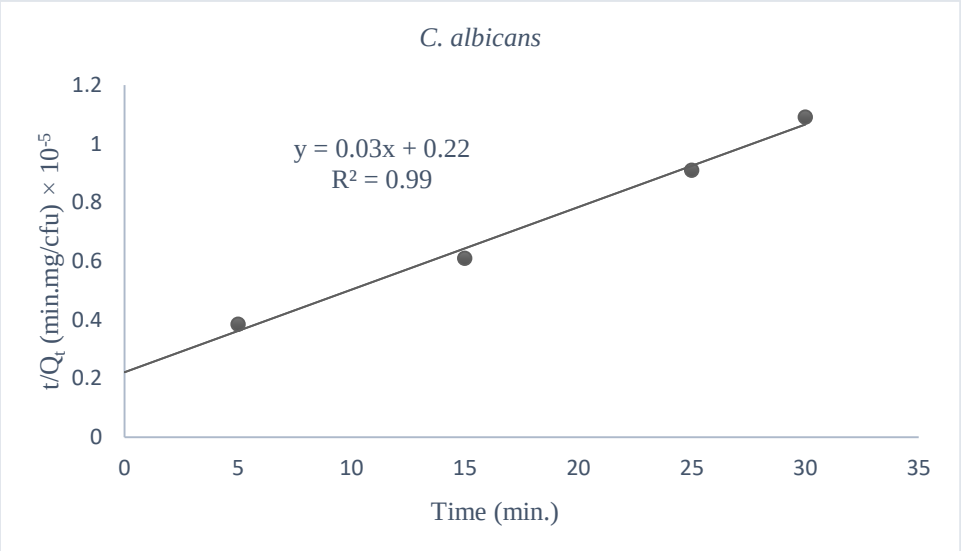

Fig: 4.22: *Pseudo-second order kinetic model of adsorption for C. albicans on HAp*

Table 4.5: Different parameters of pseudo-first order and pseudo-second order kinetics model for adsorption of fungi

S/N	Kinetics model	Rate constants	Q_e (cfu/mg) × 10^5	R^2
1.	Pseudo-first order	0.09 (cfu min^{-1} mg^{-1})	22.79	0.96
2.	Pseudo-second order	0.36×10^{-12} (mg min^{-1} cfu^{-1})	35.46	0.99

The larger value of correlation coefficient for pseudo-second order kinetics model (R^2 = 0.99) than pseudo-first order model (R^2 = 0.96) indicates that most of the fungal cells adsorb on hydroxyapatite following the pseudo-second order equation.

4.2.3 Adsorption study of *S. aureus* on HAp

1. Calibration curve

The calibration curve of different concentrations of *S. aureus* on hydroxyapatite is shown in **Figure 4.23.**

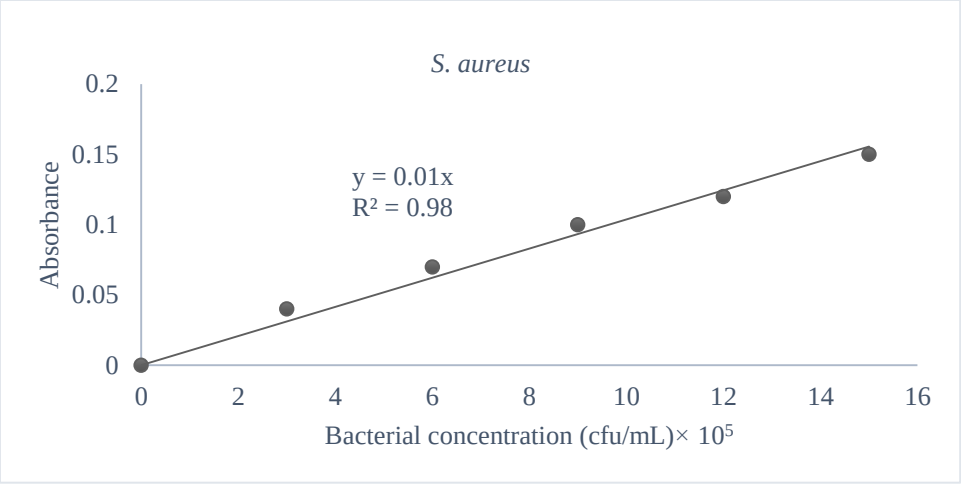

Fig 4.23: *Plot of absorbance against bacterial concentration*

2. Adsorption study

A plot of *S. aureus* adsorbed against bacterial equilibrium concentrations is shown in **Figure 4.24.**

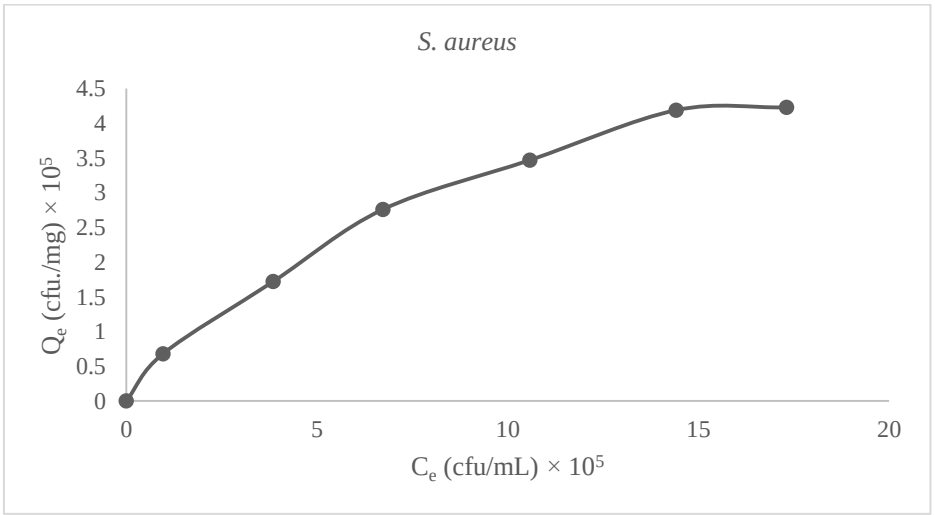

Fig 4.24: *Plot of bacteria adsorbed against bacterial equilibrium concentration*

It shows that the adsorption of bacteria on HAp increases upto the bacterial equilibrium concentration 15×10^5 cfu/mL. Plateau is formed in a plot of bacteria adsorbed against bacterial equilibrium concentration beyond this equilibrium concentration which indicates that no bacterial adsorption occurs. It is a major sign to find the adsorption capacity of HAp to adsorb *S. aureus* suspension. Most of the adsorption sites of HAp are completely covered by monolayer of *S. aureus* and further adsorption is stopped.

A linearized Freundlich curve for the adsorption of *S. aureus* is shown in **Figure 4.25.**

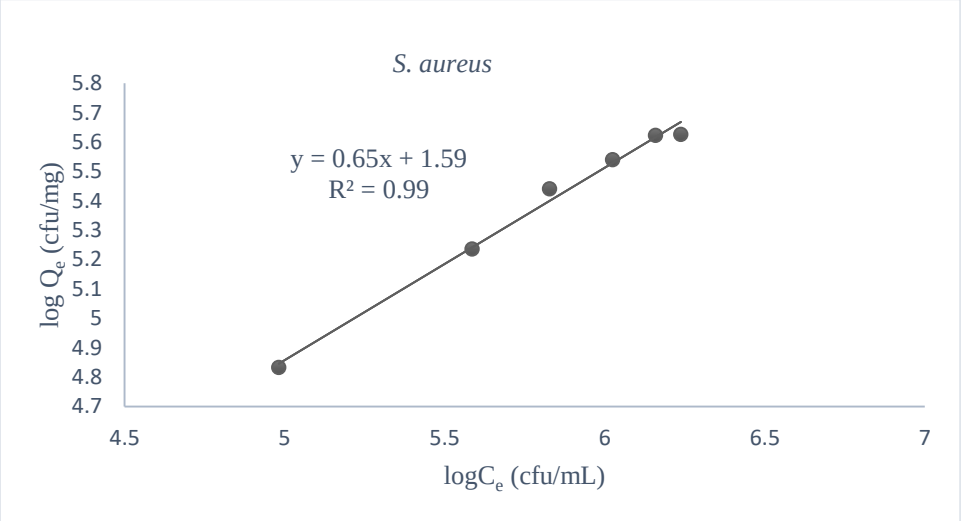

Fig 4.25: *Linearized Freundlich plot of $logQ_e$ versus $logC_e$ for S.aureus*

Further, a langmuir plot is drawn as shown in **Figure 4.26.**

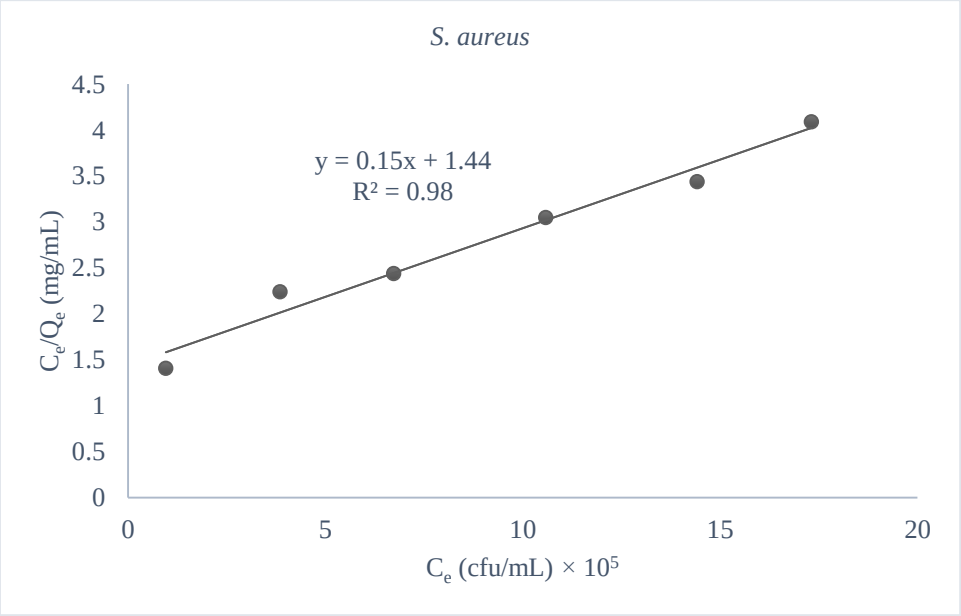

Fig 4.26: *Linearized Langmuir plot of C_e/Q_e against S. aureus equilibrium concentration (C_e)*

Slope of the line obtained from the above Langmuir plot is found to be 0.1493. The maximum number of bacteria adsorbed on 1 mg of HAp is calculated as

Q_m = 1/0.15 = 6.7× 10^5 cfu/mg. It shows that 1 mg of HAp could adsorb 6.7 × 10^5 number of *S. aureus*.

Table 4.6: Different parameters of Langmuir and Freundlich model for *S. aureus*

Langmuir model			
	Q_m (cfu/mg)	b (mL/cfu)	R^2
S. aureus	6.7 × 10^5	1.03 × 10^{-6}	0.98
Freundlich model			
	$\log K_f$ (cfu/mg)	n	R^2
S. aureus	1.59	1.53	0.99

In case of adsorption of *S. aureus* onto HAp surface, the lower value of Langmuir constant 'b' indicates the weak interaction between bacteria (adsorbate) and hydroxyapatite (adsorbent).The correlation coefficients of Langmuir and Freundlich adsorption isotherm of *S. aureus* were 0.98 and 0.99 respectively. This shows that the experimental data fitted with the Freundlich model.

3. Adsorption kinetics study

The adsorption kinetics study establishes the relationship between contact time of HAp and the adsorbed bacterial concentration. Bacterial suspension having concentration 27 × 10^5 cfu/mL was used and the kinetics plot of bacteria adsorbed against time is as shown in figure shown in **Figure 4.27**.

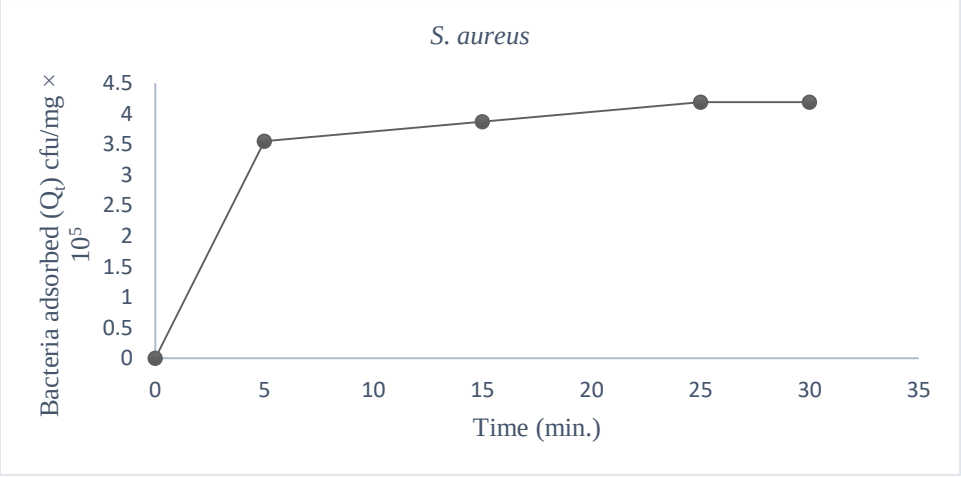

Fig 4.27: *Adsorption kinetics of S. aureus adsorbed onto HAp surface*

It shows that the adsorption of bacteria on HAp increases upto 5 minutes. Plateau is formed in a plot of bacteria adsorbed against contact time beyond 5 minutes which indicates that no bacterial adsorption occurs after this. Most of the adsorption sites of HAp are completely covered by monolayer of *S. aureus* and further adsorption is stopped.

For kinetic studies pseudo-second order model was employed to the experimental kinetics data which is shown in in **Figure 4.28.**

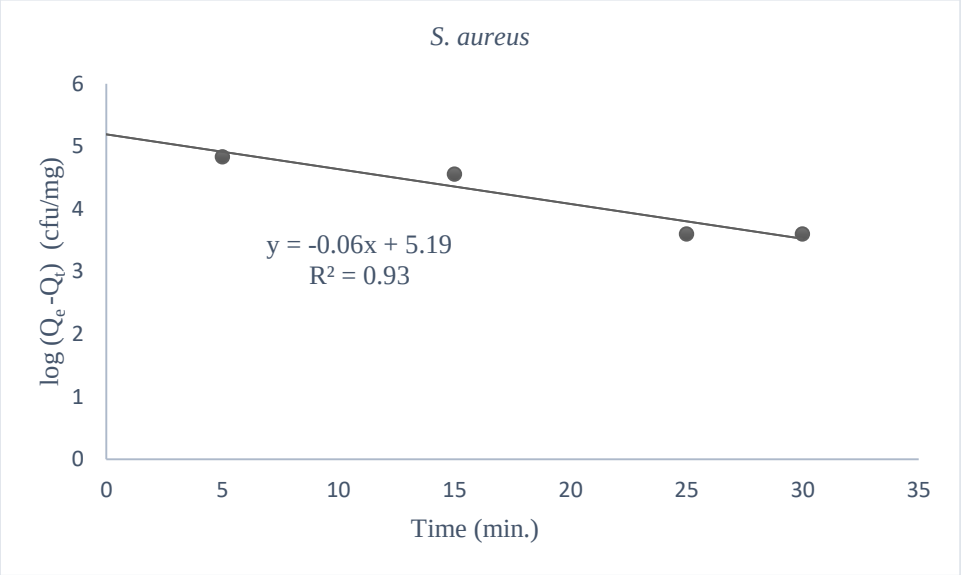

Fig 4.28: *Pseudo-first order kinetics model of adsorption for S. aureus on HAp*

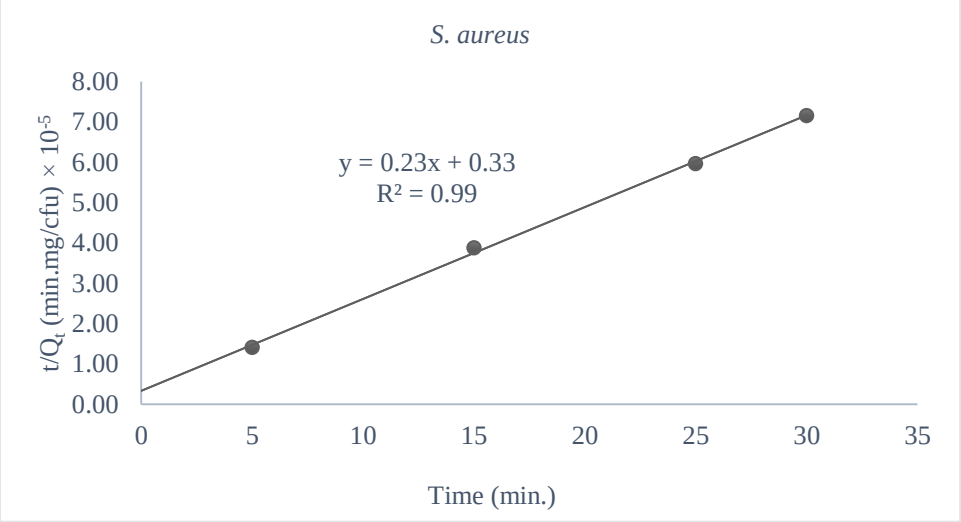

Fig 4.29: *Pseudo-second order kinetics model of adsorption for S. aureus on HAp*

Table 4.7: Different parameters of pseudo-first order and pseudo-second order kinetics model for *S. aureus*

S.N.	Kinetics model	Rate constants	Q_e (cfu/mg) × 10^5	R^2
1.	Pseudo-first order	0.13 (cfu mg^{-1} min^{-1})	1.5	0.93
2.	Pseudo-second order	15.51 × 10^{-12} (mg min^{-1} cfu^{-1})	4.39	0.99

The larger value of correlation coefficient for pseudo-second order kinetics model (R^2 = 0.99) than pseudo-first order model (R^2 = 0.93) indicates that all bacteria adsorb on hydroxyapatite following the pseudo-second order equation.

4.2.4 Adsorption study of *A. baumanii* on HAp

1. Calibration Curve

The calibration curve of different concentrations of *A. baumanii* on hydroxyapatite is shown in **Figure 4.27.**

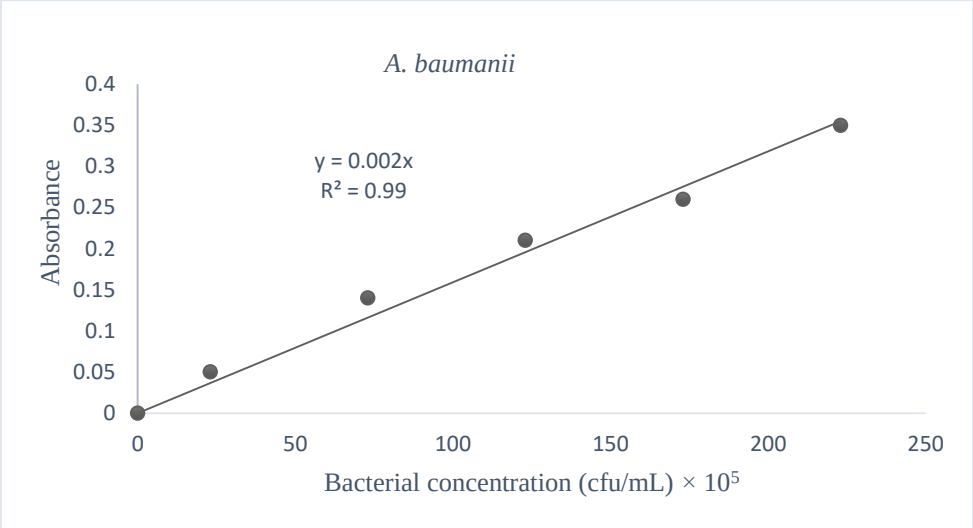

Fig 4.30: Plot of absorbance against bacterial concentration of A. baumanii

2. Adsorption study

A plot of *A. baumanii* adsorbed against bacterial equilibrium concentration is shown in **Figure 4.31.**

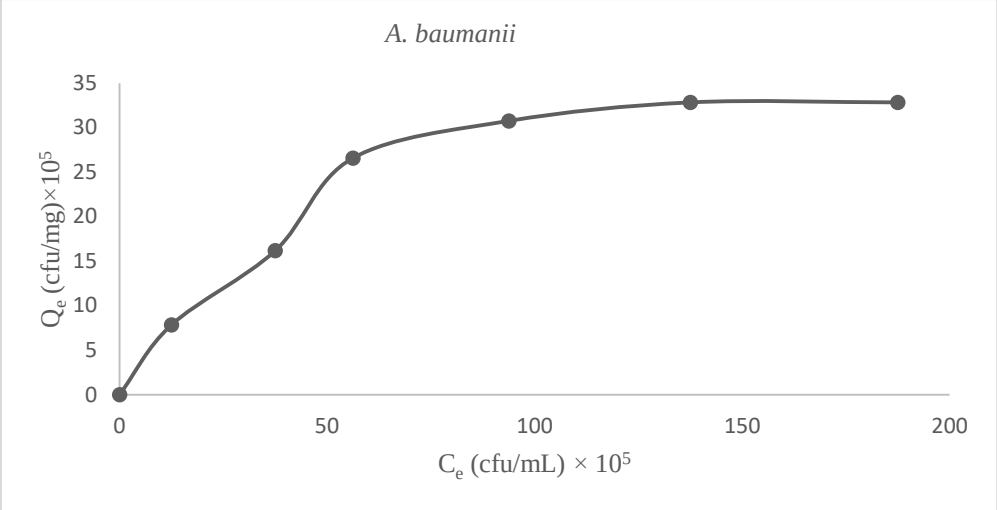

Fig 4.31: *Plot of A .baumanii adsorbed (Q_e) against equilibrium concentration (C_e)*

It shows that the adsorption of bacteria on HAp increases upto the bacterial equilibrium concentration 137.5 × 10^5 cfu/mL. Plateau is formed in a plot of bacteria adsorbed against bacterial equilibrium concentration beyond this equilibrium concentration which indicates that no bacterial adsorption occurs. It is a major sign to find the adsorption capacity of HAp to adsorb *A. baumanii* suspension. Most of the adsorption sites of HAp are completely covered by monolayer of *A. baumanii* and further adsorption is stopped.

A linearized Freundlich curve for the adsorption of *A. baumanii* on HAp is shown in **Figure 4.32.**

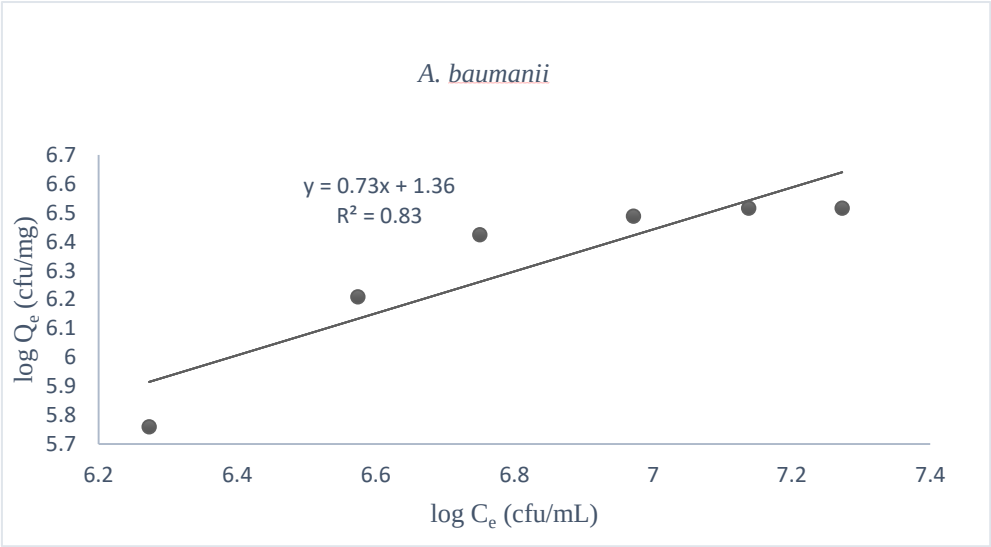

Fig 4.32: *Linearized Freundlich plot of logQ_e against logC_e for A. baumanii*

Further, a langmuir plot is drawn as shown in **Figure 4.33.**

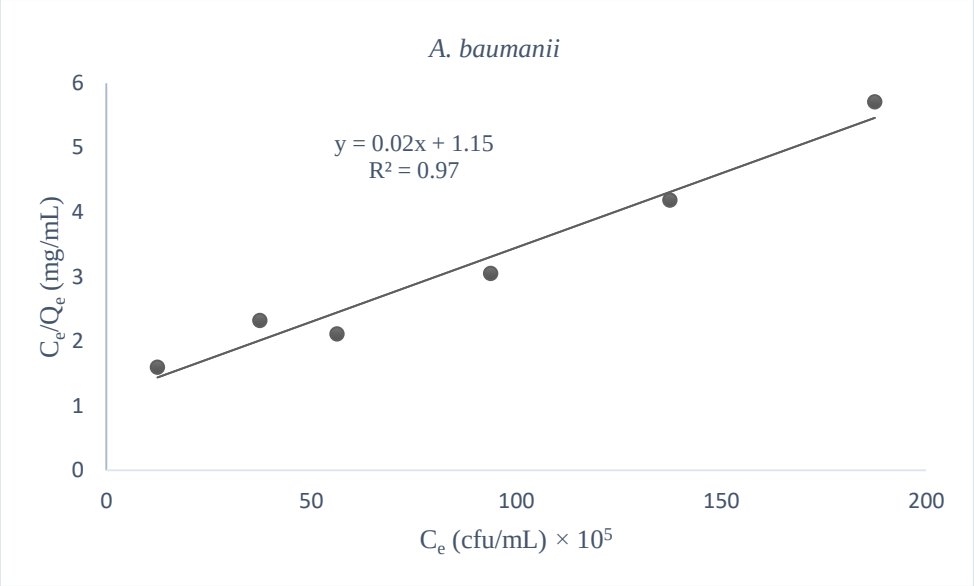

Fig 4.33: *Linearized Langmuir plot of C_e/Q_e against A. baumanii equilibrium concentration (C_e)*

Slope of the line obtained from the above Langmuir plot is found to be 0.023. The maximum number of bacteria adsorbed on 1 mg of HAp is calculated as

$Q_m = 1/0.02 = 43.47 \times 10^5$ cfu/mg. It shows that 1 mg of HAp could adsorb 43.47×10^5 number of *A. baumanii.*

Table 4.8: Parametrers of Langmuir and Freundlich constants for *A. baumanii*

Langmuir model			
	Q_m (cfu/mg)	b (mL/cfu)	R^2
A. baumanii	43.47×10^5	5.02×10^{-7}	0.97
Freundlich model			
	$\log K_f$ (cfu/mg)	n	R^2
A. baumanii	1.36	1.80	0.92

In case of adsorption of *A. baumanii* onto HAp surface, the lower value of Langmuir constant 'b' indicates the weak interaction between bacteria (adsorbate) and hydroxyapatite (adsorbent).The correlation coefficients of Langmuir and Freundlich adsorption isotherm of *A. baumanii* were 0.97 and 0.92 respectively. This shows that the experimental data fitted with the Langmuir model.

3. Adsorption kinetics study

For the adsorption kinetics study, the initial bacterial concentration was used as 236×10^5 cfu/mL and the plot is shown in **Figure 4.34.**

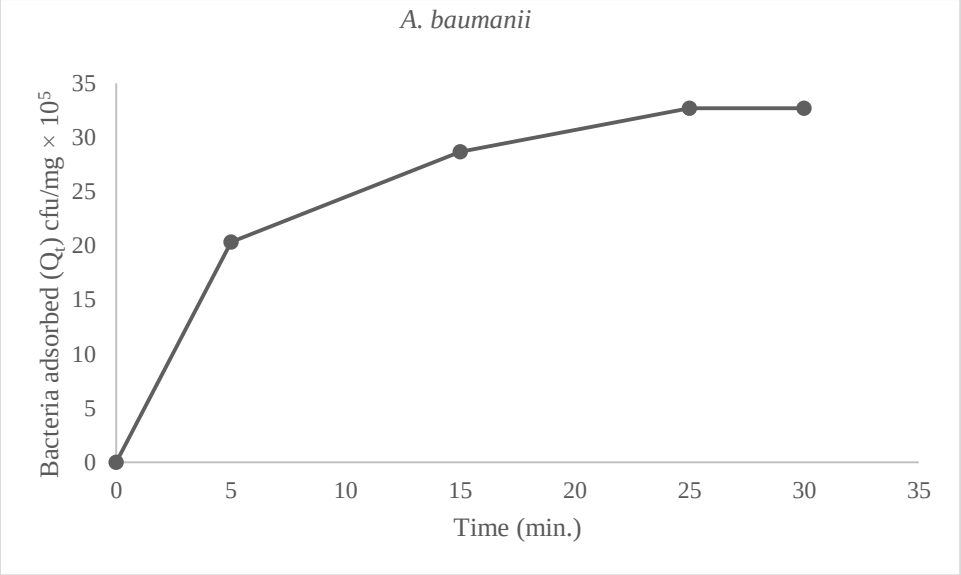

Fig 4.34: *Adsorption kinetics of A. baumanii onto HAp surface*

It shows that the adsorption of bacteria on HAp increases upto 25 minutes. Plateau is formed in a plot of bacteria adsorbed against contact time beyond 25 minutes which indicates that no bacterial adsorption occurs after this. Most of the adsorption sites of HAp are completely covered by monolayer of *A. baumanii* and further adsorption is stopped. For kinetic studies pseudo-second order model was employed to the experimental kinetics data which is shown in **Figure 4.35.**

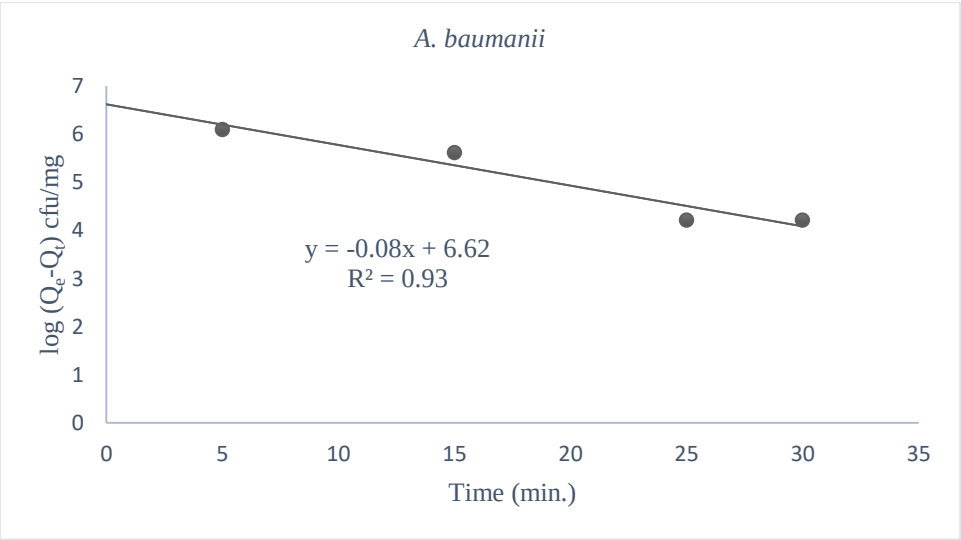

Fig 4.35: *A plot of pseudo-first order kinetic model for the adsorption of A. baumanii on HAp*

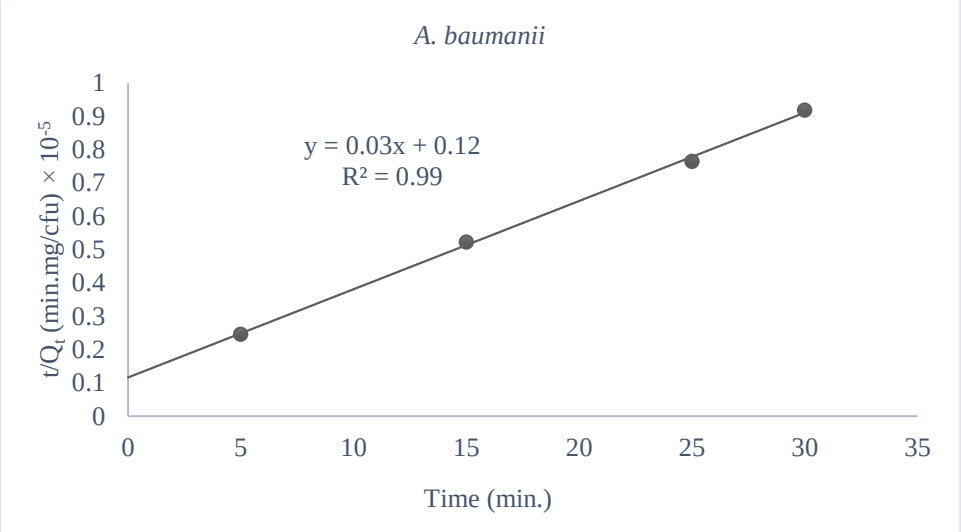

Fig 4.36: *A plot of pseudo-second order kinetic model for the adsorption of A. baumanii on HAp.*

Table 4.9: Parameters of pseudo-first order and pseudo-second order kinetics model for the adsorption of *A. baumanii*.

S.N.	Kinetics model	Rate constants	Q_e (cfu/mg)×10^5	R^2
1.	Pseudo-first order	0.19 (cfu mg^{-1} min^{-1})	41.76	0.93
2.	Pseudo-second order	0.6×10^{-12} (mg min^{-1} cfu^{-1})	38.02	0.99

The larger value of correlation coefficient for pseudo-second order kinetics model (R^2 = 0.99) than pseudo-first order model (R^2 = 0.93) indicates that most of the bacteria adsorb on hydroxyapatite following the pseudo-second order equation.

4.3 Qualitative Analysis for Antimicrobial Activity of Hydroxyapatite

4.3.1 Antibacterial activity

The antibacterial activities of HAp extracted at 750^0C after acid and base treatment were evaluated. For this study, different concentrations of HAp were used as 25, 50, 100, 200 mg/mL against *E. coli, S. aureus, Bacillus sp.* and *A. baumanii* and the result are shown in **Figure 4.37.**

E .coli (ATCC 25923)

Staphylococcus aureus (ATCC 25923)

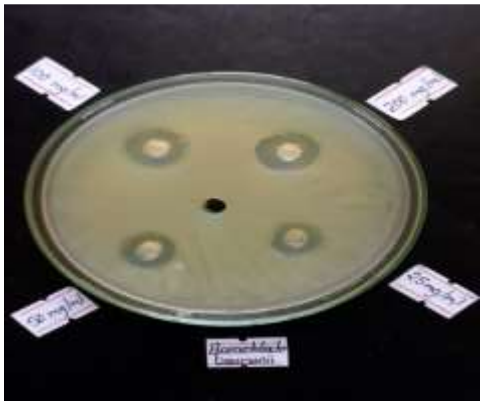

Acinetobacter baumanii (ATCC 19606)

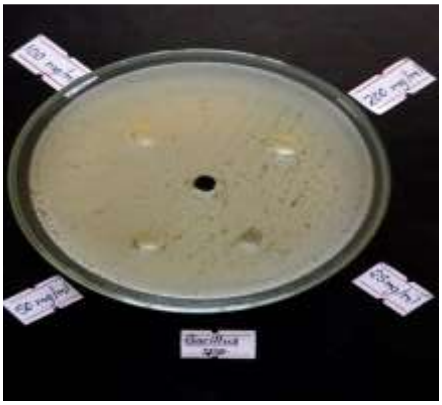

Bacillus spp.

Fig 4.37: *Antibacterial activity of HAp against E. coli, S. aureus, A. baumanii and Bacillus spp.*

The diameters of inhibition zone of HAp with different concentrations against *E. coli, S. aureus, Bacillus sp., A. baumanii* are tabulated in **Table 4.10.**

Table 4.10: The diameters of ZOI of HAp with different concentrations against different bacteria

Tested bacteria	Gram staining	Zone of inhibition for HAp an negative control (mm)	Zone of inhibition of HAp at different concentrations (mm)			
			25	50	100	200
E .coli	-ve	-	-	-	-	-
S. aureus	+ve	-	-	-	-	-
A. baumanii	-ve	-	9	11	14	15
Bacillus spp.	-ve	-	-	-	-	-

Note: '-ve' means Gram negative , '+ve' means Gram positive and '-' means no zone of inhibition

Negative control = DMSO (No zone of inhibition)

For the adsorption experiment of bacteria, *E. coli* and *S. aureus* were used. From antibacterial test of such bacteria, it was shown that HAp couldn't damage the bacterial cell even in higher concentrations. So, it is confirmed that these bacteria adsorbed on HAp surface in viable form.

The antibacterial effect of HAp was pronounced only in *A. baumanii*. The zone of inhibition is substantially increased with increase in concentration of HAp as depicted from above table. Larger zone of inhibition signifies the greater number of bacteria killed by HAp.

Due to larger surface area (144.89 m^2/g) of prepared hydroxyapatite, the interaction with bacterial surface increases resulting the inhibitory effect upon *A. baumanii.* It is a Gram –ve bacteria. The cell wall of this bacteria is thinner with less amount of peptidoglycan (a type of sugar) along with lipoproteinous nature. The antibacterial activity against this bacteria is related to the production of reactive oxygen species like OH^-, H_2O_2 and O_2^{2-} by hydroxyapatite nanoparticles on its surface. These species are responsible for fatal damage to bacterial cell. Similarly, the surface defects and aggregates on hydroxyapatite particles make an abrasive surface ordering on HAp surfaces. These are correlated to the mechanical damage of bacterial cell membrane (Resmim *et al*., 2019).

4.3.2 Antifungal activity

The antifungal activity of HAp extracted at 750^0C after acid and base treatment was evaluated. For this study, different concentrations of HAp were used as 25, 50, 100, 200 mg/mL against *C. albicans*. **Figure 4.38** depicts the result.

Fig 4.38: *Antifungal activity of HAp against Candida albicans*

For the adsorption experiment of fungi, *C. albicans* was used. It is a unicellular fungi. From antifungal test of such fungi, it was shown that HAp couldn't damage the fungal cell even in higher concentrations. So, it is confirmed that this fungi was adsorbed on HAp surface in viable form. Fungal cell wall is similar to the plant cell wall. It consists of a complex carbohydrate chitin. Probably, the complex cell wall structure of fungi didn't allow the HAp particles to enter the fungal cytoplasm for its lysis. There was no any inhibition zone present in any concentrations of HAp. It shows HAp was unable to destroy the fungal cell.

4.3.3 Minimal Inhibitory Concentration (MIC) and Minimal Biocidal Concentration (MBC) study for HAp against *A. baumanii*

Hydroxyapatite showed the antimicrobial property towards the *A. baumanii* (ATCC 19606) which was confirmed from the antimicrobial screening test. To know the MIC and MBC values of HAp against this bacteria, another test in sterile 96 well plate was carried out as depicted from **Figure 4.39.**

HAp (mg/mL)	Antibiotic (mg/mL)
200	0.25
100	0.125
50	0.0625
25	0.0312
12.5 (MIC)	0.0156 (MIC)
6.25	0.008
3.125	0.004
1.625	0.002

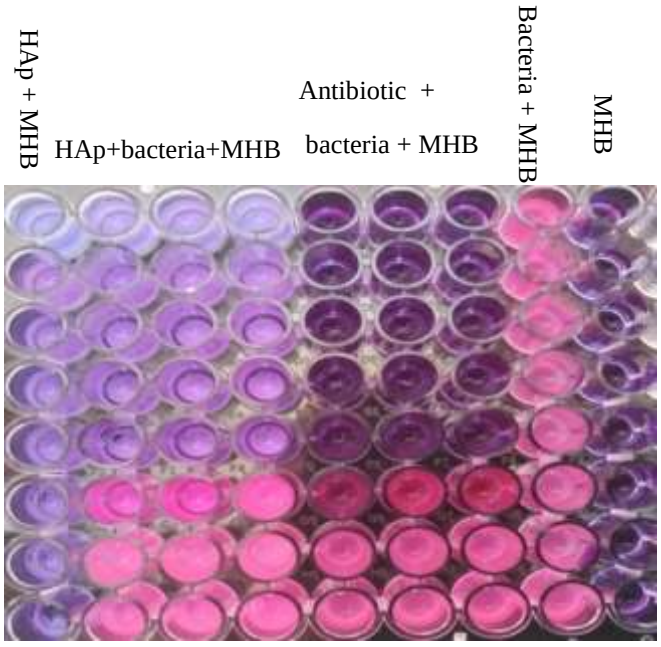

Fig 4.39: *MIC determination of HAp in sterile 96 well plate using Rsazurin as a redox indicator*

MIC value of synthesized HAp against *Acinetobacter baumanii* was found to be 12.5 mg/mL while the standard antibiotic solution showed 0.0156 mg/mL. The synthesized HAp had little antimicrobial property as compared to the antibiotic solution. It is not as potent as the antibiotic solution in terms of antimicrobial property. Above this MIC value, HAp could inhibit the bacterial growth so that the initial purple colour of

Resazurin did not change into final pink colour of Resorufin due to the absence of NADH dehydrogenase enzyme.

MBC is calculated by culturing the solution from the well having higher amount of HAp in NA plate as shown in **Figure 4.40.**

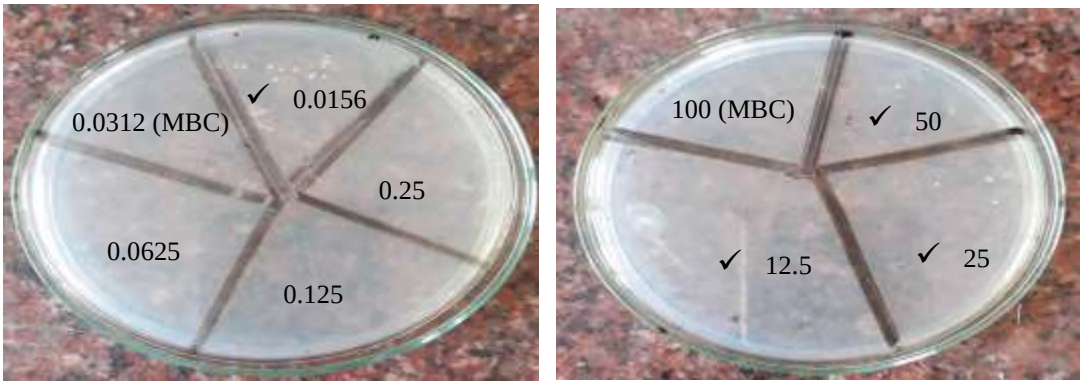

(A) (B)

Fig 4.40: *Different concentrations of (A) antibiotic solutions and (B) HAp for the determination MBC*

MBC value of synthesized HAp against *Acinetobacter baumanii* was found to be 100 mg/mL while the standard antibiotic solution showed 0.0312 mg/mL. The synthesized HAp had little antimicrobial property as compared to the antibiotic solution. Above this MBC value, HAp could kill the bacteria as confirmed by the absence of colony in NA plate as shown above. However, below the MBC value, there were colony showing the survival of bacteria.

CHAPTER 5: CONCLUSIONS

In this work, hydroxyapatite (HAp) was extracted from bio-waste namely caprine (goat) bone from two different methods such as chemical and thermal treatment only and chemical method followed by thermal treatment. Thus produced hydroxyapatites were characterized by XRD, FTIR, SEM analyses.

The broad diffraction peaks and their peak position at about 2θ = 26.21, 29.28, 32.12, 32.53, 33.26, 40.16, 47.04, 49.81, 50.84 and 51.61^{o} for different bone powders prepared from different methods suggest the synthesized nanoparticles were hydroxyapatite (based on JCPDS card number 9-0432). FTIR result showed that NaOH/HCl treated bone powder calcined at 750^0 C is the best one as compared to others due to presence of peak responsible for OH^-. So, it was taken for further microbial adsorption and antimicrobial study. The average crystallite size of such HAp was found to be ± 45.79 nm. The rod shape hydroxyapatite with porous agglomerate was found through SEM analysis. Similarly, the pH_{PZC} and specific surface area were calculated as 7.2 and 144.89 m^2/g by pH drift and methylene blue adsorption method respectively.

Microbial adsorption studies were performed by using extracted nano-HAp as an adsorbent and different microorganisms as adsorbate at neutral pH. Modelling of experimental data were performed using Freundlich and Langmuir adsorption isotherm model. The maximum adsorption capacities (Q_m) on HAp were found to be 32.57 × 10^5, 6.7 × 10^5, 37.17 × 10^5 and 43.47 × 10^5 cfu/mg for *E. coli, S. aureus, C. albicans* and *A. baumanii* respectively. The contact time required for maximum adsorption of particular microorganism was found to be a different value for different concentrations of particular microorganisms. For *E. coli* with different concentrations (212 × 10^5 and 236 × 10^5 cfu/mL), time required for maximum adsorption was found to be 15 and 5 min. respectively. For *S. aureus* using 27 × 10^5 cfu/mL and 30 × 10^5 cfu/mL concentrations, it was found to be 5 and 15 min. respectively. However, it was same for both concentrations (126 × 10^5 and 140 × 10^5 cfu/mL) in case of *C. albicans*. For *A. baumanii* using 236 × 10^5 cfu/mL, it was found to be 25 min. respectively. Pseudo-second order kinetics model was fitted for the adsorption of all microorganisms.

HAp didn't show any antimicrobial effect upon *E. coli, S. aureus* and *C. albicans* even at higher concentrations. This shows that the microorganisms adsorb on HAp during the adsorption experiment were in viable form. However, HAp showed good

antibacterial activity upon *A. baumanii*, a Gram –ve bacteria. MIC and MBC values of HAp against this bacteria were found to be 6.25 and 100 mg/mL respectively.

Thus, hydroxyapatite was synthesized from bio-waste caprine (goat) bone which can be used as an adsorbent in microbial adsorption and an antimicrobial agent.

CHAPTER 6: RECOMMENDATIONS FOR FURTHER STUDY

HAp could be characterized further using Transmission Electron Microscopy (TEM) and Energy Dispersive X-ray analysis (EDX) for better surface morphology and elemental analysis.

Hydroxyapatite is the chief inorganic constituent of teeth. Several bacteria (particularly *S. mutans*) are found to be inhabitant in mouth responsible for dental plaque formation. The exact mechanism upon biofilm formation could be studied using HAp as an adsorbent model.

Microorganisms could be immobilised on the surface of HAp that lead to a synergistic effect for the improvement of removal efficiencies of metal ions. These systems are also tested for solutions containing both metallic ions at the same time, and are shown to be effective also in these cases. These positive results suggest that this approach could be applied also to HAp of different origin. Moreover, these systems could be tested on other metallic ions (i.e. Pb (II)) and in experiments with column configuration.

Hydroxyapatite powder could be used to concentrate the spoilage and pathogenic microorganisms present in very low concentration among meat and fruit sample. This could give result in very short time introducing a rapid testing method.

REFERENCES

Aghayan, M. A., & Rodriguez, M. A. (2012). Influence of fuels and combustion aids on solution combustion synthesis of bi-phasic calcium phosphates (BCP). *Materials Science and Engineering C, 32* (8), 24646-2468. https://doi.org/10.1016/j.msec.2012.07.027.

Akram, M., Ahmed, R., Shakir, I., Ibrahim, W. A., & Hussain, R. (2014). Extracting hydroxyapatite and its precursors from natural resources. *Journal of Material Science, 49* , 1461–1475.

Ayers, R. A., Douglas, B. E., Guglielmo, G., Yi, H. C., Zhim, F., & Yahia, L. (2006). Combustion synthesis of porous biomaterials. *Journal of Biomedical Materials Research Part A, 81A*(3), 634-643. https://doi.org/10.1002/jbm.a.31017.

Baig, A. A., Fox, J. L., Young, R. A., Wang, Z., Hsu, J., Higuchi, W. I., . . . Ostuka, M. (1999). Relationships among carbonated apatite solubility, crystallite size, and microstrain parameters. *Calcified Tissue International, 64*, 437-449.

Barakat, N. M., Khil, M. S., Omran, M. A., Sheikh, F. A., & Kim, H. Y. (2009). Extraction of pure natural hydroxyapatite from the bovine bones bio-waste by three different method. *Journal of Materials Processing Technology, 209* (7), 3408-3415. https://doi.org/10.1016/j.jmatprotec.2008.07.040.

Beem, J. E., Hurley, C. G., Nesbitt, W. E., Croft, D. F., Marks, R. G., Cisar, J. O., & Clark, W. B. (1996). Fimbrial-mediated colonization of murine teeth by *Actinomyces naeslundii*. *Oral Microbiology Immunology, 11*(4), 259-265. https://doi.org/10.1111/j.1399-302X.1996.tb00179.x.

Berry, E. D., & Siragusa, G. R. (1997). Hydroxyapatite adherence as a means to concentrate bacteria. *Applied and Enviromental Microbiology, 63* (10), 4069-4074.

Bigi, A., Cojazii, G., Panzavolta, S., Ripamonti, A., Roveri, N., Romanello, M., . . . Moro, S. (1997). Chemical and structural characterization of the mineral phase from cortical and trabecular bone. *Journal of Inorganic Biochemistry, 68*(1), 45-51. https://doi.org/10.1016/S0162-0134(97)00007-X.

Brooks, T. (1981). *Hydoxyapatite.* San Diego, California: Calbiochem Brand Biochemicals .

Cai, R., Wang, H., Cao, M., Hao, L., Jiang, S., & Xinjiang, L. (2015). Synthesis and antimicrobial activity of mesoporous hydroxylapatite/zinc oxide nanofibers. *Materials and Design, 87*, 17-24. https://doi.org/10.1016/j.matdes.2015.08.004.

Cao, Y. L., Zhang, C. B., & Huang, J. F. (2005). Synthesis of hydroxyapatite nanoparticles in ultrasonic precipitation. *Ceramics International, 31*(8), 1041-1044. https://doi.org/10.1016/j.ceramint.2004.11.002.

Chang, B. S., Lee, C. K., Hong, K. S., Youn, H. J., Ryun, H. S., & Chung, S. S. (2000). Osteoconduction at hydroxyapatite with various pore configuration. *Biomaterials, 21*(12), 1281-1298. https://doi.org/10.1016/S0142-9612(00)00030-2.

Chen, B. H., Chen, K. I., Ho, M. L., Chen, N. H., Chen, W. C., & Wang, C. K. (2009). Synthesis of calcium phosphates and porous hydroxyapatite beads prepared by emulsion method. *Materials Chemistry and Physics, 113*(1), 365-371. https://doi.org/10.1016/j.matchemphys.2008.06.040.

Cho, J. S., & Kang, Y. C. (2008). Nano-sized hydroxyapatite powders prepared by flame spray pyrolysis. *Journal of Alloys and Compounds, 464*(1-2), 282-287. https://doi.org/10.1016/j.jallcom.2007.09.092.

Clark, W. B., & Gibbons, R. J. (1977). Influence of salivary components and extracellular polysaccharide synthesis from sucrose on the attachment of Streptococcus mutans 6715 to hydroxyapatite surfaces. *Infection and Immunity, 18*(2), 5154-523.

Clark, W. B., Bammann, L. L., & Gibbons, R. J. (1978). Comparative estimates of bacterial affinities and adsorption sites on hydroxyapatite surface. *Infection and Immunity, 19* (3), 846-853.

Clark, W. B., Lane, M. D., Beem, J. E., Bragg, S. L., & Wheeler, T. T. (1985). Relative hydrophobicities of *Actinomyces viscosus* and *Actinomyces naeslundii* strains and their adsorption to saliva treated hydroxyapatite. *Infection and Immunity, 47*,, 730-736.

Cowan, M. M., Taylor, K. G., & Doyle, R. J. (1987). Energetics of the initial phase of adhesion of *Streptococcus sanguis* to hydroxyapatite. *Journal of Bacteriology, 169*, 2995-3000. https://doi.org/10.1128/jb.169.7.2995-3000.1987.

Durucan, C., & Brown, P. (2000). Tricalcium phosphate hydrolysis to hydroxyapatite at and near physiological temperature. *Journal of Materials Science : Materials and Medicine, 11*, 365-371.

Elliott, J. C., Mackie, P. E., & Young, R. A. (1980). Monoclinic hydroxyapatite. *Science,180*(4090), 1055-1057.

Elshikh, M., Ahmed, S., Funston, S., Dunlop, P., McGaw, M., Marchant, R., & Banat, I. M. (2016). Resazurin-based 96-well plate microdilution method for the determination of

minimum inhibitory concentration of biosurfactants. *Biotechnology Letter, 38*, 1015-1019. https://doi.org/10.1007/s10529-016-2079-2.

Fathil, M. H., Hanifi, A., & Mortazavi, V. (2008). Preparation and bioactivity evaluation of bone-like hydroxyapatite nanopowder. *Journal of Materials Processing Technology 202*(1-3), 536-542. https://doi.org/10.1016/j.jmatprotec.2007.10.004.

Fu, H. Z., Wang, M. H., & Ho, Y. S. (2013). Mapping of drinking water research: a bibliometric analysis of research output during 1992-2011. *Science of the Total Enviroment, 443*, 757-765. https://doi.org/10.1016/j.scitotenv.2012.11.061.

Gergely, G., Weber, F., Lukcas, I., Toth, A. L., Horvath, Z. E., Mihaly, J., & Balazsi, C. (2010). Preparation and characterization of hydroxyapatite from eggshell. *Ceramics International* (36), 803-806. https://doi.org/10.1016/j.ceramint.2009.09.020.

Gibbons, R. J., Etherden, I., & Moreno, E. C. (1985). Contribution of stereochemical intearctions in the ashesion of S. sanguis C5 to experimental pellicles. *Journal of Dental Research, 64* (2), 96-101. https://doi.org/10.1177%2F00220345850640021801.

Gibbons, R. J., Moreno, E. C., & Spinell, D. M. (1976). Model delineating the effects of a salivary pellicle on the adsorption of *S. miteor* onto hydroxyapatite. *Infection and Immunity, 14* (4), 1109-1112.

Gomez, J. M., Torrent, J. B., Boix, T., Fraile, J., & Rodriguez, R. C. (2001). Precipitation of stoichiometric hydroxyapatite by a acontinuous method. *Crystal Research and Technology, 36*, 15-26. https://doi.org/10.1002/1521-4079(200101)36:1%3C15::AID-CRAT15%3E3.0.CO;2-E.

Goodman, P. A., Li, H., Gao, Y., Lu, Y. F., Stenger-Smith, J. D., & Redepenning, J. (2013). Preparation and characterization of high surface area, high porosity carbon monoliths from pyrolyzed bovine bone and their performance as supercapacitor electrodes. https://doi.org/10.1016/j.carbon.2012.12.066.

Haberoka, K., Bucko, M. M., & Miecznik, J. B. (2006). Natural hydroxyapatite - its behaviour during heat treatment. *Journal of the European Chemical Society, 26*, 537-542. https://doi.org/10.1016/j.jeurceramsoc.2005.07.033.

Heidari, F., Razavi, M., Ghaedi, M., & Forooghi, M. (2017). Investigation of natural properties of hydroxyapatite samples prepared by cold isostatic pressing method. *Journal of Alloy and Compounds, 693*, 1150-1156. https://doi.org/10.1016/j.jallcom.2016.10.081.

Hillman, J. D., Houte, J. V., & Gibbons, R. J. (1970). Sorption of babcteria to human enamel powder. *Journal of Oral Biology and Medicine, 15*, 899-903. https://doi.org/10.1016/0003-9969(70)90163-9.

Hong, L., MinYing, L., & ChangRen, Z. (2008). Processing of nanocrystalline hydroxyapatite particles via reverse microemulsions. *Journal of Materials Science, 43*, 384-389.

Huang, W., Zhang, H., Huang, Y., Wang, W., & Wei, S. (2011). Hierarchial porous carbon obtained from animal bone and evaluation in electric double-layer capacitors. *Carbon, 49*, 838-843. https://doi.org/10.1016/j.carbon.2010.10.025.

Huang, Y. C., Hsiao, P. C., & Chai, H. J. (2011). Hydroxyapatite extracted from fish scale: Effects on MG63 osteoblast-like cells. *Ceramics International, 37* (6), 1825-1831. https://doi.org/10.1016/j.ceramint.2011.01.018.

Itatani, K., Tsugawa, T., Umeda, T., Musha, Y., Davies, L. J., & Koda, S. (2010). Preparation of submicrometer-sized porous spherical hydroxyapatite agglomerates by ultrasonic spray pyrolysis technique. *Journal of the Ceramic Society of Japan, 118*(1378), 462-464. https://doi.org/10.2109/jcersj2.118.462.

Itodo, A. U., Abdulrahman, F. W., Hassan, L. G., Maigandi, S. A., & Itodo, H. U. (2010b). Application of methylene blue and iodine adsorption number for the measurement of specific surface area by four acid and salt treated activated carbon. *New York Science, 3* (5), 25-33.

Khoo, W., Nor, F. M., Ardhyananta, H., & Kurniawan, D. (2015). Preparation of natural hydroxyapatite from bovine femur bones using calcination at various temperatures. *Procedia Manufacturing, 2*, 196-201. https://doi.org/10.1016/j.promfg.2015.07.034.

Kinnari, T. J., Esteban, J., Martin-de-Hijas, N. Z., Sanchez-Munoz, O., Sanchez-Salcedo, S., Colilla, M., . . . Gomez-Barrena, E. (2007). Influence of surface porosity and pH on bacterial adherence to hydroxyapatite and biphasic calcium phosphate bioceramics. *Journal of Medical Microbiology, 58*(1), 132-137. https://doi.org/10.1099/jmm.0.002758-0.

Kong, L., Ma, J., & Boey, F. (2002). Nanosized hydroxyapatite powders derived from cprecipitation process. *Journal of Material Science*, 1131-1134.

Krzesinska, M., & Majewska, J. (2015). Physical properties of continuous matrix of porous natural hydroxyapatite related to the pyrolysis temperature of animal bones precursors. *Journal of Analytical and Applied Pyrolysis, 116*, 202-204. https://doi.org/10.1016/j.jaap.2015.09.009.

Kumar, A. R., & Kalainathan, S. (2010). Sol-gel synthesis of nanostructured hydroxyapatite powder in presence of polyethylene glycol. *Physica B: Condensed Matter, 405*(13), 2799-2802. https://doi.org/10.1016/j.physb.2010.03.067.

Kuttapan, S., Dennis, M., & B., N. M. (2016). Biomimetic composite scaffolds containing bioceramics and collagen/gelatin for bone tissue engineering - A mini review. *International Journal of Biologocal Macromolecules, 93*, 1390-1401. https://doi.org/10.1016/j.ijbiomac.2016.06.043.

Kutty, M. G., & Ramesh, S. (2000). Sintering behaviur and properties of commercial hydroxyapatite. *Ceramics International, 26*, 221-230.

Langmuir, I. (1916). The constitution and fundamental properties of solids and liquids. Part I. Solids. *Journal of American Chemical Society, 38*, 2221-2295. https://doi.org/10.1021/ja02268a002.

Largitte, L., & Pasquier, R. (2016). A review of the kinetics adsorption models and their application to the adsorption of lead by an activated carbon. *Chemical Engineering Research and Design, 109*, 495-504. https://doi.org/10.1016/j.cherd.2016.02.006.

Liu, G. B., & Ma, X. Y. (2009). Hydroxyapatite: hexagonal or monoclinic ? *Crystal Growth and Design, 9*(7), 2992-2994. https://doi.org/10.1021/cg900156w.

Mandal, S., Pal , U., & Dey, A. (2016). Natural origin hydroxyapatite scaffold as potential bone tissue engineering substitute. *Ceramics International, 14*(16), 18338-18346. https://doi.org/10.1016/j.ceramint.2016.08.165.

Markovic, M., Fowler, B. O., & Tung, M. S. (2004). Preparation and comprehensive characterization of a calcium hydroxyapatite reference material. *Journal of Research of the National Institute of Standards and Technology, 109*(6), 553-568. https://dx.doi.org/10.6028%2Fjres.109.042.

Martinez-Vazquez, F. J., Cabanas, M. V., Paris, J. L., Lozano, D., & Vallet-Regi, M. (2014). Fabrication of novel Si-doped hydroxyapatite/gelatine scaffolds by rapid prototyping for drug delivery and bone regeneration. *Acta Biomaterialia, 15*, 200-209. https://doi.org/10.1016/j.actbio.2014.12.021.

Meneghini, C., Dalconi, M. C., Nuzzo, S., Mobilio, S., & Wenk, R. H. (2003). Rietveld refinement on X-ray diffraction patterns of bioapatite in human foetal bones. *Boiphysics, 84* (3), 2021-2029. https://doi.org/10.1016/S0006-3495(03)75010-3.

Mochales, C., Wilson, R. M., Dowker, P. S., & Ginebra, M. P. (2011). Dry mechanosynthesis of nanocrystalline calcium deficient hydroxyapatite: structural characterization. *Journal of Alloys and Compounds, 509*, 7389-7394. https://doi.org/10.1016/j.jallcom.2011.04.033.

Moreno-Pirajan, J. C., Gomez-Cruz, R., Garcia-Cruz, V. S., & Giraldo, L. (2010). Binary system Cu(II)/Pb(II) adsorpttion on activated carbon obtained by pyrolysis of cow bone study. *Journal of Analytical and Applied Pyrolysis, 89*, 122-128. https://doi.org/10.1016/j.jaap.2010.06.007.

Nasiri, T. B., Honarmandi, P., & Ebrahimi, R. K. (2009). Synthesis of nanosized single hydroxyapatite via mechanochemical method. *Material Letters, 63*, 543-546.

Neira, I. S., Guitian, F., Taniguichi, T., Watanabe, T., & Yoshimura, M. (2008). Hydrothermal synthesis of hydroxyapatite whiskers with sharp faceted hexagonal morphology. *Journal of Materials Science, 43*, 2171-2178.

O'Brien, W. J., Fan, P. L., Loesche, W. J., Walker, M. C., & Apostolids, A. (1978). Adsorption of *Streptococcus mutans* on chemically treated hydroxyapatite. *Journal of Dental Research, 57*(9-10). https://doi.org/10.1177%2F00220345780570091601.

Ofudje, E. A., Rajendran, A., Adeojun, A. I., Idowu, M. A., Kareem, S. O., & Pattanayak, D. K. (2017). Synthesis of organic derived hydroxyapatite scaffold from pig bone waste for tissue engineering applications. *Advanced Powder Technology*, *29*(1), 1-8. https://doi.org/10.1016/j.apt.2017.09.008.

Olsson, J., & Krasse, B. (1976). A method of studying adherence of oral streptococci to solid surfaces. *Journal of Dental Research, 84*, 20-28. https://doi.org/10.1111/j.1600-0722.1976.tb00457.x.

Ooi, C. Y., Hamdi, M., & Ramesh, S. (2006). Properties of hydroxyapatite produced by annealing of bovine bone. *Ceramics International* (33), 1171-1177. https://doi.org/10.1016/j.ceramint.2006.04.001.

Orstavik, D., Kraus, F. W., & Henshaw, L. C. (1974). In vitro attachment of Streptococci to the tooth surface. *Infection and Immunity*, 794-800.

Payne, M. J., & Kroll, R. G. (1991). Methods for the separation and concentration of bacteria from foods. *Trends Food Science and Technology, 12*, 315-319. https://doi.org/10.1016/0924-2244(91)90734-Z.

Piccirillo, C., Pereira, M. A., Pullar, R. C., Tobaldi, D. M., Pintado, M. E., & Castro, P. M. (2013). Bacteria immobilization on hydroxyapatite surface for heavy metals removal. *Journal of Enviromental Management*(121), 87-95. https://doi.org/10.1016/j.jenvman.2013.02.036.

Posner, A. S., Perloff, A., & Diorio, A. F. (1958). Refinement of the hydroxyapatite structure. *Acta Crystallographica, 11*(4), 308-309. https://doi.org/10.1107/S0365110X58000815.

Pramanik, S., Agrawal, A. K., Rai, K., & Garg, A. (2007). Development of high strength hydroxyapatite by solid state sintering process. *Ceramics International, 33*, 419-426. https://doi.org/10.1016/j.ceramint.2005.10.025.

Ramesh, S., Loo, Z. Z., Tan, C. Y., Kelvin, W. J., Ching, Y. C., Tarlochan, F., . . . Sarhan, A. A. (2018). Characterization of biogenic hydroxyapatite derived from animal bones for biomedical applications. *Ceramics International*. *44*(9), 10525-10530. https://doi.org/10.1016/j.ceramint.2018.03.072.

Reddy, M. P., Venugopal, A., & Subrahmanyam, M. (2007). Hydroxyapatite-supported Ag-TiO_2 as *Escherichia coli* disinfection photocatalyst. *Water Research, 41*(2), 379-386. https://doi.org/10.1016/j.watres.2006.09.018.

Rolla, G., & Melsen, B. (1975). Desorption of protein and bacteria from hydroxyapatite by fluoride and monofluorophosphate. *Caries Research, 9*, 66-73. https://doi.org/10.1159/000260144.

Rouhani, P., Taghavinia, N., & Rouhani, S. (2010). Rapid growth of hydroxyapatite nanoparticles using ultrasonic irradiation. *Ultrasonics Sonochemistry, 17*(5), 853-856. https://doi.org/10.1016/j.ultsonch.2010.01.010.

Ruksudjarit, A., Pengpat, K., Rujijanagul, G., & Tunkasiri, T. (2008). Synthesis and characterization of nanocrystalline hydroxyapatite from natural bovine bone. *Current Applied Physics*, *8*(3-4), 270-272. https://doi.org/10.1016/j.cap.2007.10.076.

Sanosh, K. P., Cheoi, C. M., Balakrishnan, A., Kim, T. N., & Seong, C. J. (2009). Preparation and characterization of nano-hydroxyapatite powder using sol-gel techn. *Bulletin of Materials Science, 32*, 465-470.

Seol, Y., Park, D. Y., Park, J. Y., Kim, S. W., Park, S. J., & Cho, D. (2013). A new method of fabricating robust freeform 3D ceramic scaffolds for bone tissue regeneration. *Biotechnology and Bioengineering, 110*(5), 1444-1455.

Shipman, P., Foster, G., & Schoeninge, M. (1984). Burnt bones and teeth: an experimental study of colour, morphology, crystal structure and shrinkage. *Journal of Archaeological Science, 11,* 307-325. https://doi.org/10.1002/bit.24794.

Shojai, M. S., Khorasani, M. T., Khoshdargi, E. D., & Jamshidi, A. (2013). Synthesis methods of nanosized hydroxyapatite in diverse structures. *Acta Biomaterilia, 9*(8), 7591-7621. https://doi.org/10.1016/j.actbio.2013.04.012.

Sionkowska, A & Kozlowska, J. (2010). Characterization of collagen/hydroxyapatite composites sponges as a potential bone substitute. *International Journal of Biological Macromolecules, 47*(4), 483-487. https://doi.org/10.1016/j.ijbiomac.2010.07.002.

Smith, C. B., & Smith, D. A. (1977). An x-ray diffraction investigation of age-related changes in the crystal structure of bone apatite. *Calcified Tissue Research, 22,* 219-226.

Sobczak, A., Kowalski, Z., & Wzore, Z. (2009). Preparation of hydroxyapatite from animal bones. *Acta of Bioengineering and Biomechanics, 11* (4).

Sturgeon, J. L., & Brown, P. W. (2009). Effects of carbonate on hydroxyapatite formed from Calcium hydrogen phosphate and other phospahe salt. *Journal of Material Science : Materials and Medicine, 20,* 1787-1794.

Sun, R. X., Yao, L. V., Niu, Y. R., Zhao, H. X., Cao, D. S., Tang, J., . . . Chen, K. Z. (2017). Physicochemical and biological properties of bovine-derived porous hydroxyapatite/collagen composite and its hydroxyapatite powders. *Ceramics International, 43*(18), 16792-16798. https://doi.org/10.1016/j.ceramint.2017.09.075.

Tarsil, R., Muzzarelli, A. R., Guzman, C., & Pruzzo, C. (1997). Inhibition of *Streptococcus mutans* adsorption to hydroxyapatite by low molecular weightcChitosans. *Journal of Dental Research, 76* (2), 665-672. https://doi.org/10.1177%2F00220345970760020701.

Teshima, K., Lee, S. H., Sakurai, M., Kameno, Y., Yubuta, K., & Suzuki, T. (2009). Well formed one dimensional hydroxyapatite crystals grown by an enviromentally friendly flux method. *Crystal Growth and Design, 9,* 2937-2940. https://doi.org/10.1021/cg900159j.

Tong, W., Glimcher, M. J., Katz, L. J., Kuhn, L., & Eppell, S. J. (2003). Size and shape of mineralites in young bovine bone measured by atomic force microscopy. *Calcified Tissue International, 72*(5), 592-598.

Vacca-Smith, M. A., & Bowmen, W. H. (1998). Binding properties of *Streptococcal glucosyltransferases* for hydroxyapatite, saliva coated hydroxyapatite, and bacterial surfaces. *Archives of Oral Biology, 43*(2), 103-110. https://doi.org/10.1016/S0003-9969(97)00111-8.

Walters, M. A., Lang, Y. C., Bluementhal, N. C., LeGeros, R. Z., & Konsker, L. A. (1990). A Raman and infrared spectroscopic investigation of biological hydroxyapatite. *Journal of Inorganic Biochemistry, 39*(3), 193-200. https://doi.org/10.1016/0162-0134(90)84002-7.

Weeekamp, A. H., & McBride, B. C. (1980). Adherence of *Streptococcus salivarius* HB and HB-7 to oral surfaces and saliva-coated hydroxyapatite. *Infection and Immunity, 30*, 150-158. https://doi.org/0019-9567/80/10-0150/09$02.00/0.

Wheeler, T. T. (1983). Influence of physicochemical parameters on adsorption of *Actinomyces viscosus* to hydroxyapatite surfaces. *Infection and Immunity, 39*, 1095-1101. https://doi.org/0019-9567/83/031095-07$02.00/0.

Xingyuan, G., Xiao, P., Liu, J., & Shen, Z. (2005). Fabrication of nanostructured hydroxyapatite via hydrothermal synthesis and spark plasma sintering. *Journal of the American Ceramic Society, 88*(4). https://doi.org/10.1111/j.1551-2916.2005.00198.x.

Yogananda, C. P., Selvarajan, V., Goudouri, O. M., Paraskevopoupos, K. M., & Dongfeng, J. W. (2011). Preparation of bovine hydroxyapatite by transferred arc plasma. *Current Applied Physics, 11*(3), 702-709. https://doi.org/10.1016/j.cap.2010.11.035.

Zamora, N., Esteban, J., Kinnari, T. J., Celdran, A., Granizo, J. J., & Zafra, C. (2007). In vitro evaluation of the adhesion to polypropylene sutures of non-pigmented, rapidly growing bacteria. *Clinical Microbiology Infection, 13*, 902–907. https://doi.org/10.1111/j.1469-0691.2007.01769.x.

Zhang, H. G., & Zhu, Q. (2006). Preparation of fluoride substituted hydroxyapatite by a molten salt synthesis route. *Journal of Material Science: Materials in Medicine, 17*, 691-695. https://doi.org/10.1007/s10856-006-9679-7.

Zhou, J., Zhang, X., Chen, J., Zeng, S., & Groot, K. D. (1993). High temperature characteristics of synthetic hydroxyapatite. *Journal of Material Science: Materials and Medicine, 5*, 83-85.

Zhuofan, C., Baoxin, H., Haobo, P., & Darvell, B. W. (2009). Solubility of bovine-derived hydroxyapatite by solid titration, pH 3.5–5. *Crystal Growth and Design, 9*(6), 2816-2820. https://doi.org/10.1021/cg900070v.

APPENDICES

Table 1: Crystallite size of bone powder calcined at 750^0C

S.N.	2θ	θ (radian)	Cos θ	FWHM	FWHM (radian) 10^{-2}	Crystallite size (nm)	Average size (nm)
1	26.22	0.23	0.97	0.21	0.36	39.14	36.02
2	29.28	0.25	0.96	0.21	0.36	38.94	
3	32.12	0.28	0.96	0.21	0.38	37.62	
4	32.53	0.28	0.95	0.26	0.46	31.28	
5	33.29	0.29	0.95	0.22	0.38	37.13	
6	40.16	0.35	0.93	0.22	0.39	37.35	
7	47.04	0.41	0.91	0.25	0.44	34.22	
8	49.8	0.43	0.9	0.25	0.44	34.61	
9	50.84	0.44	0.9	0.25	0.44	34.38	
10	51.69	0.45	0.9	0.24	0.43	35.48	

Table 2: Crystallite size of bone powder calcined at 950^0C

S.N.	2θ	Θ (radian)	Cos θ	FWHM	FWHM (radian) 10^{-2}	Crystallite size (nm)	Average size (nm)
1	26.21	0.22	0.97	0.27	0.47	30.24	31.67
2	29.24	0.25	0.96	0.24	0.41	34.66	
3	32.12	0.28	0.96	0.29	0.52	27.72	
4	33.22	0.28	0.95	0.27	0.47	30.35	
5	34.37	0.3	0.95	0.24	0.42	33.94	
6	40.12	0.35	0.93	0.25	0.44	32.82	
7	47	0.41	0.91	0.27	0.47	31.56	
8	49.79	0.43	0.90	0.28	0.49	31.67	
9	50.8	0.44	0.90	0.26	0.46	32.73	
10	51.59	0.45	0.90	0.28	0.48	31.65	

Table 3: Crystallite size of bone powder calcined at 750^0C after base treatment

S.N.	2θ	θ (radian)	Cos θ	FWHM	FWHM (radian) 10^{-2}	Crystallite size (nm)	Average size (nm)
1	26.05	0.23	0.97	0.26	0.45	31.23	30.63
2	26.88	0.23	0.97	0.12	0.22	63.83	
3	29.15	0.25	0.96	0.29	0.51	27.74	
4	31.96	0.28	0.96	0.21	0.37	38.1	
5	32.21	0.28	0.96	0.72	0.02	11.34	
6	33.14	0.28	0.96	0.31	0.54	26.74	
7	34.24	0.29	0.96	0.32	0.55	26.28	
8	40.02	0.34	0.94	0.33	0.57	25.58	
9	46.9	0.4	0.92	0.31	0.54	27.73	
10	49.67	0.43	0.91	0.32	0.54	27.78	

Table 4: Crystallite size of bone powder calcined at 750^0C after acid + base treatment

S.N.	2θ	θ (radian)	Cos θ	FWHM	FWHM (radian) 10^{-2}	Crystallite size (nm)	Average size (nm)
1	26.1	0.22	0.97	0.16	0.27	51.31	45.79
2	29.17	0.25	0.97	0.17	0.3	46.57	
3	32	0.28	0.96	0.18	0.32	44.95	
4	32.41	0.28	0.96	0.18	0.31	45.5	
5	33.14	0.29	0.96	0.17	0.3	46.84	
6	34.29	0.29	0.95	0.16	0.29	49.43	
7	40.04	0.35	0.94	0.18	0.31	47.5	
8	46.93	0.41	0.92	0.20	0.35	42.82	
9	49.71	0.43	0.91	0.22	0.38	39.34	
10	50.72	0.44	0.9	0.20	0.35	43.59	

Table 5: Determination of λ_{max} for methylene blue solution

S.N.	Concentration of methylene blue solution (ppm)	Absorbance
1	0	0
2	1	0.139
3	2	0.204
4	3	0.291
5	4	0.371
6	5	0.458
7	6	0.546
8	7	0.591
9	8	0.718
10	9	0.753

Table 6: Calibration curve for methylene blue solution

S.N.	Wavelength (nm)	Absorbance
1	400	0.02
2	450	0.018
3	500	0.019
4	550	0.029
5	600	0.073
6	645	0.098
7	650	0.128
8	655	0.131
9	660	0.135
10	665	0.139
11	670	0.133
12	675	0.111
13	700	0.028
14	750	0.012
15	800	0.012

Table 7: Determination of specific surface area

S.N.	Initial concentration (C_i) (mg/L)	Equilibrium concentration (C_e) (mg/L)	Methylene blue adsorbed per unit mass ($Q_{e)}$ (mg/g)	C_e/Q_e (g/L)
1	50	16.65	16.67	0.99
2	100	48.04	25.97	1.85
3	150	87.76	31.11	2.82
4	200	131.48	34.26	3.84
5	250	181.95	34.02	5.35
6	300	228.65	35.67	6.41

Table 8: Determination of pH_{PZC} of HAp surface

S.N.	Initial pH	Final pH	ΔpH
1	2.1	3.45	-1.35
2	3.22	4.26	-1.04
3	3.98	5.74	-1.76
5	5.2	6.54	-1.34
6	6.14	6.74	-0.6
7	7.24	7.08	0.16
8	8.12	7.15	0.97
9	9.08	7.44	1.64
10	10.13	7.92	2.21

Table 9: Calibration curve of *E. coli*

S.N.	Bacterial concentration (cfu/mL) × 10^5	Absorbance
1	0	0
2	24	0.06
3	48	0.12
4	72	0.15
5	96	0.19
6	120	0.23

Table 10: Adsorption of *E. coli* on HAp

Initial volume of Bacterial suspension (V) = 5mL

Mass of HAp used in each (M) = 15 mg

Contact time = 30 mins.

Optimum pH = 7

S.N.	Bacterial initial concentration cfu/mL × 10^5 (C_i)	Bacterial equilibrium concentration cfu/mL × 10^5 (C_e)	Bacteria adsorbed cfu/mg × 10^5 (Q_e)	C_e/Q_e (mg/mL)	logC_e	logQ_e
1	0	0	0	0	-	-
2	24	15	3	5	1.17	0.47
3	72	50	7.33	6.82	1.69	0.86
4	120	85	11.67	7.28	1.92	1.06
5	164	120	14.67	8.18	2.07	1.16
6	212	160	17.33	9.23	2.2	1.23
7	236	185	17	10.88	2.26	1.23

Table 11: Adsorption kinetics study of *E. coli* on HAp

S.N.	Time (min.)	Bacterial initial concentration cfu/mL × 10^5 (C_i)	Bacterial equilibrium concentration cfu/mL × 10^5 (C_e)	Bacteria adsorbed cfu /mg × 10^5 (Q_t)	t/Q_t	log ($Q_e - Q_t$) cfu/mg	Adsorption %
1	0	0	0	0	-	-	0
2	5	212	187	8.33	0.6	5.95	11.79
3	15	212	165	15.67	0.95	5.22	24.52
4	25	212	165	15.67	1.59	5.22	24.52
5	30	212	165	15.67	1.91	5.22	24.52

Table 12: Effect of adsorbent dose on adsorption of *E. coli*

S.N.	Amount taken (g)	Bacterial equilibrium concentration (cfu/mL) × 10^5	Adsorption %
1	0.01	220	9.09
2	0.02	215	11.15
3	0.03	195	19.42
4	0.04	180	25.61
5	0.05	175	27.68
6	0.06	165	31.81
7	0.07	160	33.88
8	0.08	160	33.88

Table 13: Calibration curve of *C. albicans*

S.N.	Fungal Concentration (cfu/mL) × 10^5	Absorbance
1	0	0
2	14	0.03
3	28	0.07
4	42	0.1
5	56	0.13
6	70	0.16

Table 14: Adsorption of *C. albicans* on HAp

Initial volume of fungal suspension (V) = 5mL

Mass of HAp used in each (M) = 15 mg

Optimum pH = 7

S.N.	Fungal initial concentration cfu/mL × 10^5 (C_i)	Fungal equilibrium concentration cfu/mL × 10^5 (C_e)	Fungi adsorbed cfu/mg × 10^5 (Q_e)	C_e/Q_e (mg/mL)	logC_e	logQ_e
1	0	0	0	0	-	-
2	28	4	8	0.5	0.6	0.9
3	84	17	22	0.77	1.23	1.34
4	112	26	29	0.9	1.41	1.46
5	126	39	29	1.34	1.59	1.46
6	140	52	29	1.79	1.71	1.46

Table 15: Adsorption kinetics of *C. albicans* on HAp

S.N.	Time (min.)	Fungal initial concentration cfu/mL × 10^5 (C_i)	Fungal equilibrium concentration cfu/mL × 10^5 (C_e)	Fungi adsorbed cfu /mg × 10^5 (Q_t)	t/Q_t	log ($Q_e - Q_t$)	Adsorption %
1	0	0	0	0	-	-	-
2	5	126	86.96	13	0.38	6.20	30.98
3	15	126	52.17	25	0.6	5.64	58.59
4	25	126	43.48	27.51	0.91	5.17	68.94
5	30	126	43.48	27.51	1.09	5.17	68.94

Table 16: Calibration curve of *S. aureus*

S.N.	Bacterial concentration (cfu/mL) × 10^5	Absorbance
1	0	0
2	3	0.04
3	6	0.07
4	9	0.1
5	12	0.12
6	15	0.15

Table 17: Adsorption of *S. aureus* on HAp

Initial volume of bacterial suspension (V) = 5mL

Mass of HAp used in each (M) = 15 mg

Contact time = 30 mins

Optimum pH = 7

S.N.	Bacterial initial concentration cfu/mL × 10^5 (C_i)	Bacterial equilibrium concentration cfu/mL × 10^5 (C_e)	Bacteria adsorbed cfu/mg × 10^5 (Q_e)	C_e/Q_e (mg/mL)	logC_e	logQ_e
1	0	0	0	0	-	-
2	3	0.96	0.68	1.41	4.98	4.83
3	9	3.85	1.72	2.24	5.58	5.23
4	15	6.73	2.76	2.44	5.82	5.44
5	21	10.58	3.47	3.05	6.02	5.54
6	27	14.42	4.19	3.44	6.15	5.62
7	30	17.31	4.23	4.09	6.24	5.62

Table 18: Adsorption kinetics of *S. aureus* on HAp

S.N.	Time (min.)	Bacterial initial concentration cfu/mL × 10^5 (C_i)	Bacterial equilibrium concentration cfu/mL × 10^5 (C_e)	Bacteria adsorbed cfu/mg × 10^5 (Q_t)	t/Q_t	log ($Q_e - Q_t$)	Adsorption %
1	0	0	0	0	-	-	-
2	5	27	16.35	3.55	1.4	4.83	39.44
3	15	27	15.38	3.87	3.87	3.55	43.04
4	25	27	14.42	4.19	5.96	3.6	46.6
5	30	27	14.42	4.19	7.15	3.6	46.6

Table 19: Calibration curve of *A. baumanii*

S.N.	Bacterial concentration (cfu/mL) × 10^5	Absorbance
1	0	0
2	23	0.05
3	73	0.14
4	123	0.21
5	173	0.26
6	223	0.35

Table 20: Adsorption of *A. baumanii* on HAp

Initial volume of Bacterial suspension (V) = 5 mL

Mass of HAp in each (M) = 15 mg

Contact time = 30 mins.

Optimum pH = 7

S.N.	Bacterial initial concentration cfu/mL × 10^5 (C_i)	Bacterial equilibrium concentration cfu/mL × 10^5 (C_e)	Bacteria adsorbedcfu /mg × 10^5 (Q_e)	C_e/Q_e (mg/mL)	log C_e	logQ_e
1	36	18.75	5.75	1.59	1.09	0.89
2	86	37.50	16.17	2.31	1.57	1.20
3	136	56.25	26.58	2.11	1.75	1.42
4	186	93.75	30.75	3.04	1.97	1.48
5	236	137.5	32.83	4.18	2.13	1.51
6	286	187.5	32.83	5.76	2.27	1.51

Table 21: Adsorption kinetics study of *A. baumanii* on HAp

S.N.	Time (min.)	Bacterial initial concentration cfu/mL × 10^5 (C_i)	Bacterial equilibrium concentration cfu/mL × 10^5 (C_e)	Bacteria adsorbed cfu/mg × 10^5 (Q_t)	t/Q_t	log ($Q_e - Q_t$)	Adsorption %
1	0	0	0	0	-	-	-
2	5	236	175	20.33	0.17	6.09	25.85
3	15	236	150	28.67	0.46	5.62	36.44
4	25	236	138	32.67	0.76	4.21	41.73
5	30	236	138	32.67	0.91	4.21	41.73